

# **The Role and Implementation of Compliance in Legged Locomotion**

Jonathan W. Hurst

CMU-RI-TR-08-48

Submitted in Partial Fulfillment of the  
Requirements for the Degree of  
Doctor of Philosophy in Robotics



Robotics Institute  
Carnegie Mellon University  
Pittsburgh, Pennsylvania

2008

Thesis Committee:  
Jessica Hodgins, Chair  
Alfred A. Rizzi  
Matt Mason  
J. Kenneth Salisbury, Stanford University

Copyright © 2008 by Jonathan W. Hurst. All rights reserved.



## Abstract

Many robots excel at precise positioning and trajectory tracking using software control, and most successful robotic applications utilize this ability—examples include CNC machining, robotic welding, painting, and pick-and-place circuit board assembly. The mechanical design of these robots focuses on rigid transmissions and minimizing compliance in the structure, so the software controller can accurately track a desired position as a function of time, regardless of any disturbance forces. However, there is a class of tasks for which rigid actuation is not ideal: physical interaction with the world, especially interaction that involves an impact or kinetic energy transfer. Animals tend to excel at these tasks, and far outperform the best robots. Examples include walking, running, catching a ball, gripping a piece of fruit firmly but without causing damage, and many types of assembly tasks.

For dynamic behaviors such as running, the performance limitations of a robot are often due to limitations of the mechanical design. A robot is an integrated system of electronics, software, and mechanism, and each part of the system limits or enables the behavior of the whole. While some behaviors can easily be implemented through simple actuators and direct software control, a running machine requires mechanical design that is specialized for the task. Among other things, physical springs are essential for a robust and efficient running gait, to store energy, provide high mechanical power, and overcome bandwidth limitations of traditional actuators. An ideal kinematic design, where the joints and links are perfectly sized and placed for the desired task, and motors that exceed the force and speed requirements of the task are not sufficient for successful dynamic interactions. Inertia, transmission friction, and other dynamic effects have a significant role in the behavior of a robot.

We are building running and walking machines with a focus on mechanical design to enable efficient and robust gaits. The defining characteristic of a running gait is spring-like behavior; all running animals, from small insects to large mammals, exhibit a center-of-mass motion that resembles a bouncing ball or a pogo stick. The spring-like behavior is implemented with the assistance of physical springy elements, such as tendons, and not entirely through software or neural control. Energy cycles back and forth between the ballistic trajectory of the body and the compression of the leg spring. To exhibit this behavior, our robots incorporate a mechanical spring that is tuned to absorb and release the energy of a running gait at the appropriate frequency. Electric motors act in series with this spring to add or remove energy from the cycle to modify or control the running gait.

Our first prototype machine is a single actuator mounted to a bench, called the Actuator with Mechanically Adjustable Series Compliance, or AMASC. The stiffness and the no-load position of the joint are mechanical configurations that can be independently adjusted using two separate motors, and it is a test platform to verify and refine several design ideas for leg joints of running and walking robots. After significant testing and design revision, we incorporated the ideas behind the AMASC into the design of a full bipedal robot, the Biped with Mechanically Adjustable Series Compliance, or BiMASC. A single leg prototype of the BiMASC was constructed and tested, and after some final revisions, we have built the Electric Cable Differential (ECD) Leg. The ECD Leg derives its name from the construction—using electric motors, cable drives, and mechanical differentials to actuate the system. One ECD Leg, named Thumper, is assembled as a monopod and installed in our laboratory at the Robotics Institute to study the role of compliance in running gaits. Two ECD Legs are assembled as a biped named MABEL, which is installed in Professor Jessy Grizzle’s Laboratory at the University of Michigan and will serve as a platform to explore novel control ideas.

In this thesis, we demonstrate that physical springs are extremely important for supporting a running gait. Additionally, through experiments on the ECD Leg, we demonstrate that there is an

energetically optimal leg stiffness. The design and construction of the robots in this thesis are an exploration of methods for adjusting the leg stiffness to obtain the optimal stiffness for a running gait. The AMASC and BiMASC utilize co-contraction of antagonistic springs to tune the stiffness to a desired value. The ECD leg, in contrast, utilizes both active control of the motor and kinematic adjustments to control the stiffness behavior of the leg. We suggest that that co-contraction of antagonistic springs is energetically expensive, and that active control of a leg to modify its inherent stiffness might be energetically cheaper, with the same functionality.

The ECD leg successfully hopped in place, as well as at speed. Thumper and MABEL demonstrate, for the first time, a cable drive paired with series elasticity for a running machine. The AMASC is the first demonstration of series elasticity implemented via a mechanical differential, and the BIMASC, Thumper, and MABEL all utilize this same concept. The mechanical design of the ECD leg contains many novel ideas that will be utilized in future walking and running machines.

## Acknowledgments

This thesis work was made possible through the help and support of friends, colleagues, advisors, and the Robotics Institute community. While I have benefitted from the many conversations, seminars, contacts, and facilities here, I would like to specifically thank a few people who have had a significant impact on my life and on my work.

Al Rizzi agreed at the outset to help me pursue my interests in legged locomotion as my advisor, taking on quite an educational project. Al has taught me to be a better communicator, both in publications and in presentations, and to think bigger, looking for fundamental ideas that will have impact and significance. Al supported the construction of the AMASC prototype actuator out of his discretionary money, which led to the subsequent work in this thesis. With Al's encouragement and support, I was able to attend several important conferences, such as the Dynamic Walking meetings, and to maintain and pursue important relationships with members of the academic community that have and will continue to impact my career.

Joel Chestnutt, a fellow Robograd, worked together with me on many of the systems described in this thesis, motivated by a shared vision of making legged robots that can get around in the world. We had countless discussions about the design of the mechanical systems, drawing diagrams on the whiteboard and making up notation to describe differentials and cable drives. With Joel driving the detailed implementation, we created software to control the devices, and made them all work.

Professor Jessy Grizzle, from the University of Michigan, took a risk and agreed to collaborate with me in creating a walking, running biped robot. This collaboration has allowed me to create the bipedal robot that was a major achievement of my graduate studies, and has resulted in a machine that Jessy can use for years to come in control system development. As I have neared completion and looked forward to an academic career, Jessy has gone to great lengths to assist my efforts and ensure my success. As a result of his efforts, I will have a running start at my new faculty position, with a set of tools and a monopod robot ready to go. It has made a significant impact, and I sincerely appreciate it. May the collaboration continue.

Jessica Hodgins assumed responsibility as my advisor for the last portion of my thesis work. She has provided resources at the moment they were needed, such as a lab space that had been recently vacated, and funding to hire an undergraduate assistant for robot experiments. At the time, I did not realize how necessary these things were to the success of my research. In addition, she has provided valuable advice and paper comments, and integrity and reliability through all interactions.

Matt Mason has served on my thesis committee during graduate school, and has been supportive in sometimes subtle ways. Matt has always been tolerant of unconventional methods of thinking about problems, and I never felt pressure to do things a certain way. Matt has been a great soundboard, asking one or two questions that get right to the center of the problem, sometimes exposing poor assumptions or gaps in logic. Matt served as the local Principal Investigator on the NSF sub-contract from Professor Grizzle and the University of Michigan, paving the way for the work to begin and parts to be made for the ECD Legs.

Pras Velagapudi and Brian Kirby volunteered their time to design the custom electronics on the ECD Leg. We had a number of meetings to make decisions about the system, and they both provided invaluable expertise and advice for specifying the commercial components of the system. They designed the two custom circuit boards, and helped to debug them. Brian and Pras also helped to design and build the large power supply that powers the robot.

Steven Zhang, during the second semester of his first year of college, came every day to help with the final software edits and experiments on the ECD Leg. Together, we finished the experiments just in time.

David Conner and Sarjoun Skaff, my long-time office-mates, tolerated a thousand questions about LaTeX and Matlab, and constant complaints about computers in general. We had many technical discussions, talking through ideas and refining them. After many political discussions, we still agree to disagree, and have a beer together.

Ralph Hollis has been an ally and friend since my undergraduate years, and is the director of the Microdynamic Systems Lab, my home lab throughout graduate school. There are so many interesting projects and so much useful equipment in the lab, it has been a fantastic place to do research in robotics.

Stephanie Matvey helped with all matters concerning money, especially when I was building the ECD Leg, buying a hundred different items and barraging her with receipts. Thank you for keeping such meticulous records and for making my life a lot easier.

After making it through the first year of courses together, a number of classmates became good friends, all responsible for making my time in graduate school into a great experience. Damion, Jeremy, Alik, Maayan, Liz, Rachel, Brian, Tom, Krissie, and others will hopefully always keep in touch.

Last and most important, my wife, Kelly. With any other uncertainties in life and career, she is the constant, and I know she will be there. Although she finished her Ph.D. before me and likes to rub it in a little, she knows what is involved, and it helps to know we're in it together.

Financially, this work was supported in part by NSF grant 0413251 through Professors Matt Mason and Al Rizzi, by NSF grants ECS-0322395 and ECS-0600869 through Professor Jessy Grizzle at the University of Michigan, by an NSF fellowship, an IGERT fellowship, and by Carnegie Mellon University.

# Contents

<b>1</b>	<b>Introduction</b>	<b>1</b>
1.1	Contributions . . . . .	2
<b>2</b>	<b>Background and Related Work</b>	<b>5</b>
2.1	The Spring-Loaded Inverted Pendulum . . . . .	5
2.2	Tuned Leg Stiffness . . . . .	7
2.3	Using Leg Stiffness for Gait Control . . . . .	8
2.4	Using Leg Stiffness for Disturbance Rejection . . . . .	9
2.5	Creating Spring-Like Behavior . . . . .	10
2.6	SLIP model running robots . . . . .	10
2.7	Other Robots . . . . .	11
2.8	Variable Compliance Mechanisms . . . . .	12
2.9	Variable Compliance Outside of Legged Locomotion . . . . .	12
2.10	Cable Drive Systems . . . . .	12
<b>3</b>	<b>Actuators for Running</b>	<b>15</b>
3.1	Electric Gearmotors and Inelastic Collisions . . . . .	15
3.2	Adding Series Springs . . . . .	16
3.2.1	Power Density of a Series Spring System . . . . .	17
3.2.2	Energy Efficiency of a Series Spring System . . . . .	18
3.3	Tuned Spring: Stiffness Adjustment . . . . .	19
3.3.1	Co-Contraction of Antagonistic Springs . . . . .	19
3.3.2	Adjusting Stiffness Behavior: Alternative Methods . . . . .	20
<b>4</b>	<b>The AMASC Design</b>	<b>21</b>
4.1	Mechanical Design . . . . .	22
4.2	Control System Design . . . . .	28
4.3	Simulation, Results and Comparison . . . . .	29
4.3.1	Static Compliance Characterization . . . . .	29
4.3.2	Dynamic Actuator Simulation . . . . .	35
4.3.3	Running Simulation . . . . .	37
4.4	Discussion . . . . .	40
4.4.1	SEA comparison . . . . .	40
4.4.2	The AMASC as a Manipulator . . . . .	40
<b>5</b>	<b>BiMASC</b>	<b>43</b>
5.1	Background . . . . .	48
5.1.1	Comparable Robots . . . . .	48

5.2	Philosophy . . . . .	48
5.3	Mechanical Design . . . . .	49
5.3.1	Design Choices . . . . .	50
5.3.2	Layout of Differentials . . . . .	51
5.3.3	Cables . . . . .	54
5.4	Discussion . . . . .	55
<b>6</b>	<b>The Electric Cable Differential Leg</b>	<b>59</b>
6.1	Robot Software and Simulation . . . . .	59
6.2	Robot Controller . . . . .	61
6.3	Mechanical Design . . . . .	62
6.3.1	System Notation . . . . .	62
6.3.2	Mechanical Differentials in General . . . . .	63
6.3.3	Mechanical Differential Configuration and Notation for Thumper . . . . .	65
6.3.4	Pulley Workspace . . . . .	70
6.4	Results and Discussion . . . . .	75
<b>7</b>	<b>Conclusions and Future Work</b>	<b>83</b>
7.1	Future Work . . . . .	83
7.2	Discussion . . . . .	84
7.3	Conclusions . . . . .	85
	<b>Appendices</b>	<b>87</b>
<b>A</b>	<b>Derivation of a Mechanical Differential</b>	<b>89</b>
<b>B</b>	<b>Energy Storage in Antagonistic Spring Pairs</b>	<b>93</b>
B.1	Antagonistic vs. Parallel Springs . . . . .	93
B.2	Stiffness Adjustment . . . . .	95
	<b>References</b>	<b>96</b>

# Chapter 1

## Introduction

Legged robots must be capable of running in a dynamic fashion over realistic terrain if they are to be useful in the real world. Realistic terrain varies in geometry, with rises and dips, and in dynamic properties, such as ground stiffness or damping. A legged robot should be able to hop up a flight of stairs, hop on stones across a river, and transition between hard and soft surfaces with minimal effect on its gait. It should be able to run in a grassy field where the ground surface may be soft dirt or rock, and may be lower or higher than expected. In addition, a legged robot should achieve this agility with energetic efficiency and reliability.

Current legged robots cannot achieve these goals. A number of robots meet the common definition of running, *to move swiftly on foot so that both feet leave the ground during each stride*, but this definition is not specific enough to include many of the goals of a running gait, such as stability, robustness over rough terrain, and energy efficiency. Running by the dictionary definition is not a useful goal in itself, because a gait that has an aerial phase is not necessarily good for locomotion. A robot may follow the same nominal trajectory as a human running in steady-state, but be unable to respond as effectively to an unexpected disturbance.

Running can be defined more specifically as *what animals do when they move swiftly on foot so that both feet leave the ground during each stride*. Animals are a refined mass-spring oscillatory system that store and release energy in an efficient manner throughout each stride, with high reliability and controllability. Our goal is to capture the essence of the physics and dynamics exhibited by a running animal, rather than merely mimic the trajectory. The dynamics of the center of mass of a running animal are well approximated by a mass on a spring, like a pogo stick; with the kinetic energy during flight being converted to potential energy in the leg spring during the stance phase, and back again to kinetic energy of flight. Thus, our goal for running within the framework of a mass-spring system, and an alternative definition of running, is *to move swiftly on foot so that gait energy is primarily stored in leg springs during stance*.

Most current legged robots do not have the physical capacity to meet our goal of running. They tend to use gearmotors or similar actuators, which react poorly to the rapid changes in force and velocity associated with the impacts of the foot with the ground during running. In addition, most actuators have insufficient power output to rapidly lift a robot off the ground and produce a running gait; and they certainly lack energetic efficiency when doing repeated positive and negative work to serve as virtual springs. Running is far more than a kinematic trajectory; it involves dynamic behaviors.

It is our conjecture that for a mass-spring running motion, a robot should incorporate mechanical leg springs that are tuned to the correct stiffness for the gait, speed, and running surface. Energy can be stored at each foot contact and returned with each liftoff; the springs handle much of the power required to accelerate the robot off the ground and decelerate on impact, without damping

the mechanism. Because the springs are mechanical, the response time is essentially instantaneous. The idea of a tuned mechanical leg spring has been demonstrated on some robots, which have the capacity to run in an efficient manner on a hard, flat surface [Ahmadi and Buehler, 1999, Raibert, 1986, Zeglin, 1999, 1991].

The correct leg stiffness is specific to a particular gait, speed, and ground surface, and it may be beneficial for robots to be able to actively adjust the leg spring. Animals, in contrast to robots, regularly adjust leg stiffness to compensate for changes in gait, speed, or ground stiffness [Ferris et al., 1999, Weyand et al., 2000]. Most robots do not have the ability to dynamically adjust leg stiffness, and changes in ground stiffness will affect the running gait in ways that cannot be corrected, which can lead to consequences in energy efficiency or robustness. Even for a robot that can control leg stiffness, the stiffness control strategies must still be determined. Understanding the control strategies of animal runners is difficult, because direct measurements are challenging, and it is yet more difficult to determine the reasons behind such a strategy.

With this thesis, we explore the role of leg stiffness in running gaits through literature research, simple mathematical arguments, simulation, and experimentation with prototype robotic systems. The discussion begins with the importance of physical springs for a running system. We examine control of leg stiffness in a running gait, and methods of implementing the stiffness control in a mechanical system. A benchtop prototype, the Actuator with Mechanically Adjustable Series Compliance (AMASC), demonstrates some ideas about implementation of variable stiffness. Experiments on the AMASC validate its functionality, and simulations of running robots that incorporate the AMASC behavior show successful running gaits. Based on the ideas from the AMASC, I designed and built a single leg prototype for the Biped with Mechanically Adjustable Series Compliance (BiMASC). After some initial testing, the BiMASC design was revised, and three Electric Cable Differential (ECD) Legs were constructed: one as a monopod, named Thumper, and two as a biped, named MABEL. The ECD Leg is the final revision of this thesis work, and Thumper is the primary platform for the experiments on leg compliance in running in our lab at the Robotics Institute. MABEL is installed in Professor Jessy Grizzle's laboratory at the University of Michigan, and serves as their platform for development of walking and running controllers.

This thesis is a step towards our long-term goal, which is to attain the stability, efficiency, and robustness benefits created by the physics and dynamics of a correctly designed running system. Mimicking the appearance of an animal gait is not our goal; instead we seek to understand why the gait is robust, stable, and efficient. We are not focusing on careful foot placement or navigating extreme rough terrain. We are interested in the low-level dynamic system comprised of natural dynamics and low-level software control, in the cyclical motion of running and walking, and developing stable cycles that are energetically efficient and robust to the myriad small disturbances of somewhat uneven terrain. However, it is our hope that following principles of increasing efficiency, robustness, and stability will result in control strategies and gaits that are similar to those of animals. Such a relation would be a qualitative measure that we are approaching a similar solution to presumably similar goals.

## 1.1 Contributions

This dissertation is a guide to creating mechanical systems for robot running, with three different example implementations: the AMASC, a benchtop prototype actuator, the BiMASC, an monopod prototype, and the ECD leg, built into both a successfully hopping monopod named Thumper and a successfully walking biped named MABEL. In the past, many different robots with dramatically different mechanical designs and software controllers have been designed for running, and a few

have been successful, while many have not. It is sometimes unclear what the limitations are—would a better software controller yield successful and efficient running, or are there mechanical design limitations that no software control could overcome? A mechanical system always has some inherent natural dynamics, such as motor inertia, which can interfere with software control. For the robots built as part of this thesis work, the natural dynamics are carefully considered as an important part of the design process. I have attempted to “meet in the middle” between software control and mechanical system, by creating a mathematical model that the mechanical system must match as closely as possible, and is sufficiently simple that effective software controllers can be readily designed. More generally, this thesis work explores the “grey line” between what parts of the running behavior may be exhibited through software control, and what parts are better implemented through natural dynamics.

Running generally involves some discussion of leg stiffness. Stiffness can be defined as “the resistance of an elastic body to deflection or deformation by an applied force,” and simulation of stiffness through software control of an actuator is sometimes sufficient, depending on the bandwidth of the actuator and the requirements of the application. For a running system, I have shown that physical springs are important to isolate the motor inertia from the regular ground impacts, and to cyclically store and release levels of energy at a rate that would otherwise overwhelm most actuators. Furthermore, I show through simulation and through experiment on the ECD Leg hopping robot that there is a specific, energetically optimal leg stiffness for a particular gait, ground speed, and hopping height.

The first demonstration mechanism built as part of this thesis work is the Actuator with Mechanically Adjustable Series Compliance. It is a bench-mounted prototype based on the idea that the optimal stiffness of a running gait will change as the gait or the environment changes. Through co-contraction of antagonistic springs in the AMASC, the stiffness and set point of a single joint can be configured; but unlike previous mechanisms, the AMASC can hold this stiffness with no energetic cost and freely change the set point. A mechanical differential is used to transform the deflection of two individual springs into a combined deflection, which controls the stiffness of the joint, and an opposed deflection, which applies a torque to the joint.

Other innovations on the AMASC include the pairing of energy-storing series elasticity with a cable drive. This pairing is ideal for the application of legged locomotion, combining benefits of both ideas, and avoiding a few of the limitations. A cable drive transmits high torques while weighing less than gears, eliminates backlash, has low frictional losses, and can transmit power over joints so motors can be located remotely from the actuated joints. The cable drive has a limited range of motion, which is not a problem for knee or hip joints of legged machines. As with many transmissions, cable drives are sensitive to damage caused by force spikes due to impacts, but the addition of series elasticity eliminates this problem.

The implementation of the series elasticity is a contribution in itself. The springs are mounted to the stationary base of the robot, and differentials allow them to act in series between the actuator and the end-effector. Series springs generally move back and forth with the set point of the actuator, adding their mass to that of the actuated joint; but in the AMASC, the springs are mounted to the base of the robot, stationary with respect to the motor mount. By placing the springs on the base of the robot, it is much easier to use large springs that store plenty of energy, using readily available materials.

At a higher level of system design, I discuss and demonstrate several methods of stiffness control and stiffness adjustment in this dissertation. The AMASC adjusts stiffness through co-contraction, and the BiMASC design demonstrated that the energetic cost for using antagonistic springs is high. The ECD Leg demonstrates active methods of stiffness adjustment, along with the experiments to show an optimal physical leg stiffness. Based on the experiences documented in this dissertation,

future robot designers can make better-informed choices about the implementation of spring-like behavior and the control of leg stiffness for running robots.

## Chapter 2

### Background and Related Work

Like many areas of robotics, there is a broad range of research which applies to legged locomotion. There are also many different ideas on how to approach legged locomotion. In this section we primarily discuss topics and references which are useful for the thesis research, beginning with spring-mass models of running that apply generally to running animals of any size, and to many robots, including ours. We then focus on the leg stiffness of the spring-mass model, citing work that shows a preferred leg stiffness for specific gait and environmental parameters. Moving into the realm of physical machines, we cite some previous work that implements spring-like behavior in running robots, and also some mechanisms that are capable of adjusting their stiffness. Finally, there is a brief discussion of cable drives, which form the basis for many of the machines built as part of this thesis work.

#### 2.1 The Spring-Loaded Inverted Pendulum

A simple, mathematical model for running is important for analytical treatment of a running robot or animal. Without a mathematical model of running, analyses and controllers are intuitive at best. Theory can be derived based on the simple mathematical model, and then applied to answer questions about animals or to develop controllers for SLIP-type running robots. In addition, a mathematical model provides the basis for a good simulation.

The Spring Loaded Inverted Pendulum (SLIP) model, shown in Figure 2.1 is the basis for most of the work on legged locomotion, implicitly and explicitly, both in biomechanics and robotics. It is a mass on top of a spring, which bounces like a pogo stick. The SLIP model provides a reasonable approximation to the center of mass (CoM) motion of an animal in a running gait, regardless of the number of legs, the size of the animal, or the running gait employed [Full and Farley, 2000, Blickhan and Full, 1993, Dickinson et al., 2000, Blickhan, 1989, Farley and Ferris, 1998]. Animals as diverse as ghost crabs and elephants exhibit running gaits that can be approximated by the SLIP model [Blickhan et al., 1993, Hutchinson et al., 2003]. Successful running robots also exhibit SLIP model behavior, such as the Planar Hopper, ARL Monopod II and CMU Bowleg Hopper, and most likely were designed specifically to do so [Raibert, 1986, Ahmadi and Buehler, 1999, Zeglin and Brown, 1998].

Animals as well as many running robots are far more complicated than a basic SLIP, because they may have knees, hips, nonlinear springs, and leg mass, among other discrepancies. Although all degrees of freedom are not captured in the SLIP model, the concept of templates and anchors provides a manner of reconciling the more complex model with the basic SLIP [Full and Koditschek, 1999]. A template is defined as the simpler model, in this case a SLIP, and an anchor is defined as the manner by which the complex model follows the template. For example, each joint of an animal

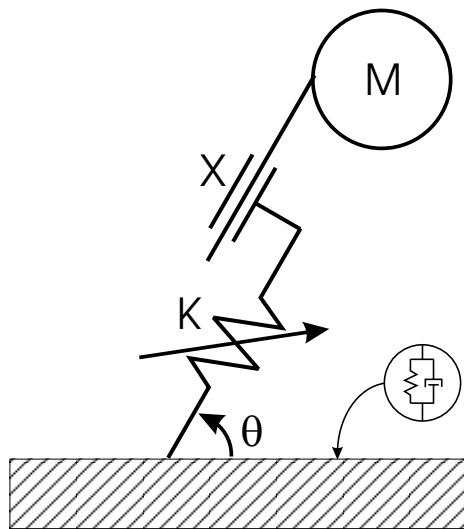


Figure 2.1: The Spring Loaded Inverted Pendulum. Prismatic joint X, variable spring stiffness K, leg angle  $\theta$ .

leg might be “anchored” to the leg length of the template (the SLIP model) by a specific function. Constraints are imposed and degrees of freedom are lost, but the templates and anchors provide a structured way to simplify a highly complex mechanism.

Even with a clear mathematical model, controlling a running robot is a relatively abstract task. Concepts such as stride length, hopping height, and forward speed are not directly linked with leg stiffness, touchdown angle, or leg length, the variables over which we have direct control. One way to simplify the control problem is to link the control inputs with the gait parameters using a forward map of the stance dynamics. A forward map can describe the state of the SLIP at the peak of the flight phase, given the state of the SLIP at the peak of the previous flight phase [Schwind, 1998]. The forward map describes the dynamics of a SLIP in response to a set of inputs; it is particularly useful for this thesis work, because the location and amount of energy stored in the spring or in the kinetic energy of the SLIP model are explicitly calculated. Schwind and Koditschek developed an approximate return map, which calculates the set of control inputs for a desired result [Schwind and Koditschek, 2000, Schwind, 1998, Schwind and Koditschek, 1995]. It is potentially useful for controller development—given a desired result, the control inputs can be calculated and implemented.

There are many gait variables, and the best stride length, hopping height, or forward speed for a given task may not be obvious. Choosing a gait that requires the minimum energy input is a good choice in most situations, assuming other requirements are met, such as gait stability. Minimum energy likely means minimum control input, in the case of a largely passive spring-mass runner. Schwind and Koditschek showed that a completely passive equilibrium gait exists for a particular SLIP, where each stance phase is identical to the last [Schwind and Koditschek, 1997a,b]. The equilibrium gait could be a good choice for a nominal running gait, and a potential trajectory for a software controller to follow. In the presence of disturbances, a software controller would be required to return the system to the equilibrium gait.

## 2.2 Tuned Leg Stiffness

In general, carefully choosing leg stiffness is important, for a variety of reasons. Leg stiffness that is too high causes energetically wasteful ground deformations, high stresses in the body, and high acceleration of sensors or other sensitive components. Leg stiffness that is too low results in a long stance time and larger deflection of the leg, possibly reaching compression limitations of the leg or hip angle limits. A long stance time is more expensive energetically, because the animal or robot must hold its weight against gravity for a longer period of time, assuming the motor is in series with the leg spring.

Tuned leg stiffness is also important for passive stability properties of legged locomotion. Seyfarth, Geyer and Gunther showed that the SLIP model becomes self-stabilized if the leg stiffness is properly adjusted and a minimum running speed is exceeded, for certain angles of attack [Seyfarth et al., 2001]. Full, Kubow, Schmitt, Holmes and Koditschek showed similar results in both computer simulation of a running cockroach and mathematical analyses; the model demonstrated passive stability in its running gait and an optimal leg spring stiffness for maximum passive stability [Full et al., 2002, Schmitt and Holmes, 2000a,b]. These mathematical and simulation case studies argue that a particular leg stiffness will maximize the passive stability of a SLIP model running gait. In contrast, this thesis work primarily addresses energetic efficiency as a function of leg stiffness; we hope that the leg stiffness for peak energetic efficiency is similar to that required for passive stability.

Previous work has established that choosing a specific leg stiffness for a specific gait is arguably useful. However, what if the desired gait changes slightly? A different forward speed, hopping

height, or stride length will change the optimal leg stiffness. Changing external conditions, such as ground properties, will also change the optimal leg stiffness.

## 2.3 Using Leg Stiffness for Gait Control

Although adjustable leg stiffness is generally not implemented on running robots, prior theoretical and biomechanical work indicates that varying the leg stiffness is one good method for controlling a running gait. Only three terms are required to describe a cyclic running gait based on the SLIP model, and leg stiffness affects one or more of the three terms [Schwind and Koditschek, 1997a]. Hodgins and Raibert used the planar biped to experimentally demonstrate control of foot placement using leg stiffness, as well as hopping height and forward velocity [Hodgins and Raibert, 1991]. To our knowledge, this is the sole example of robotic leg stiffness control in a running gait.

Evidence suggests that many animals vary leg stiffness to control their running gait and alter their center of mass motion, within the constraints of the SLIP model. Researchers have sought to better understand the role of compliance control in animal running through experiments limiting one parameter of the SLIP model. By restricting obvious control methods (such as touchdown angle), more obscure methods (such as leg stiffness) can be observed. Ferris and Farley restricted humans to hopping in place, removing leg touchdown angle as a control variable. When subjects were tested at constant ground stiffness but instructed to alter hopping frequency, subjects adjusted leg spring stiffness [Full and Farley, 2000]. Another experiment forced runners to run at stride frequencies higher and lower than normal for a given running speed, thus artificially restricting hip angle, again observing that runners adjust leg stiffness [Farley and Gonzalez, 1996].

As an empirical observation of the effects of static leg stiffness, I visited the National Aviary in Pittsburgh, and watched a number of flightless birds walking and running. Because they have very long legs with long tendons, it is unlikely that they are able to significantly change leg stiffness. As the bird walked, I chased it. To initiate a running gait, it first hopped rather high, and when running at a slow speed, maintained a very high (and presumably inefficient) hopping height. As it ran faster, the hopping height was reduced in what appeared to be an approximately inversely proportional relationship with forward speed. This observation would agree with the predictions of a SLIP model with invariant leg stiffness; hopping height and forward speed would have an inversely proportional relationship.

Another similar observation involves the hexapod RHex. There are a number of different gaits available, and it has been shown that RHex exhibits SLIP-like behavior [Altendorfer et al., 2002]. Each of RHex's six legs has a single degree of freedom at the hip; thus the SLIP model is restricted to only hip angle control, and cannot vary spring set point or spring stiffness. As RHex runs at faster and faster speeds, the body sinks closer and closer to the ground, until at the highest speed, the legs are deflecting a very significant amount and the body nearly touches the ground. The hopping height is lower at higher running speeds, and cannot be changed unless the legs are replaced; a specific running speed appears to correspond to a specific hopping height.

Common wisdom in the athletic running community is that faster running is achieved by increasing stride length, increasing stride frequency (likely achieved by increasing leg stiffness), or both [Joyner et al., 1999]. Most biomechanics publications make the claim that animals prefer to change speed by changing stride length (perhaps by controlling hip angle at touchdown), while leg stiffness remains constant [Full and Farley, 2000, McMahan and Cheng, 1990, Farley et al., 1993b, Full and Tu, 1991, Farley et al., 1993a]. A few others claim that step length changes little with speed for normal running on a hard surface, implying stiffness control of the leg [McMahan, 1985]. Another study shows that faster speeds result from higher ground reaction forces rather than stride

frequency, also implying stiffness control [Weyand et al., 2000]. The discrepancy may arise from testing at different running speeds; most experiments involve running at low to moderate speeds, where runners seem to prefer a stride length change over a leg stiffness change. Only in experiments with high-speed running do subjects maintain a relatively consistent stride length over a range of speeds. In personal conversations, Bob Full, Dan Ferris, and Claire Farley have agreed that animals probably use leg stiffness for speed control at higher speeds. In general, lower speeds and slower stride frequencies result from lower leg stiffness, while higher speeds and stride frequencies result from higher leg stiffness.

The top speed of animal running may even be limited by the maximum achievable leg stiffness. A study of robotic running claimed that for a given leg length, running speed is largely limited by leg stiffness [Koechling, 1989]. Two studies on human running have shown that human sprinters exhibit very high leg stiffness compared to standard running [Chelly and Denis, 2001, Kuitunen et al., 2002]. Exhibiting high leg stiffness is energetically expensive for animal runners, so it is understandable that they do it only for the highest-energy running gaits. However, this limitation does not necessarily exist for robotic runners, so control of leg stiffness may or may not be more useful for robots than it is for animals.

## 2.4 Using Leg Stiffness for Disturbance Rejection

Discussion has thus far focused on control of a running gait on flat, hard floors, but leg stiffness control is also useful when running over terrain with varying stiffness. Analysis of the SLIP model shows that without leg stiffness control, the center of mass displacement and ground contact time will change, affecting the gait significantly. The gait change may not cause the runner to fall, but it would slow down or speed up the forward speed, or change the hopping height, or change the stride length. There would be a reduction in efficiency, because the leg spring would no longer be tuned to the ideal stiffness. This effect is observed indirectly in humans and other animals, who control leg stiffness when ground surfaces change. For example, Full, Farley, and Ferris showed that humans hopping in place will adjust leg stiffness to maintain constant global stiffness in response to changes in surface stiffness at a given hopping frequency [Full and Farley, 2000, Ferris and Farley, 1997]. During unrestricted running over varying terrain, human runners compensate for ground surface changes by varying leg stiffness, and maintain a relatively consistent center of mass motion [Ferris et al., 1999, Farley et al., 1998, Ferris et al., 1998, Kerdok et al., 2002].

Maintaining a constant center of mass motion is beneficial, despite the fact that changing leg stiffness costs energy. Hopping higher than necessary requires more energy storage in the leg, leading to higher spring restitution losses. Hopping high also increases flight time, allowing trajectory errors to build. Alternatively, hopping too low increases the risk of hitting obstacles and requires faster leg swing recoveries, which may require high power at the hip. Although these reasons are largely speculative, animals do control leg stiffness to maintain a consistent center of mass motion, indicating some benefit.

The importance of leg stiffness adjustment changes with animal scale, and leg stiffness may or may not be important for small robots [Heglund and Taylor, 1988]. As animals scale in size, their dynamic properties and gaits change as well; larger animals take slower strides and have stiffer legs. The ground stiffness, of course, does not change with animal size; thus, the relative stiffness between the animal leg and the ground is dramatically different for runners of different size. Most ground surfaces are much stiffer than a mouse's legs, but are relatively softer than a horse's leg spring. A 50% change in ground stiffness may require a 50% change in leg stiffness from a horse to maintain a constant global stiffness, but only 1% change in leg stiffness from a mouse. Because

the mouse's leg compliance dominates the dynamics of the gait, the ground can more easily be approximated as a rigid surface.

## 2.5 Creating Spring-Like Behavior

Thus far, I have discussed literature establishing that leg stiffness is one method of control for disturbance rejection and gait change, and that animals use this method. However, creating a robotic mechanism that can correctly exhibit the desired behavior is a challenge. Animals have different mechanical limitations than robots, but still provide a useful example; they create spring-like behavior by using tendons as internal physical springs, storing and returning energy with each stride [Cavagna, 1970, Cavagna et al., 1977, Alexander, 1990].

Storing and returning energy using tuned physical springs dramatically reduces the overall energy consumption for a runner. In addition, using springs(tendons) in series with motors (muscles) allows animals to minimize the power output of their muscles [Roberts, 2002]. The muscles move little during the highest forces in the middle of stance, allowing the tendons do most of the work [Roberts et al., 1997]. Similarly, animals can maximize their power output while jumping by tuning the muscles to an optimal stiffness [Arampatzis et al., 2001, Seyfarth et al., 2000].

Properly tuned physical springs not only improve efficiency and reduce power requirements of a legged system, but they can also create passive stability [Full et al., 2002]. Animals sometimes use a timed, pre-planned trajectory in conjunction with the natural dynamics of the system to create desirable passive stability characteristics - often referred to as "preflexes" [Kubow and Full, 1999, Horita et al., 2002]. Although some muscle activation is required, the dynamic response is not controlled by any neural feedback, differentiating preflexes from stretch reflexes [Duncan and McDonagh, 2000].

Robotics researchers are far from understanding how to implement the natural dynamics and real-object interaction demonstrated by biology. There is a body of research in force control, which is somewhat applicable to legged locomotion, because springs can be compared to a force-control system where the force is proportional to the displacement. Some research in force control suggests that passive springs are an important part of the mechanism [Pratt and Williamson, 1995, Robinson et al., 1999, Robinson, 2000]. Certainly, standard actuation methods have physical limitations on impedance and bandwidth response for force control, suggesting that some non-standard mechanical designs are needed [Eppinger and Seering, 1987, Lawrence, 1989]. For a force-control system to have a reasonable execution speed and disturbance rejection, it has been shown that there should be at least as much compliance in the mechanism as there is in the software controller [Schutter, 1987]. Thus, even if energy efficiency in running is not a concern, physical springs are still a good idea.

## 2.6 SLIP model running robots

Many robots have been built that exhibit SLIP-like behavior. They all utilize mechanical springs of some sort; either air springs in the Raibert hoppers, a steel coil spring in the ARL Monopods and Uniroo, or fiberglass springs in the CMU Bowleg hoppers and in RHex [Raibert, 1986, Gregorio et al., 1997, Rad et al., 1993, Ahmadi and Buehler, 1999, 1995, Zeglin, 1991, Zeglin and Brown, 2002, Zeglin, 1999, Zeglin and Brown, 1998, Altendorfer et al., 2002]. Energy is stored and released with each stride, much like animals use tendons as springs in series with muscles. These robots, most notably the ARL Monopod II and the CMU Bowleg, are very energetically efficient compared

to non-SLIP legged robots. The ARL Monopod II is a good example of the use of natural dynamics in the mechanical design; it can take several hops with all power turned off.

Most current running robots have manually tuned leg stiffness, and are not capable of varying leg stiffness on the fly. However, these robots are generally not subject to changes in ground stiffness; therefore, leg stiffness adjustment is not necessary for disturbance rejection. Many values of leg stiffness will result in successful (though not optimal) running, so a robot with no leg stiffness adjustment can still control its forward speed, hopping height, or stride length, though not all independently [Raibert, 1986]. RHex is an outdoor robot, and does encounter ground stiffness changes on a regular basis. It is extremely capable over a variety of terrain, but some tuned gaits work noticeably better on specific surfaces. For example, the high-speed running gait is relatively smooth and fast on pavement, but a transition to softer grass can cause the robot to start bouncing out of control, requiring the driver to switch to a more robust (and slower) gait.

There are several key differences between the work of Hodgins and Raibert and this thesis work. Most importantly, the focus of this thesis is on the energy consumption of a particular stride length and leg stiffness rather than the effective control of a particular gait parameter. For the implementation of leg stiffness, the planar hopper used a pressurized single-sided air cylinder. Because the cylinder had air pressure on only one side, there was a significant pre-load to the leg spring, which changed with the value of the initial air pressure. Thumper uses fiberglass springs in series with an electric motor, which can be replaced between experiments, and do not affect other aspects of the robot dynamics. The effects of this difference on the dynamics of the robot are difficult to predict, but Thumper's leg springs are more similar to a basic SLIP model.

## 2.7 Other Robots

Most legged robots do not incorporate mechanical springs tuned for a SLIP model running gait, instead relying on rigid gearmotors, in the hope that all necessary dynamics can be exhibited through software control. BIP2000, Johnnie, Rabbit, H6, Asimo, and QRIO are all examples of rigid gearmotor robots [Sardain et al., 1998, Gienger et al., 2001, Chevallereau et al., 2003, Nishiwaki et al., 2000, Nagasaka et al., 2004]. Some of these robots are intended for running, and some of them are successful in achieving a brief aerial phase. However, none exhibit SLIP-like behavior, and they are all far more energy-consumptive than a robot with passive springs such as the ARL Monopod II. QRIO and Rabbit are capable of an aerial phase in which both feet are off the ground, but it is short relative to the rest of the gait, and the robots do not store gait energy internally as in a traditional running gait [Chevallereau and Aoustin, 2001, Chevallereau et al., 2008].

Spring Flamingo and M2 are both bipedal robots based on the MIT Series Elastic Actuator [Paluska, 2000, Pratt and Williamson, 1995, Robinson, 2000, Robinson et al., 1999]. The actuator was designed for improved force control, and utilizes small, stiff springs in series with a motor and transmission to reduce force spikes during an impact. The springs are not used for energy storage, but do improve force control in the presence of impacts. Spring Flamingo succeeded in planar walking both with bird-like knees and with forward knees and kneecaps [Pratt and Pratt, 1998].

An important point to be made is that adding compliance is useful only when properly designed, and is a hindrance if mistuned to the wrong stiffness. For example, researchers at Waseda University built a biped with antagonistic compliant joints [Yamaguchi and Takanishi, 1997]. The joints were built with variable compliance to mimic the joints of a human, rather than to implement principles of locomotion. The robot walked much more slowly and tentatively than a comparable rigidly-actuated robot, presumably because the compliance was not tuned for a specific task, and thus the

compliance became a hindrance rather than a help. It is possible that the series springs on M2 also hindered its operation, by causing uncontrolled oscillations in many of the robot joints immediately following a ground impact.

## 2.8 Variable Compliance Mechanisms

The design and implementation of a mechanism with variable stiffness is a challenge. Several variable compliance mechanisms have been developed, some for manufacturing or manipulation tasks involving constrained contact or impacts, which benefit from the high bandwidth of passive dynamics [Laurin-Kovitz et al., 1991, Nahar and Sugar, 2003, Morita and Sugano, 1995, Bicchi et al., 2003, Bicci and Tonietti, 2004].

Most of these mechanisms rely on two antagonistic motors, co-contracting nonlinear springs to change the stiffness of a driven joint. As in animals, this co-contraction uses energy, because the motors must apply force to compress the springs. Some mechanisms use a leaf spring which is shortened or lengthened to adjust the stiffness, which avoids the energy inefficiency of antagonistic motors. One drawback to these mechanisms is that they offer very little energy storage. The springs are small, and while they do offer changes in stiffness, a legged locomotion application would saturate the springs.

Air cylinders such as those used on the Planar Biped have plenty of energy storage for a running gait [Hodgins and Raibert, 1991]. The main drawbacks to using air springs are energy inefficiency, with losses due to seal friction and air compression hysteresis, and also inelastic collisions with hard stops on both touchdown and liftoff. The Planar Biped's air cylinders are pre-loaded springs, so there is an additional energy loss on touchdown when the force must rise to the pre-load value. In addition, powering the robot with air pressure requires that the robot carry a large air compressor, or be tethered. For all of these mechanism types, including air springs, the stiffness function cannot be adjusted or controlled. It is part of the physics of the spring design, and is likely to be difficult to model. This limitation is a disadvantage when engineering the dynamics of a mechanism; analogous to disallowing the choice of joint positions when engineering a kinematic mechanism. A designer-specified spring function is more desirable for a mass-spring system.

## 2.9 Variable Compliance Outside of Legged Locomotion

Variable compliance is potentially useful any time a robot or animal interacts dynamically with the world. This interaction includes manipulation tasks as well as legged locomotion. Variable compliance has been implemented in robot arms as a method of maximizing performance while ensuring safety during human interaction. The stiffness is adjusted to be high at low speeds, allowing for high positional accuracy, and low at high speeds, resulting in a softer impact [Bicchi et al., 2003, Bicci and Tonietti, 2004].

Biomechanics studies have shown that humans vary arm stiffness during reaching motions, an indication that control of variable compliance may be important for robot arms as well [Bennett, 1992].

## 2.10 Cable Drive Systems

Most of this thesis work utilizes steel cables rather than gears or belts for power transmission. While cable drives have been in use for some time in high-precision devices such as telescopes, which

require zero backlash, they are not as commonly used as more standard gearmotors or hydraulic systems. For most applications, the cable drive is too complex to implement (because no commercial cable drive transmissions are sold), takes too much space, and has too much stretch to be useful for most position-controlled devices. However, Townsend showed that a high-speed cable drive, where the speed reduction is near the end-effector, can increase the stiffness of the transmission by a factor of 100. The efficiency of the drive can be very high, approaching 96%, because most of the contact is pure rolling contact, like a ball bearing. Energy losses are caused by localized stretching of the cable as it wraps around a pulley, while under load [Townsend, 1988]. Townsend also invented the cable differential, which is used on the Barrett WAM Arm to transmit power from two parallel motors to perpendicular degrees of freedom [www.barrett.com].

Cable drives are most commonly used in haptic devices, because the high efficiency allows for good transmission of torque from the motor rotor to the end-effector, and because the regular change in force from positive to negative necessitates zero backlash for good haptic performance. The Phantom haptic devices from SensAble Technologies are among the most popular cable-drive haptic devices [www.sensable.com].



## Chapter 3

### Actuators for Running

While a general-purpose actuator would provide ideal flexibility for software controller development on a running robot, all actuators have natural dynamics that can limit the authority of the software controller. Therefore, the best approach is to begin the robot design with a specification for the dynamic behavior of the machine. In other words, many aspects of the control should be designed before any mechanical system is created, so the natural dynamics of the actuator can assist and enable the behavior of the machine rather than imposing limitations.

While several successful running and walking machines have used pneumatic and hydraulic power, many designers opt for the simplicity and robustness of electric motors. Pneumatics have limitations on the control rate, due to small tubes, valves, and limitations on the power supply, especially for untethered machines. We do not discuss details of pneumatic actuators. Hydraulic actuators have similar limitations to electric gearmotors in their bandwidth, their energy inefficiency in cyclic motion, and their power output. They differ from electric motors in that they can hold their position against a force with no work expenditure, but they burn the same amount of energy when moving at a given rate whether or not they apply force. In addition, they tend to leak oil, and require more support machinery such as a hydraulic pump and accumulator. Hydraulic actuators may be appropriate for a running robot, and most of the discussion in this chapter can be applied to hydraulic actuators. However, we primarily discuss electric motors because of the dynamic simplicity and relevance to robot designs.

#### 3.1 Electric Gearmotors and Inelastic Collisions

A simple design for a legged robot would utilize an electric gearmotor at each joint. To apply appropriate torques at the joints with sufficiently low-mass actuators, large gear reductions are required, sometimes as high as 100 : 1. Several groups have built bipedal robots using this design, and some intended to make the robots run as well as walk. The problem with this approach to running is that most of the kinetic and potential gait energy is lost with each hop to an inelastic collision with the ground, and in addition, the forces of impact increase the potential for damage to the mechanism.

A spring-free, gearmotor-actuated running robot is represented in Figure 3.1(a). Because there is no physical spring, all behavior of the leg must be exhibited by the software through the motor. The entire mass of the robot (including the mass of the motor) is represented by  $M$ , and the leg is assumed to be massless. However, the rotational inertia of the motor cannot be lumped into the overall mass of the robot; it is represented by the variable  $I$ , and after the rotational inertia of the motor is converted to linear inertia by the conversion ratio  $r$ , the overall reflected inertia at the joint of the robot is  $\frac{I}{r^2}$ . For a typical harmonic-drive gearmotor on a humanoid robot with  $r = 0.01$ , the resulting reflected motor inertia can approach that of the robot mass,  $M$ .

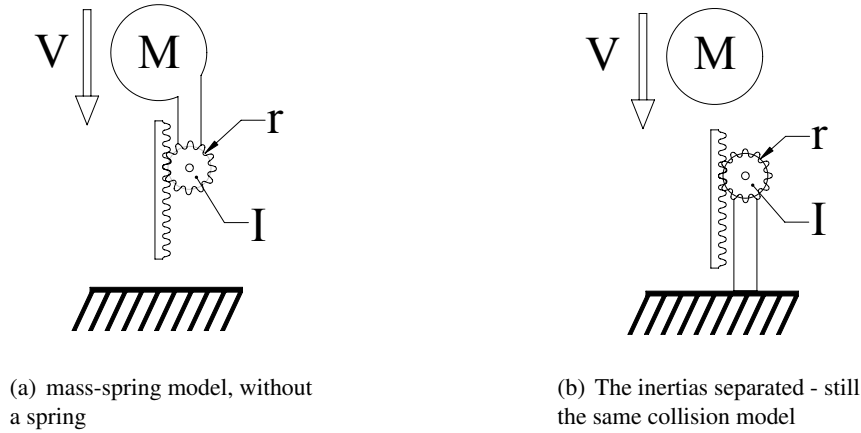


Figure 3.1: Figures representing the mass-spring model, with the physical spring removed. The inertia of the motor is represented by  $I$ , the mass of the robot by  $M$ , the conversion from motor angular velocity to linear velocity by a fictional pulley radius  $r$ , and the velocity of the robot just before collision by  $V$ .

Because the rotor inertia and the robot mass are uncoupled, the robot leg may be moved to the ground without affecting the model, as shown in Figure 3.1(b). The rotor begins at rest, and after collision, has some speed that matches that of the mass. If the kinetic energy just prior to impact is represented as  $T_0$ , the rotor inertia is represented as  $I$ , the conversion from rotational to linear motion is represented by a fictional pulley radius  $r$ , and  $M$  is the robot's total mass, then the energy lost to an impact is

$$T_{loss} = \frac{I}{Mr^2 + I} T_0 \quad (3.1)$$

$$(3.2)$$

and the remaining energy, stored in the downward motion of the robot and the rotation of the motor, is

$$T_{final} = \frac{Mr^2}{Mr^2 + I} T_0. \quad (3.3)$$

$$(3.4)$$

If the effective inertia of the motor rotor ( $\frac{I}{r^2}$ ) is the same as the robot's mass, then half the kinetic energy from flight will be lost to the inelastic collision. Even after the collision, any remaining energy must be converted through the motor and transmission inefficiencies, which are compounded when energy must pass into the system and then out. In effect, very little energy can be recovered. Most will be lost instantly during collision, much of the rest to motor inefficiencies.

### 3.2 Adding Series Springs

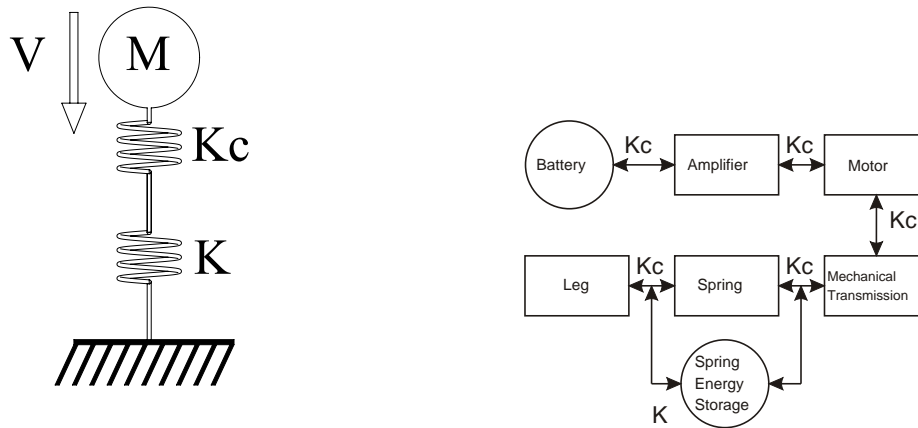
Minimizing the reflected inertia of the motor can reduce the energy lost to inelastic collisions, but in practice, it is difficult to create a motor with low reflected inertia and the high torque required

for running. A series spring can also be used to decouple the motor inertia and the load inertia, eliminating the inelastic collision and associated energy loss during impacts. Both methods are used in force-control applications [Townsend and Salisbury, 1989, Kanade and Schmitz, 1985, Schutter, 1987, Pratt and Williamson, 1995], which are similar in many ways to the implementation of a desired spring stiffness.

A series-elastic actuator may be much more effective than a standard gearmotor at creating spring-like behavior, even when the physical spring is a different stiffness than that of the desired behavior. In this case, the software must control the motor so the overall system exhibits the desired total spring rate. In the best-case scenario of an inertia-free rotor, a proportional controller will behave like a spring, creating two springs in series - a software spring and a physical spring, as shown in Figure 3.2(a). This simplification is relatively straightforward to analyze, and provides a conservative estimate of energy use and power output due to the assumption of no inertia. Therefore, further analysis will assume perfect force control of a massless rotor, providing an ideal software spring in series with a physical spring.

### 3.2.1 Power Density of a Series Spring System

In a cyclical system such as a hopping spring-mass system, energy is transferred from external sources (kinetic energy of motion, potential energy of height) to internal sources (physical spring energy or chemical battery energy) and vice-versa, once per step. This transfer of energy is represented in Figure 3.2(b), where the energy may go into and out of the physical spring as an energy storage element (compression and extension), or through the physical spring as merely a power-transmission element (the spring translating, with no deflection). The power output will be divided between the software spring and the physical spring, depending on their stiffnesses.



(a) Our spring-mass model, with software spring rate  $K_c$  and hardware spring rate  $K$

(b) Energy flow diagram;  $K_c$  represents the energy path of stiffness behavior implemented through software control,  $K$  represents the mechanical spring stiffness.

Figure 3.2: Assuming an inertia-free actuator, the software controller can simulate a spring  $K_c$ . Acting in series with the physical spring  $K$ , the energy will flow into one or the other depending on the ratio of the stiffnesses.

If the series spring system is deflecting at some rate, the power output attributed to the software spring,  $P_{K_c}$ , is

$$P_{K_c} = \frac{K}{K_c + K} P(t), \quad (3.5)$$

where  $P(t)$  is the total power output of both springs in series,  $K_c$  is the proportional gain of the computer controller, and  $K$  is the physical spring constant. If the physical spring is perfectly tuned to match the desired stiffness, the software spring  $K_c$  becomes infinitely stiff, and it can be seen from equation 3.5 that the motor (exhibiting the rigid software spring) exerts zero shaft power.

Because springs have higher power density than electric motors, it makes sense to design a system such that the physical spring transfers as high a proportion of the power as possible. A physical spring can have nearly infinite power density, depending on its stiffness; therefore, a comparison between the power density of a spring and that of a motor must be made in the context of an application. Choosing reasonable values for a hopping robot of leg stiffness  $K = 5000 \text{ N/m}$ , hopping height of  $h = 0.25 \text{ m}$ , and robot mass of  $m = 30 \text{ kg}$ , the highest power output during stance is approximately 1 kW (RMS power is 680 W) and the maximum work stored is about 75 J. With an efficient fiberglass spring, such as those used on archery bows which have energy capacity around 1000 J/kg, a 75 g spring can store the required energy and output the desired power. In contrast, a brushless motor that can output 600 W of continuous power (such as the Emoteq Quantum series 3401, from [www.emoteq.com](http://www.emoteq.com)) weighs approximately 2.2 kg, almost 30 times the mass of the spring. Adding the necessary electronics and batteries would add to the mass considerably.

Based on this analysis, it is clear that, even ignoring the inertia of the rotor and the inefficiencies of the motor, a spring has much higher power density than an electric motor in a cyclic system. This effect has been noticed in the biomechanics community, where experiments have shown that animals use their springy tendons to amplify the power output of their muscles for jumping and running [Roberts, 2002, Seyfarth et al., 2000].

### 3.2.2 Energy Efficiency of a Series Spring System

Although avoiding inelastic collisions and reducing power requirements are compelling reasons to use physical springs, energetic efficiency of a cyclic system is also improved through the use of tuned physical springs. Again referring to Figure 3.2(b), energy can be stored and returned through the mechanical spring or through the batteries, which must first convert the mechanical energy to electrical, electrical to chemical, and back again. Assuming an overall efficiency of the spring energy storage  $e_k$  and an overall efficiency of energy storage through the motors and batteries of  $e_c$ , and given previous assumptions of a perfect software spring  $K_c$  and an inertia-free rotor, spring constant  $K$ , and leg deflection  $x$ , the equation for energy returned is

$$E_{ret} = \frac{K_c}{2(K + K_c)} K x^2 e_k + \frac{K}{2(K + K_c)} K_c x^2 e_c. \quad (3.6)$$

Because springs can store and return energy more efficiently than an electric motor system, it makes sense for the physical spring stiffness to be as close to the desired spring stiffness as possible. If our assumption of zero rotor inertia is false (and for any real system, it is), then the motor must transmit power to change the momentum of the rotor, and it will expend (and lose) more energy than in this idealized example.

### 3.3 Tuned Spring: Stiffness Adjustment

For an oscillating mass-spring system, like a running machine, matching the natural frequency of the mechanical system to the desired stride frequency will minimize the required motor power. In other words, a robot or animal of a particular size may have an optimal leg stiffness to minimize the amount of effort required to run. However, the optimal leg stiffness will change as the desired gait changes or as the environment changes. Observations from nature tell us that animals do adjust their leg stiffness in various situations [Full and Farley, 2000, McMahon and Cheng, 1990, Farley et al., 1998], but we do not have a conclusive answer as to what determines the optimal stiffness, the specific strategy they use to adjust to it, or how they make the adjustment.

There are a variety of ways to implement stiffness behavior in robotic systems, and a variety of ways to adjust the stiffness on the fly. The most common approach is to simulate spring behavior using an actuator and a feedback sensor, such as an electric motor or hydraulic actuator with a force sensor. As discussed, this method has drawbacks with bandwidth limitations, power limitations, and energy efficiency for realistic actuators. In the absence of a perfect actuator free of all dynamics or limitations, the best way to create spring-like behavior is to use a physical spring in some way.

When designing an actuator that incorporates physical springs, there are several ways to adjust, or tune, the spring stiffness to suit a particular task. There are a range of mechanical solutions, which use linkages, transmissions, or clutches to adjust stiffness. Co-contraction of antagonistic springs is a biologically-inspired approach, and the basis for the AMASC and BiMASC designs. After extensive experimentation, we found this method of stiffness adjustment to have significant drawbacks for running gaits. More promising for this particular application is a hybrid active-passive approach, where a physical spring is tuned for the standard running gait, and a series motor actively adjusts the spring forces for gait changes or other non-standard behaviors.

#### 3.3.1 Co-Contraction of Antagonistic Springs

A popular method of stiffness adjustment is co-contraction of antagonistic springs. Animals have this capability, and most robotic devices with variable stiffness use this method. With two springs opposed across a single joint, the deflection of the joint,  $x$ , stretches one spring while relaxing the other. Co-contraction of the springs,  $p$ , stretches both springs. For linear springs, the force on each spring is

$$F_1 = K(p + x) \quad (3.7)$$

$$F_2 = K(p - x) \quad (3.8)$$

and the combined force on the joint is

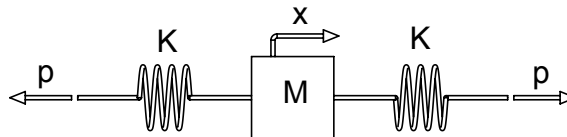


Figure 3.3: Two opposing springs in co-contraction across a single linear joint. Spring constant  $K$ , joint deflection  $x$ , joint load mass  $M$ , and co-contraction  $p$ . The co-contraction is always larger than the joint deflection, such that the springs are always in tension.

$$F_1 - F_2 = 2Kx. \quad (3.9)$$

Thus, the co-contraction  $p$  has no effect; the force  $F$  is a function of the spring constant  $K$  and the combined deflection of the two springs. For the co-contraction to affect the joint stiffness, the springs must be nonlinear. For the mathematically convenient example of a quadratic spring,  $F_1 = K(p + x)^2$  and  $F_2 = K(p - x)^2$ , the combined force on the joint is

$$F = F_1 - F_2 = 4Kpx, \quad (3.10)$$

where the co-contraction can be considered as part of the spring constant that determines the resultant forces of a joint deflection  $x$ .

The obvious drawback for co-contraction is that two actuators are required for a single joint, and they must apply forces to hold a particular stiffness even if no work is done by the joint. This drawback can be minimized by using non-backdriveable transmissions, mechanical differentials, brakes, and other mechanisms, such that joint work can be done by a large motor, and stiffness adjustment may be accomplished by a small motor with a holding brake. We implement several such ideas in our first prototype actuation system, the Actuator with Mechanically Adjustable Series Compliance, or AMASC, discussed in Chapter 4.

### 3.3.2 Adjusting Stiffness Behavior: Alternative Methods

Aside from co-contraction of antagonistic springs, the stiffness of a single spring can be adjusted by varying its effective length through some mechanical means. For example, a torsion bar can have a rigid base that rolls up and down the length, immobilizing a variable portion of the spring. A helical spring could have a rigid base that threads up and down the spring, immobilizing more or less of the coil. Or, many springs in parallel can be clutched in and out of the system.

Because “stiffness” is essentially a force profile with energy storage, a continually variable transmission (CVT) in series with a spring would be ideal; the forces could be changed arbitrarily for a particular energy transfer. The knee joint in a robot or animal leg can act as a constrained CVT, because the angle of the knee affects the mechanical advantage between the toe forces and the spring deflection. In effect, different knee angles can modify the force profile of the spring. It is not an ideal CVT, because the mechanical advantage cannot be changed arbitrarily, but mechanisms such as a knee can potentially be used to the advantage of a running gait or other dynamic behavior.

In many cases, the stiffness behavior of an actuator with series springs can be modified through active software control. In the example of a spring-mass running robot with a spring and motor in series, the spring undergoes a predictable trajectory based on the body mass and the leg stiffness, so a pre-planned motor trajectory or other simple controller can be used to modify the overall leg stiffness. In the instant after an unexpected impact, only the passive behavior of the spring will contribute to the toe force, because the inertia of the motor prevents instantaneous acceleration. After the motor begins to accelerate and move, either relaxing or compressing the spring, it can add or remove energy and modify the force profile of the spring, effectively altering its stiffness. The force profile will not be a perfect simulation of a spring, due to the inertia of the motor, but this issue may be of little consequence; it is certainly less problematic than the inelastic collision that exists with no physical spring in series with the motor. More importantly, any change in the natural spring profile will result in wasted energy by the gearmotor, so this is a tradeoff to consider.

## Chapter 4

### The AMASC Design

The Actuator with Mechanically Adjustable Series Compliance (AMASC), shown in Figure 4.1, was developed specifically for the purpose of actuating a running robot. It actuates a single degree of freedom, with a large spring in series between the electric motor and the output of the device. The spring is sized to store the energy of a running gait, so the robot may bounce on the spring much like a rider on a pogo stick, or like any animal in a regular running gait. The spring stiffness is mechanically adjustable; therefore, leg stiffness can be tuned for a particular gait or ground surface.

The AMASC is an integrated mechanism and software controller, with mechanical design choices made to closely match a simple mechanical model. The software controller is based on the same simple mechanical model, safely ignoring most of the complexities of the actual mechanism. This model is illustrated in Figure 4.2, in two different forms: one rotational, one linear.

The rotational model is physically similar to the prototype AMASC, while the linear model is a simpler form that still captures the important properties of the system. In both models, the dynamics of the system controlling the pretension,  $x_3$ , are ignored. The pretension is entirely unrepresented

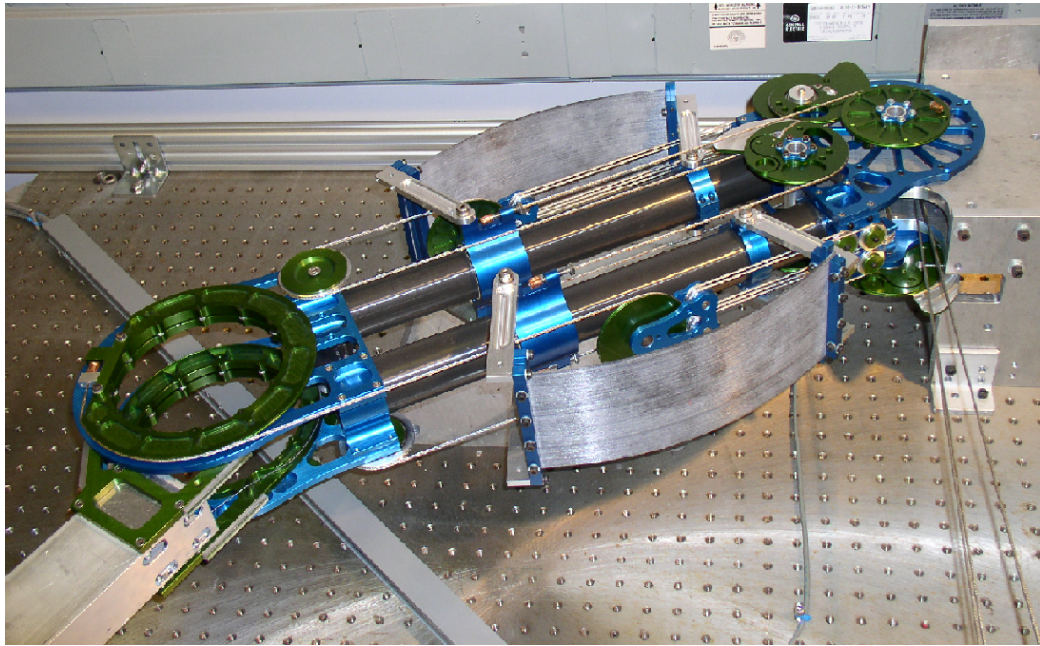


Figure 4.1: The Actuator with Mechanically Adjustable Series Compliance, or AMASC, is a prototype leg joint for a running robot.

in the linear model, and the spring stiffness,  $K_{eff}$ , is assumed to simply be a programmable value. Throughout the remainder of this chapter we will use the notational conventions of Table 4.1.

The AMASC is essentially a single compliant joint, most closely resembling a knee, endowed with engineered natural dynamics. There are two degrees of freedom, and two corresponding motors. One motor controls the spring pretension. As shown in Figure 4.2(a), there are two identical opposing springs, much like antagonistic muscles in animals. The pretension,  $x_3$ , stretches both springs, which is analogous to muscle co-contraction in animals. The knee joint does not move, but its rotational stiffness increases with the pretension, allowing the actuator to tune the stiffness aspect of its natural dynamics. The other motor controls the spring rest position ( $\theta_1$  in Figure 4.2(a) and  $x_1$  in Figure 4.2(b)), which is used as the primary energy source and controls any motions not described by the system's natural dynamics. These two motor-controlled parameters, along with the leg angle at touchdown, are the parameters necessary to control SLIP model running.

## 4.1 Mechanical Design

Many of the mechanism design challenges are common ones; for example, minimizing friction, backlash, mass, and inertia. Several specific choices were made that influence each of these attributes, such as the location and type of speed reduction, choice of materials, and type of motor. Minimizing mass was a concern throughout the design process, because the AMASC was intended as a prototype leg for a bipedal robot with approximately 1 meter leg length and 30kg total mass. Of this 30kg, 20kg are reserved for motors, batteries, and computing. This allotment leaves only 10kg for the entire framework and mechanism, including springs and power transmission. To minimize weight, all joints contain thin-section bearings, which are very light for a given load rating. All parts are machined aluminum, with the main structural members (analogous to the femur) made of thin-wall aluminum tube. The mass of this actuator prototype is approximately 4kg, and it is nearly 50% oversized.

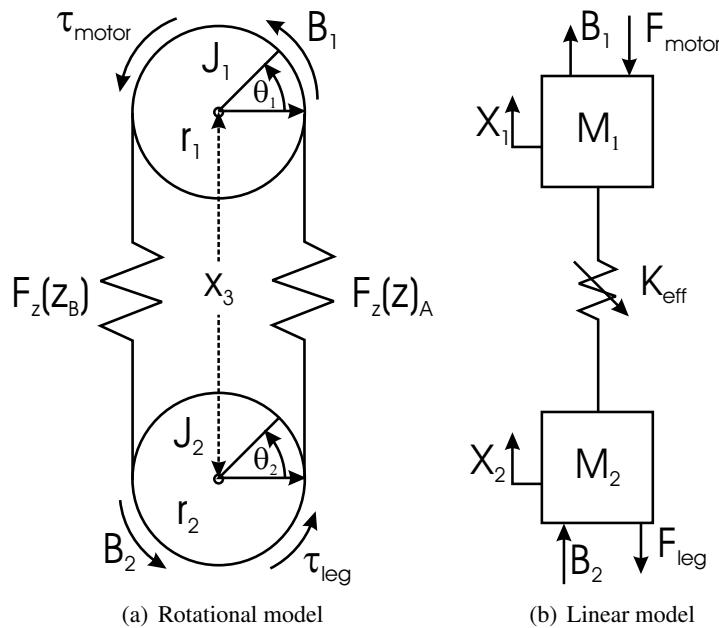


Figure 4.2: Mechanical models of the physical actuator.

variable	description
$\theta_1$	Motor position (rad)
$\theta_2$	Leg position (rad)
$r_1$	Effective radius of motor pulley (m)
$r_2$	Effective radius of end effector pulley (m)
$x_1$	$\theta_1 \cdot r_1$ , Motor position in cable length (m)
$x_2$	$\theta_2 \cdot r_2$ , Leg position in cable length (m)
$J_1$	Motor inertia ( $kg \cdot m^2$ )
$J_2$	Leg inertia ( $kg \cdot m^2$ )
$x_3$	Pretension (m)
$\Delta x$	Linear leg deflection, $\theta_2 r_2 - \theta_1 r_1$ (m)
$z$	Deflection of the cable after the pulley function: ( $x_3 + \Delta x$ ) or ( $x_3 - \Delta x$ ) (m)
$F_{eff}(x_3, \Delta x)$	Knee force, $\tau_{eff}/r_2$ (N)
$G(z)$	Spiral pulleys; spring position as a function of $z$ (m)
$y$	Deflection of the spring, before the pulleys (m)
$F_y(y)$	Force function of the spring
$F_z(z)$	Force on the cable after the pulley function

Table 4.1: Definitions of symbols describing the AMASC.

In order to create a low-friction, zero-backlash system, the AMASC utilizes a high-speed cable drive [Townsend and Salisbury, 1989]. There is some stretch in the cable transmission, which adds series compliance to the system, and is incorporated into the effective spring constant of our model. Because the cables are round, they may wrap around pulleys placed at any angle, unlike standard belts. This design freedom makes it easier to route cables through joints, allowing the motors to be located remotely. Figure 4.3 shows the cable routing, illustrating the role of each motor in the tension of the two springs. Also shown is the fact that a displacement of the leg ( $\theta_2$  or  $x_2$ ) results in displacement of the motor ( $\theta_1$  or  $x_1$ ), displacement of the springs, or some combination of the two. There is a speed reduction between the first and second pulleys not shown on the diagram; it is implemented using a combination of a block-and-tackle pulley mechanism and a difference in radii between  $r_1$  and  $r_2$ . The speed reduction is physically located near the knee joint, but diagrammatically located near the motor,  $\theta_1$ . In all of our representations, the speed reduction is shown solely as a difference between  $r_1$  and  $r_2$ . All friction related to the speed reduction is applied to  $\theta_1$  and corresponds to  $B_1$ . The inertia of the speed reduction is added to the inertia of the motor, and corresponds to  $J_1$ .

A speed reducer amplifies the motor inertia by the square of the speed reduction; this amplification appears in the relatively large values of  $J_1$ . The transmission between  $\theta_2$  and the springs has very low friction, and no speed reduction. Because the high-frequency behavior of the system is generally handled by the springs, low friction and inertia are most important in this part of the AMASC. The low-frequency behaviors of the system are handled by the motor, and thus friction and inertia can be overcome by relatively low-bandwidth software compensation.

Perhaps the most important aspect of the AMASC, along with the series spring, remotely located motors, and zero-backlash cable drive, is the physically variable series compliance. As stated in Chapter 2, physical compliance is crucial for a running gait, while varying the compliance is a useful control strategy. The AMASC's physical compliance resides in unidirectional fiberglass plates, which have a relatively high work capacity on the order of 1000 J/kg. Varying the compliance of the AMASC is achieved in much the same way as in animals, with co-contraction of opposing nonlinear springs.

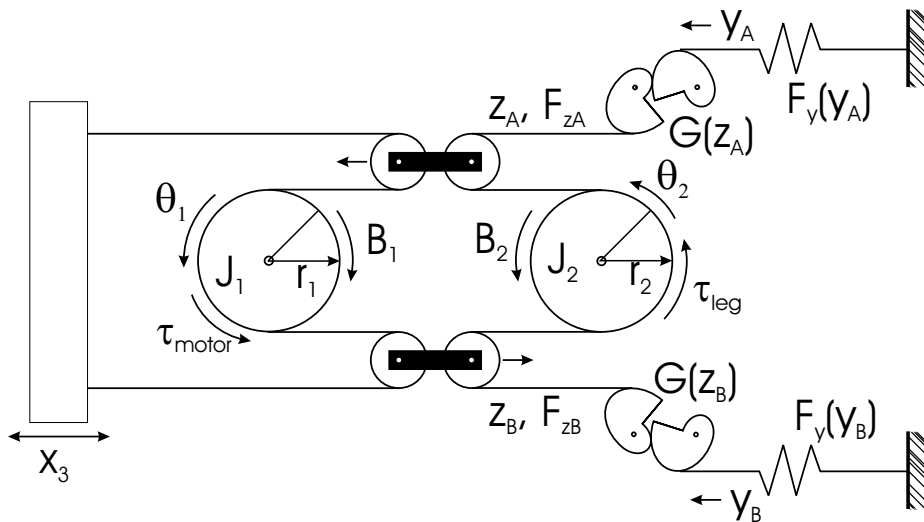


Figure 4.3: Cable routing diagram of the AMASC.  $J_1$  and  $J_2$  are pinned in place but can rotate freely; the spiral pulleys are also pinned in place but free to rotate. The remaining four pulleys are floating, and can move sideways as well as rotate. Refer to Table 1 for notation descriptions.

In the case of animals, the nonlinear spring is the muscle/tendon combination; in the case of the AMASC, the nonlinear spring is formed by a fiberglass plate in series with a set of spiral pulleys. The reduction ratio of the pulleys varies proportionally with the fiberglass spring deflection, to create some output spring function, such as  $F_z(z) = Kz^2$ . Placing two such spring functions in direct opposition results in a single effective spring force function,  $F_{eff}$ . The resulting effective spring force is calculated by substituting  $(x_3 + \Delta x)$  and  $(x_3 - \Delta x)$  for  $z$ , where  $x_3$  represents the pretension on the two nonlinear springs and  $\Delta x$  represents the deflection from their rest position  $(x_2 - x_1)$ . Combining the two forces results in

$$F_{eff}(x_3, \Delta x) = F_z(x_3 + \Delta x) - F_z(x_3 - \Delta x). \quad (4.1)$$

For the simple example of quadratic springs,  $F_z(z) = Kz^2$ :

$$\begin{aligned} F_{eff} &= K(x_3 + (x_2 - x_1))^2 - K(x_3 - (x_2 - x_1))^2 \\ F_{eff} &= K(x_3^2 - 2x_3x_1 + 2x_3x_2 + x_1^2 - 2x_1x_2 + x_2^2) - \\ &\quad K(x_3^2 + 2x_3x_1 - 2x_3x_2 + x_1^2 - 2x_1x_2 + x_2^2) \\ F_{eff} &= 4Kx_3(x_2 - x_1) \end{aligned}$$

In this manner, the stiffness of the resulting system can be changed by adjusting the pretension,  $x_3$ . Notice that the pretension affects the force as much as the displacement  $(x_2 - x_1)$ . The effective spring force  $F_{eff}$  is linear with respect to displacement (in this specific case), but its stiffness is now adjustable. In practice, the rate at which this parameter can be varied depends on the actuator and transmission used. Our prototype is intended for relatively slow changes at low force, such as during the flight phase of a running gait.

The pulley function,  $G(z)$ , is a design freedom and can be changed to impart a nearly arbitrary function to the spring/pulley system,  $F_z(z)$ . Logarithmic spiral pulleys were initially chosen because the spring function of the bending fiberglass plates was unknown, because the desired spring function was unknown, and because two logarithmic spirals mesh correctly and provide a stiffening function [Chironis, 1965]. Our logarithmic spiral pulleys are described by the following equations:

$$\begin{aligned} R_1 &= Ae^{k\phi} \\ R_2 &= C - Ae^{k\phi} \end{aligned}$$

where  $\phi$  is the angle of rotation of the pulley,

$$\phi(z) = \frac{z}{r}. \quad (4.2)$$

These pulleys exhibit the velocity transfer function

$$\frac{dy}{dz} = \frac{dG}{dz}(z) = \frac{Ae^{k\frac{z}{r}}}{C - Ae^{k\frac{z}{r}}}, \quad (4.3)$$

and exhibit the position function

$$y = G(z) = r(\phi_0 - \frac{1}{k} \ln(C - Ae^{k\frac{z}{r}})). \quad (4.4)$$

The choice of a logarithmic spiral was somewhat arbitrary. Before new pulleys can be designed, however, two functions must be considered: the desired output force function,  $F_z(z)$ , and

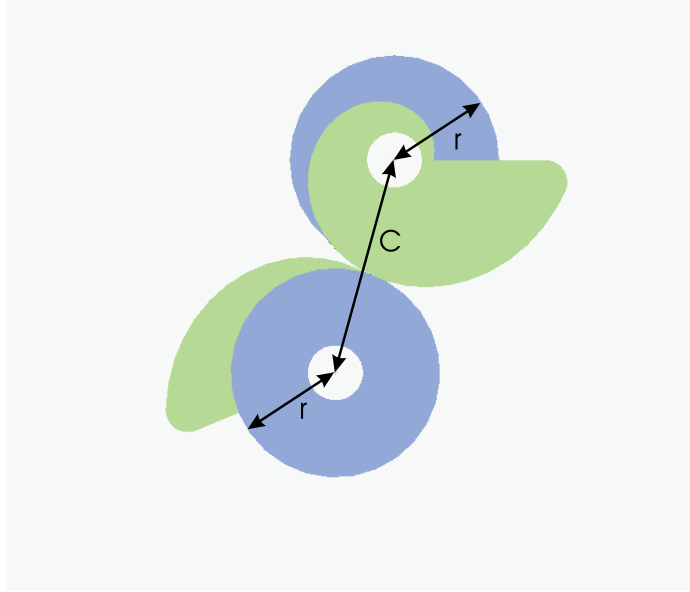


Figure 4.4: The logarithmic spiral pulleys used on the prototype AMASC.

variable	value	description
$C$	$0.1m$	center distance between axles
$r$	$0.05m$	radius of the round pulley
$k$	$0.2446489$	affects the “steepness” of the spiral
$A$	$0.017696$	scales the overall size of the spiral
$\phi_0$	$-10.2078$	position of pulley when $z = 0$

Table 4.2: Measurements of the logarithmic spiral pulleys.

the measured fiberglass spring force function  $F_y(y)$ . The desired spring force function  $F_z(z)$  can be described in terms of the pulley transmission function  $y = G(z)$ , where  $z$  is the extension of the cable out of the pulley. We calculate  $F_z(z)$  by computing the virtual work:

$$\begin{aligned}
 F_z(z)dz &= F_y(y)dy \\
 y = G(z), \quad dy &= \frac{dG}{dz}(z)dz \\
 F_z(z)dz &= F_y(G(z))\frac{dG}{dz}(z)dz \\
 F_z(z) &= F_y(G(z))\frac{dG}{dz}(z). \tag{4.5}
 \end{aligned}$$

Given the desired  $F_z$  and the spring function  $F_y$ , we can solve Equation 4.5 for the pulley function  $G(z)$ . With this pulley function, the relationship between angular velocities of two members,  $\frac{dG}{dz}(z)$ , can be determined. Given the center distance  $C$  between the pulleys, the polar equations

describing the spiral shape of both pulleys are

$$\begin{aligned} R_1 &= \frac{C \frac{dG}{dz}(z)}{1 + \frac{dG}{dz}(z)} \\ R_2 &= C - R_1. \end{aligned}$$

Even if the fiberglass springs have some unusual stiffness function  $F_y(y)$ , the spiral pulley function  $G_z(z)$  can account for it, and can create any odd output function  $F_{eff}$ . The following derivation shows that  $F_{eff}$  must be an odd function for any arbitrary  $F_z$ .

Let  $F_z(z)$  be described by a Taylor series:

$$F_z(z) = a_0 + a_1z + a_2z^2 + a_3z^3 \dots$$

We can substitute  $x_3 + \Delta x$  in for  $z$  :

$$F_z(x_3 + \Delta x) = a_0 + a_1(x_3 + \Delta x) + a_2(x_3 + \Delta x)^2 + a_3(x_3 + \Delta x)^3.$$

This equation will give us a polynomial function in terms of  $x_3$  and  $\Delta x$ :

$$F_z(x_3 + \Delta x) = F'(x_3, \Delta x).$$

We can break this function,  $F'$ , into the even and odd powers of  $\Delta x$ ,  $F'_{even}$  and  $F'_{odd}$ :

$$F'(x_3, \Delta x) = F'_{even}(x_3, \Delta x) + F'_{odd}(x_3, \Delta x).$$

The spring force at the knee becomes

$$F_{eff} = (F'_{even}(x_3, \Delta x) + F'_{odd}(x_3, \Delta x)) - (F'_{even}(x_3, -\Delta x) + F'_{odd}(x_3, -\Delta x)),$$

and because

$$\begin{aligned} F'_{even}(x_3, -\Delta x) &= F'_{even}(x_3, \Delta x) \\ F'_{odd}(x_3, -\Delta x) &= -F'_{odd}(x_3, \Delta x), \end{aligned}$$

we can substitute for  $F_z$  in Equation 4.1 and obtain the result:

$$\begin{aligned} F_{eff} &= F'_{even}(x_3, \Delta x) + F'_{odd}(x_3, \Delta x) - F'_{even}(x_3, \Delta x) + F'_{odd}(x_3, \Delta x) \\ F_{eff} &= 2F'_{odd}(x_3, \Delta x) \end{aligned}$$

The fact that  $F_{eff}$  is necessarily odd indicates that the spring function is rotationally symmetric about the origin. In other words, when deflecting the joint in one direction, the resulting force will be exactly opposite to the force that results from deflecting the joint the same amount in the other direction. This result may not be interesting in the context of legged locomotion, because most locomotion tasks will apply force in one direction only.

## 4.2 Control System Design

The control system is designed for the mechanical model shown in Figure 4.2, and is intended to accomplish two basic tasks. The first task is to adjust the mechanism configuration so its physical properties match the commanded spring stiffness. This adjustment is accomplished with a PID position controller and a spring-cancelation feed-forward torque on the pretension motor. Because the specific position of this motor,  $x_3$ , corresponds to a specific effective stiffness  $K_{eff}(x_3)$ , no further control is required.

The second task is to actively control the motor position,  $x_1$ , so that the force applied by the leg spring,  $F_z(z)$ , matches the spring force that would be created by the ideal, correctly tuned system. This ideally tuned system is shown in Figure 4.5, with desired leg stiffness  $K^*$ , and desired set point  $x_2^*$ . When the physical stiffness  $F_{eff}$  matches the desired stiffness  $K^*$ , then the motor position  $x_1$  will be commanded to match the ideal system's desired set point  $x_2^*$ . When  $F_{eff}$  does not match  $K^*$ , then  $x_1$  must move in some additional corrective trajectory.

The desired motor position  $x_1$  is calculated by setting the force of the actual springs to match the spring force of the ideal system:

$$F_{eff}(\Delta x, x_3)r_2 + \frac{B_2}{r_2}\dot{x}_2 = (x_2 - x_2^*)K^*r_2 + \frac{B_2^*}{r_2}\dot{x}_2. \quad (4.6)$$

Assuming the dependence of  $F_{eff}$  on  $\Delta x$  is linear ( $F_{eff} = K_{eff}(x_3)\Delta x$ ), we can solve this equation for  $x_1$  to calculate the desired position,  $x_1^*$ , and its derivative,  $\dot{x}_1$  :

$$x_1^* = \frac{K^*}{K_{eff}}(x_2^* - x_2) - \frac{B_2^* - B_2}{K_{eff}r_2^2}\dot{x}_2 + x_2 \quad (4.7)$$

$$\begin{aligned} \dot{x}_1^* = & -\frac{K^*}{K_{eff}}\dot{x}_2 - \frac{K^*}{K_{eff}^2}\dot{K}_{eff}(x_2^* - x_2) - \frac{B_2^* - B_2}{K_{eff}r_2^2}\ddot{x}_2 \\ & + \frac{B_2^* - B_2}{K_{eff}^2r_2^2}\dot{K}_{eff}\dot{x}_2 + \dot{x}_2. \end{aligned} \quad (4.8)$$

Note that when the mechanism matches the desired system (i.e.  $K^* = K_{eff}$  and  $B^* = B_2$ ), the above equations reduce to  $x_1^* = x_2^*$  and  $\dot{x}_1^* = 0$ .

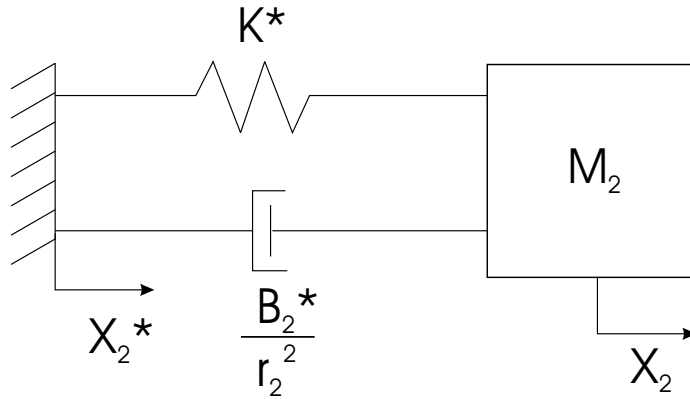


Figure 4.5: The ideal case of the AMASC, with three parameters: spring rest length,  $x_2^*$ , spring stiffness,  $K^*$ , and knee joint damping,  $B^*$ .

We then apply a PD controller on  $x_1$  to move it to the desired position, along with a feed-forward spring cancellation force to hold it against the force applied by the springs:

$$F_{\text{com}} = K_P(x_1^* - x_1) + K_D(\dot{x}_1^* - \dot{x}_1) - F_{\text{eff}}(x_3, \Delta x). \quad (4.9)$$

With the spring cancellation force, the PD control can adjust  $x_1$  as if it were an independent mass, without the attached spring and associated dynamics. There are two limitations in this approach that introduce error. First, because  $F_{\text{eff}}$  is a function composed of the logarithmic spiral pulleys and the unknown fiberglass spring function, it is necessarily an approximation. We used a linear approximation of the knee spring,  $F_{\text{eff}} = K_{\text{eff}}(x_3)\Delta x$ , introducing error between the calculated force and the applied force, most pronounced at the extremes of deflection and pretension. In addition, when using active control to implement a spring stiffness that is outside the physical range of the AMASC, the calculated location  $x_1^*$  will only be correct to the accuracy of the approximation.

The second source of error comes from the bandwidth limitation on  $x_1$ . When trying to simulate a stiffness at high frequency, the inertia of  $M_1$  will limit the acceleration of  $x_1$ , and the system will revert to the behavior of its natural dynamics, instead of the desired behavior. However, because the stiffness of the AMASC is adjustable, this error can only happen when the desired stiffness is outside the range of the mechanism, or when the mechanism is in the process of adjusting to the correct stiffness.

### 4.3 Simulation, Results and Comparison

This section describes the methods and approaches used to characterize the physical properties of the AMASC and to build an accurate simulation. After illustrating the similarity of the simulation to the real actuator, we demonstrate a simulated running robot, and compare its performance using both ideal actuation, and our simulated AMASC.

#### 4.3.1 Static Compliance Characterization

An accurate representation of the fiberglass springs and their interaction at the knee was required for correct simulation and control. To gather data on  $F_{\text{eff}}$  (shown in Figure 4.6), we applied a series of spring set point and pretension values, and recorded the motor and leg positions and the force applied by the leg. We then applied several different curve-fitting methods, to create a representation of the data in which applied force is a function of spring pretension and spring set point.

As can be seen in Figure 4.7, the AMASC spring function becomes stiffer at increasing levels of pretension. The spring function is not exactly linear in deflection, although this can be remedied through pulley design as discussed in section Section 4.1. It is also apparent in Figure 4.7 that there is some hysteresis due to mechanical friction. This friction increases with increasing tension (and higher bearing forces) in the system, as seen in Figure 4.8.

There are numerous methods that could be used to fit the available data, each with benefits and drawbacks. One of the most basic methods is a Taylor polynomial. Although the deflection curve is clearly not linear, it is a relatively flat curve; so we applied a fit that is linear in deflection and quadratic in pretension, resulting in a three-term polynomial:

$$F_{\text{eff}}(x_3, \Delta x) = a_0\Delta x + a_1x_3\Delta x + a_2x_3^2\Delta x.$$

This fit allows us to easily calculate the pretension position for a desired stiffness, and as it is linear in deflection, we can use the control equations described in Section 4.2, which assume a linear

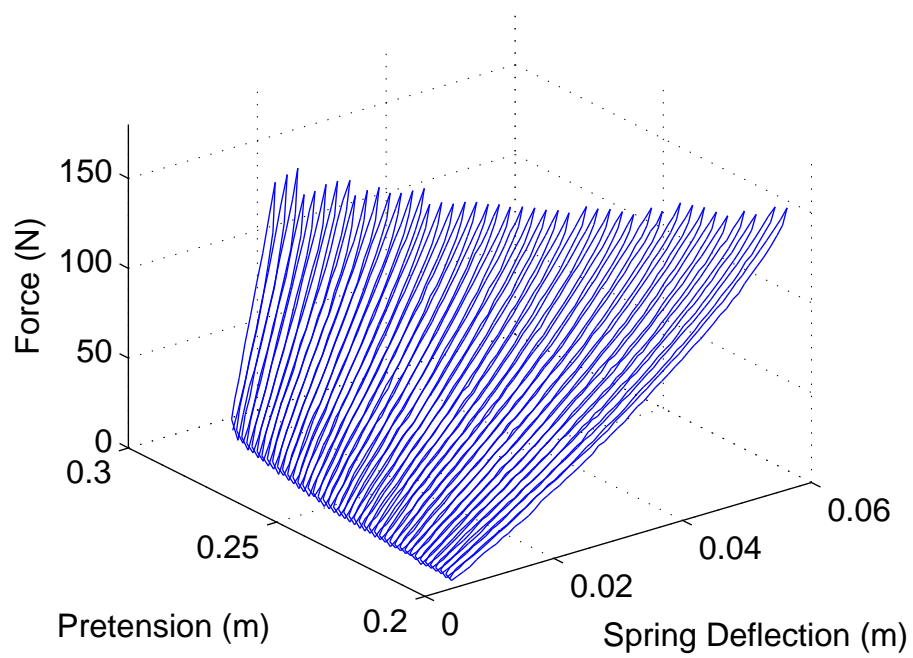


Figure 4.6: 3D plot of spring function data. Pretension units are in local coordinates of the pretension motor, while the spring deflection units are local to the springs; there is a speed reduction between them. Force is measured from a load cell, which the AMASC leg presses against.

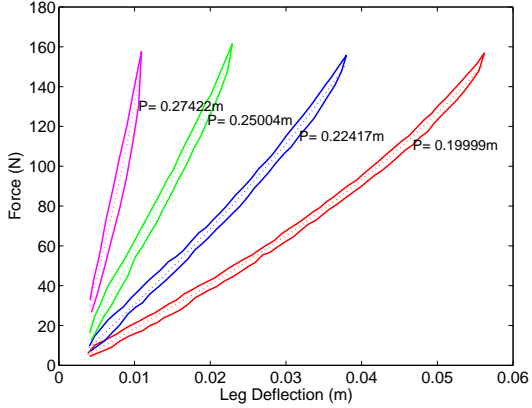


Figure 4.7: Spring force response at four different pretension settings, each with one possible curve fit (dotted line).

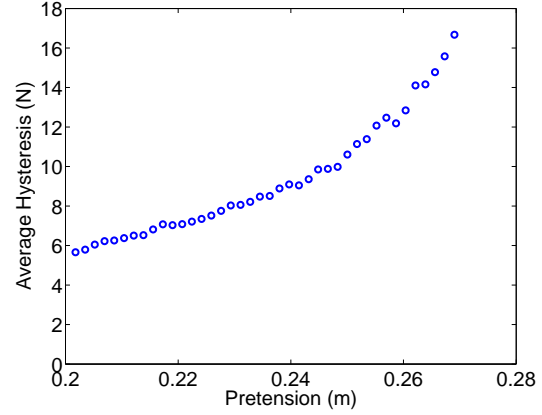


Figure 4.8: Hysteresis in the knee due to friction, shown as a function of pretension.

dependence of  $F_{eff}$  on  $\Delta x$ . It provides a reasonable fit of the data, although not as good as some other possible approaches. Figure 4.9(a) shows the absolute error between this approximation and the actual data.

A large (14-term) polynomial in both deflection and pretension yielded a much better fit than the three-term polynomial, with lower error, as shown in Figure 4.9(b). Unfortunately, this function cannot be inverted in closed form to solve for  $x_3$ , and it is not linear in deflection for use in the control system equations.

One drawback to using the polynomial fit to characterize  $F_{eff}$  is that we are ignoring the fact that the pulleys are a logarithmic spiral. This function is known, so fitting a polynomial to this known function will introduce a certain amount of unnecessary error. In addition, we would like to know the spring function of the physical springs,  $F_y(y)$ , before the force is modified by the logarithmic pulleys. Knowing the spring function of the physical springs will allow future pulley designs to compensate for undesirable properties of  $F_y$  and create the desired spring function  $F_z$ . By mathematically separating the springs from the logarithmic spirals and then applying a curve fit solely to the physical springs, our error is reduced, the polynomial is simplified, and we find that the physical springs are very nearly linear.

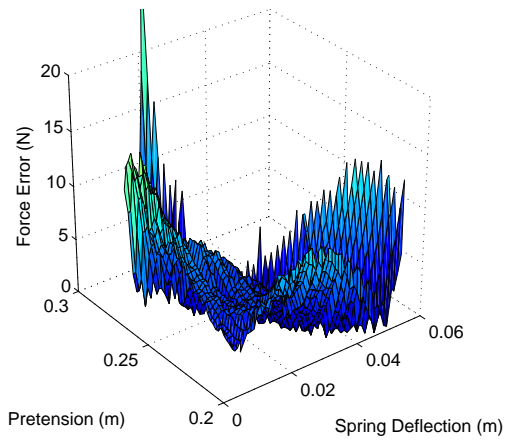
The force data collected from the actuator measures knee stiffness,  $F_{eff}$ , which is created by the two opposing springs as described in Equation 4.1. The pulley functions are known, described in Equations 4.3 and 4.4.

Substituting  $\frac{dG(z)}{dz}$  into the equation for  $F_z$  (Equation 4.5) results in

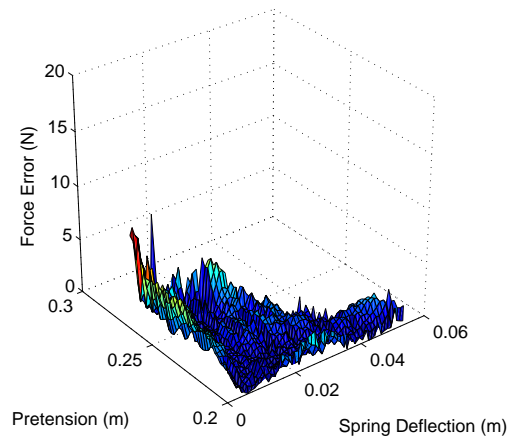
$$F_z(z) = \frac{Ae^{k\frac{z}{r}}}{C - Ae^{k\frac{z}{r}}} F_y(y).$$

If  $F_y(y)$  is represented as a Taylor series,

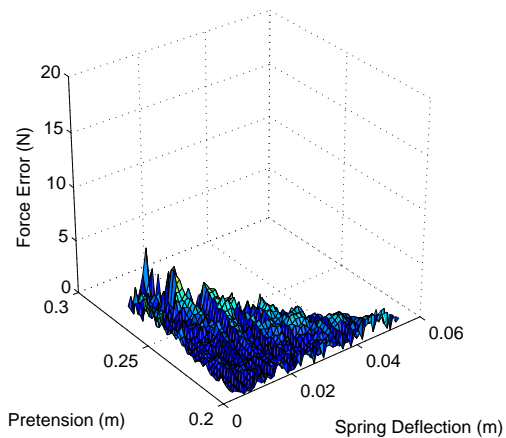
$$F_z(z) = \frac{Ae^{k\frac{z}{r}}}{C - Ae^{k\frac{z}{r}}} [a_0 + a_1y + a_2y^2 + a_3y^3 \dots],$$



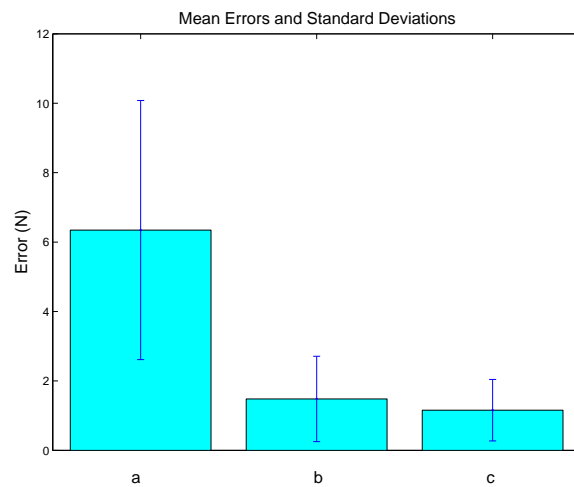
(a) 3-term polynomial, linear in deflection



(b) 14-term polynomial



(c) linear  $F_y(y)$  passed through pulleys



(d) Mean Error for data fits

Figure 4.9: Plots of absolute error between data points and curve fits.

and  $G(z)$  is substituted for  $y$ ,

$$\begin{aligned}
F_z(z) = & \\
& \frac{Ae^{k\frac{z}{r}}}{C - Ae^{k\frac{z}{r}}} \left[ a_0 + a_1 r \left( \phi_0 - \frac{1}{k} \ln(C - Ae^{k\frac{z}{r}}) \right) + a_2 \left( r \left( \phi_0 - \frac{1}{k} \ln(C - Ae^{k\frac{z}{r}}) \right) \right)^2 \right. \\
& \left. + a_3 \left( r \left( \phi_0 - \frac{1}{k} \ln(C - Ae^{k\frac{z}{r}}) \right) \right)^3 \dots \right] \tag{4.10}
\end{aligned}$$

We now have an equation for  $F_z$  in terms of a polynomial fit of  $F_y$ . We can substitute this result into Equation 4.1 to acquire an equation for  $F_{eff}$ . To simplify this equation, we construct the following definitions:

$$\begin{aligned}
H &= \frac{Ae^{k\frac{x_3+\Delta x}{r_1}}}{C - Ae^{k\frac{x_3+\Delta x}{r_1}}} \\
I &= r_1 \left( \phi_0 - \frac{1}{k} \ln(C - Ae^{k\frac{x_3+\Delta x}{r_1}}) \right) \\
J &= \frac{Ae^{k\frac{x_3-\Delta x}{r_2}}}{C - Ae^{k\frac{x_3-\Delta x}{r_2}}} \\
L &= r_2 \left( \phi_0 - \frac{1}{k} \ln(C - Ae^{k\frac{x_3-\Delta x}{r_2}}) \right)
\end{aligned}$$

By substituting these variables and Equation 4.10 into Equation 4.1, we arrive at the equation for  $F_{eff}$ ,

$$F_{eff}(x_3, \Delta x) = H(a_0 + a_1 I + a_2 I^2 + a_3 I^3 + \dots) - J(a_0 + a_1 L + a_2 L^2 + a_3 L^3 + \dots),$$

which can be factored into

$$F_{eff}(x_3, \Delta x) = a_0(H - J) + a_1(HI - JL) + a_2(HI^2 - JL^2) + \dots \tag{4.11}$$

This form is very useful for fitting a curve to the data. It allows us to calculate  $a_0 \dots a_n$ , which correspond to the physical spring force polynomial before it is passed through the pulleys. We found that using a simple linear fit of the physical spring resulted in a good approximation, as shown in Figure 4.9(c). This fit was used to generate the surface in Figure 4.10 and the dotted curves in Figure 4.7. Not only is this curve fitting method more accurate than any of the polynomial fits, it also has the advantage that it can be used to calculate spring cancelation forces for control of both  $x_1$  and  $x_3$ . A standard polynomial curve fit of  $F_{eff}$  can only calculate a spring cancelation force for  $x_1$ . In addition, because this method describes how the physical spring (before the pulley function) behaves, pulleys can be designed to provide the desired  $F_z(z)$ . Unfortunately, this fit cannot be easily inverted to solve for the desired positions of  $x_1$  or  $x_3$ . In our controller, the linear polynomial curve fit is used to calculate the desired values of  $x_1$  and  $x_3$ , while Equation 4.11 is used for spring cancelation forces and other calculations that do not require inversion.

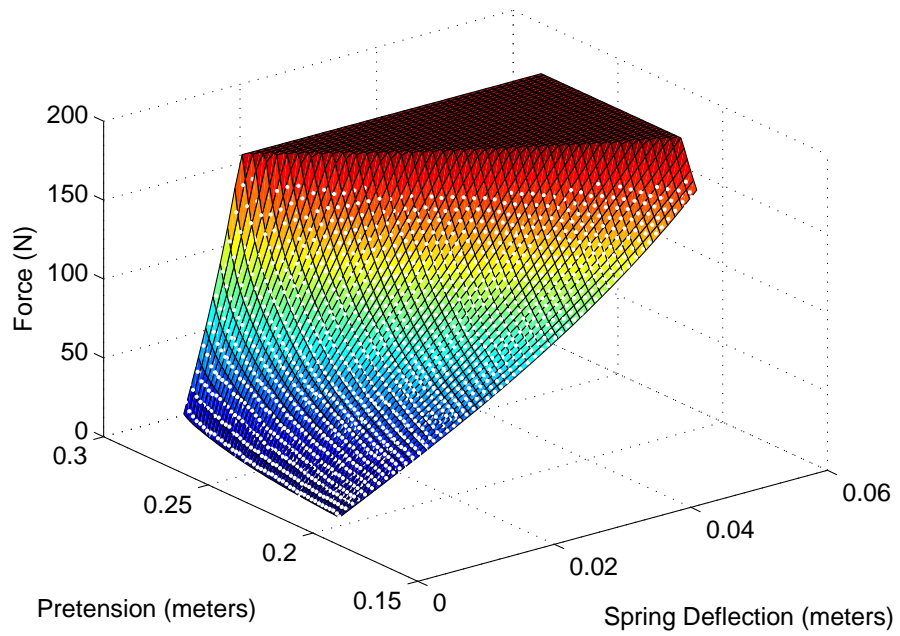


Figure 4.10: Surface plot of one spring function curve fit, with data points shown as white dots.

### 4.3.2 Dynamic Actuator Simulation

Dynamic simulation of the AMASC mechanism was done using SD/FAST (a trademark of Symbolic Dynamics, Inc. and Parametric Technology Corporation), based on the model shown in Figure 4.2(a). The springs are approximated as linear springs passed through the logarithmic spiral pulleys (i.e. the fit shown in Figure 4.9(c) and described by Equation 4.11). The dynamics of the pretension motor are approximated by a constant-velocity trajectory to the desired setting. Physical parameters such as link length and inertia were measured from the SolidWorks model and from the AMASC prototype. The values of these parameters are given in Table 4.3.

variable	value	variable	value
$J_1$	0.00134 kg·m <sup>2</sup>	$M_1 = \frac{J_2}{r_2^2}$	59.6 kg
$J_2$	0.085 kg·m <sup>2</sup>	$M_2 = \frac{J_1}{r_1^2}$	8.5 kg
$B_1$	0.0517 N·m·s/rad	$r_1$	0.00474 m
$B_2$	0.38 N·m·s/rad	$r_2$	0.1 m

Table 4.3: Physical properties used for simulation.

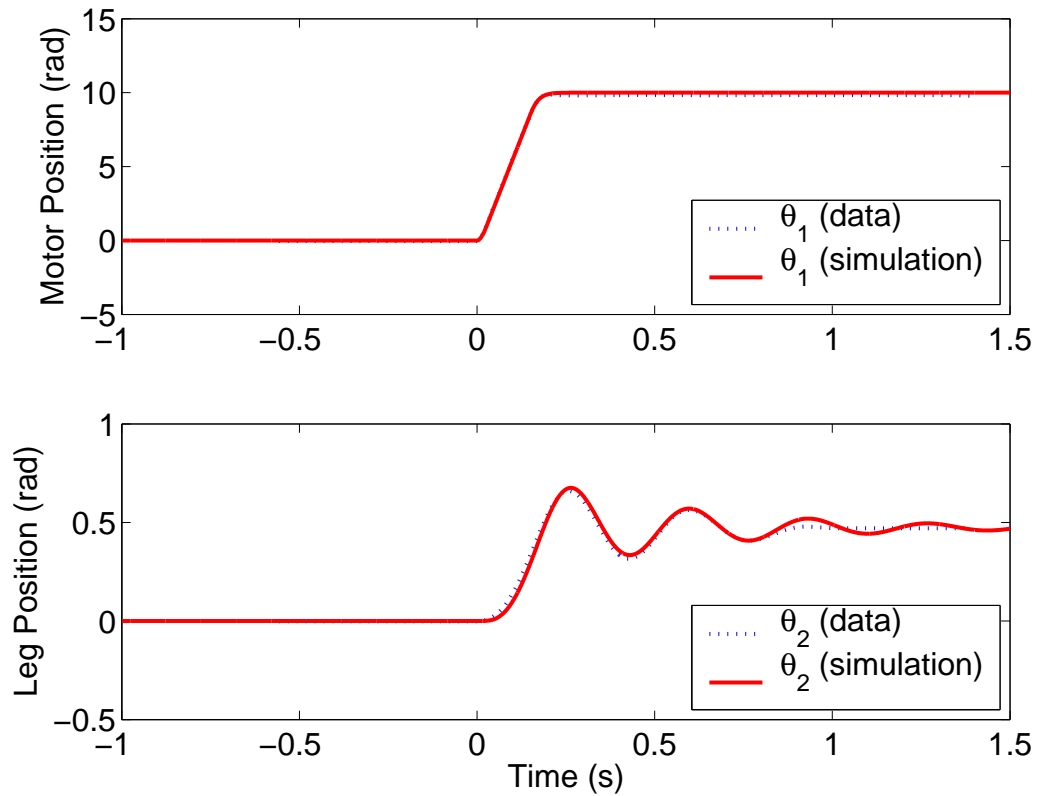


Figure 4.11: Comparison of prototype AMASC and simulated AMASC, showing motor and leg response to a step input.

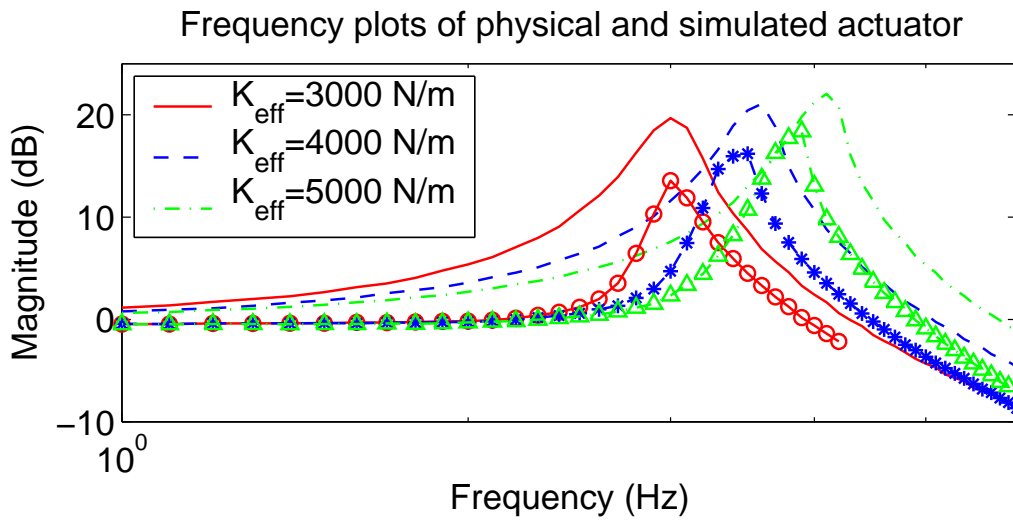


Figure 4.12: Comparison of prototype AMASC and simulated AMASC across a range of frequencies at three different stiffnesses. With a sine wave input to the motor position, the ratio of leg position to motor position is plotted, showing similar behavior between the actuator data, plotted as symbols connected by lines, and the simulation data, plotted as lines.

The prototype AMASC was initially compared to its simulation by applying a step position input to the set-point of both systems. Figure 4.11 shows that the responses are very similar. One difference is that the oscillations of the prototype AMASC are damped once the amplitude of the oscillations becomes small. We hypothesize that this is due to frictional effects that are not accurately modeled by the viscous damping included in the model.

For a more comprehensive comparison, the prototype and simulated AMASC were tested across a range of frequencies and stiffness values. Figure 4.12 shows the similar responses of the prototype and simulation as the motor is commanded a sine wave position function through a range of frequencies at a series of ascending pretension values. We hypothesize again that differences in the simulation and prototype are mostly caused by unmodeled frictional effects, such as stiction on the fiberglass springs. Part of the error may also be caused by our spring fit; it has some error, and is not an exact representation of the physical system.

These tests do not demonstrate the performance of the AMASC system, they merely show that the physical AMASC and simulated AMASC behave similarly at a range of frequencies. To measure the performance of any actuator, experiments should test how well it demonstrates desired dynamics under various conditions. For the specific case of SLIP model running, the AMASC should behave like a spring with a certain stiffness. In order to deal with frequent ground impacts during a running gait, the AMASC should exhibit this behavior to an arbitrarily high frequency, which is not possible for a standard gearmotor system.

A Bode test demonstrated the bandwidth limitations of the simulated AMASC. The input to the Bode plot was the leg position, which followed a sine wave. The output of the system is spring force. The three different Bode plots shown in Figure 4.13 represent three different commanded stiffness values  $K^*$ , with a constant physical stiffness,  $K_{eff}$ . These plots show the frequency limit of the AMASC when attempting to simulate a system softer or stiffer than its mechanical adjustment, and also demonstrate the lack of a bandwidth limit when the AMASC is tuned properly.

### 4.3.3 Running Simulation

We implemented a simulated running robot in SD/FAST based on the SLIP model. Raibert-style controllers were implemented as described in “Legged Robots that Balance” [Raibert, 1986], with slight modifications. Raibert-style hopping height controllers insert a fixed amount of energy by changing the set-point during stance, causing the hopping height to converge to some value. Our modification calculates exactly how much energy must be added for the desired hopping height and speed, and adjusts the set-point to add the appropriate amount of energy.

The running simulation was first created with an ideal actuator placed at each joint, such that we could apply any stiffness and set-point instantly. We then converted the actuator in this running simulation to the simulation of the AMASC (see Figure 4.14) as described in Section 4.3.2. Because the prototype AMASC currently has very soft springs for bench testing, we adjusted the simulation so that the simulated fiberglass springs were ten times stiffer than the prototype’s springs, which is more appropriate for a running gait. With the stiffer simulated fiberglass springs, we could reach the commanded stiffness without being outside the range of the experimental curve fits.

The simulated robot continued running with the AMASC, with no changes to the running controller from the simulation with the ideal knee spring. The resulting difference in the behavior of the running robot is shown in Figure 4.15. Note that the hopping height and stride length decrease slightly. This change is due to the fact that the set-point of the AMASC cannot change instantly, and thus slightly less energy is inserted into the running gait than with an ideal knee spring.

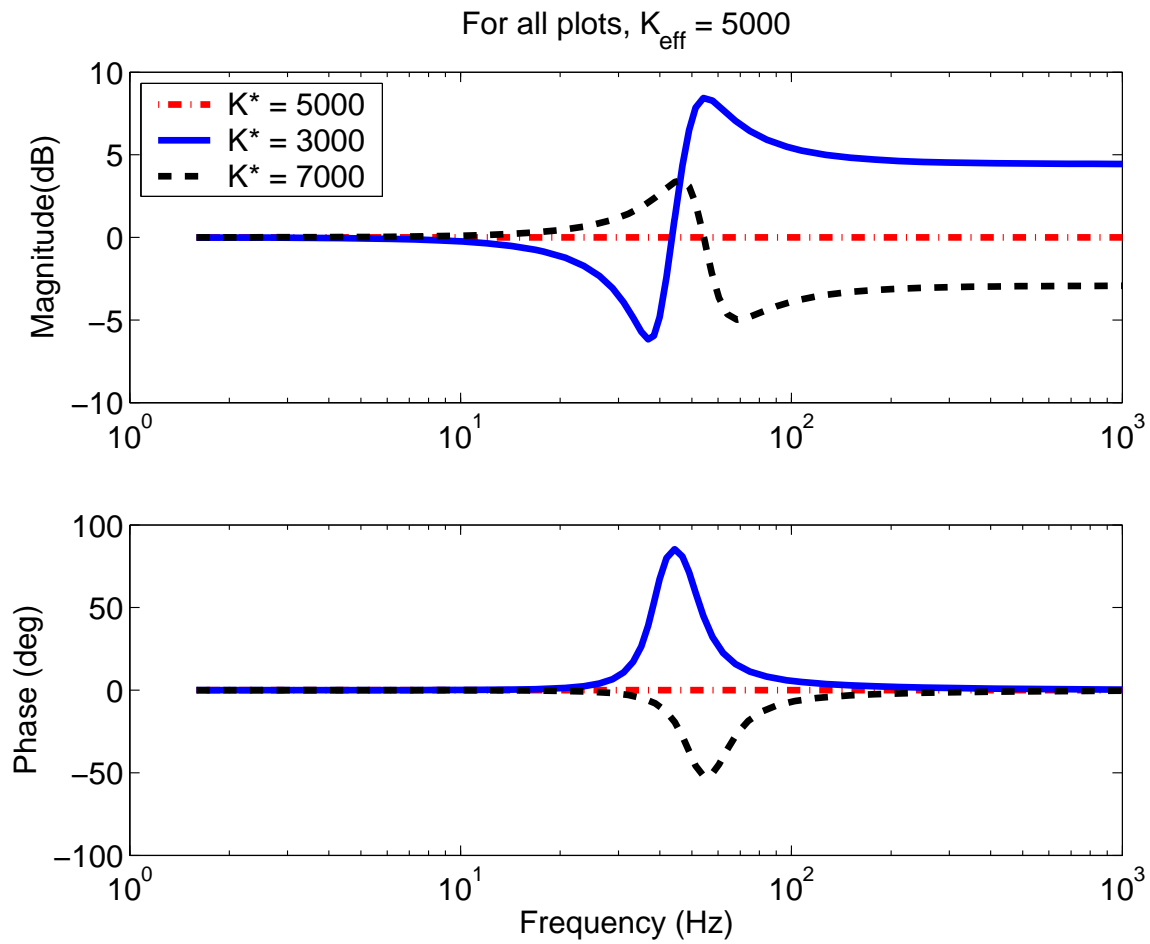


Figure 4.13: Impedance plot of the simulation. The system cannot keep up at high frequencies when improperly adjusted, but has no bandwidth limit when the system is tuned properly. Joint stiffness is in units of N/m.

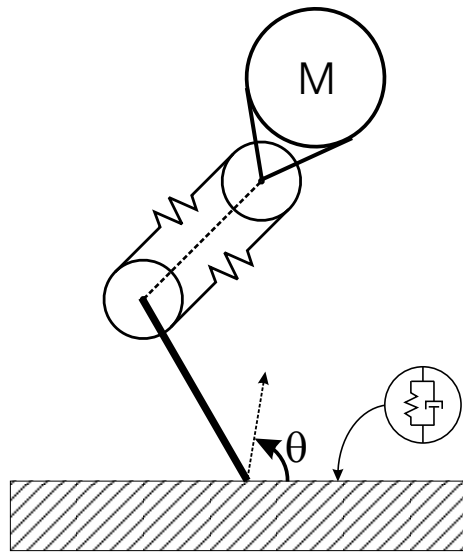


Figure 4.14: Hopping robot with the AMASC inserted as the knee spring. The vector at the toe points towards the hip joint, aligned with the effective SLIP model prismatic spring.

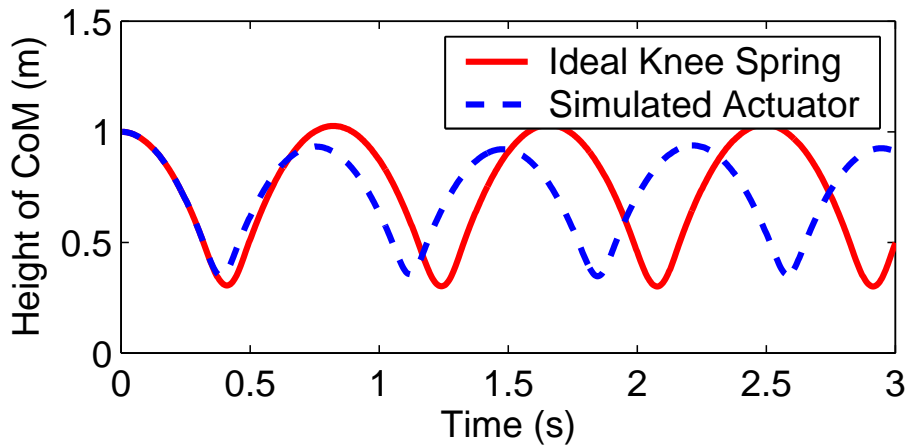


Figure 4.15: Comparison of hopping robot behavior with an ideal knee spring and a simulation of the AMASC as the knee spring.

## 4.4 Discussion

The AMASC was designed as a prototype for running robots. The spring was sized to store energy of a bouncing robot, and the software was designed to configure the AMASC to a specific set point and stiffness. However, a minor software change to control the deflection of the spring turns the AMASC into an MIT-style Series Elastic Actuator Robinson [2000]. The AMASC is compared to the MIT-SEA in this section. Aside from using the AMASC as a force controller, the variable stiffness capability has applications outside of legged locomotion, a few of which are also discussed in this section.

### 4.4.1 SEA comparison

Although the AMASC is designed to match the desired natural dynamics for a particular SLIP-model running gait, it can be operated in the same manner as the MIT Series Elastic Actuator by disabling the variable stiffness and implementing an appropriate software controller. With this modification, the AMASC has the exact same mechanical model as the SEA, but with much lower physical stiffness and about half the dynamic mass. The performance characteristics should be comparable to the SEA, and be dissimilar in a predictable fashion.

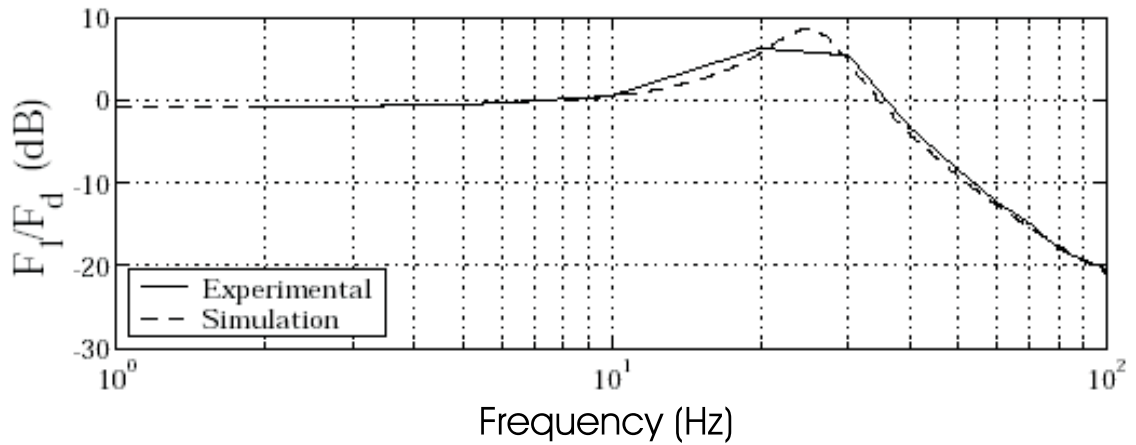
Bandwidth tests of the SEA were implemented by clamping the output shaft and measuring the applied force, while commanding a sine wave force input of increasing frequency. The motor must move some amount to preload the springs, so the desired force will be applied to the output shaft. The inertia of the motor and the software proportional gain, along with any torque limitations, will determine the upper frequency limit that is achievable by the actuator.

The AMASC has higher damping than the SEA, because a lower commanded damping ratio resulted in very large oscillations at the natural frequency, interfering with our tests. The consequence of this higher damping is a lower peak on the resulting Bode plot. The results of a physical test and a software simulation are shown in Figure 4.16(b), and can be compared to a frequency plot of the SEA in Figure 4.16(a) from David Robinson's Ph.D. Thesis [Robinson, 2000]. The structure of each graph, whether from simulation or from data, is the same. The data for the AMASC shows different peak values for different amplitudes of input excitation, which should not occur for a linear system. It is most likely due to the nonlinearity of the knee spring; while it is nearly linear, that is only an approximation of the real system. The different peak value for the AMASC and the SEA may be attributed to different motor mass and different software proportional gains.

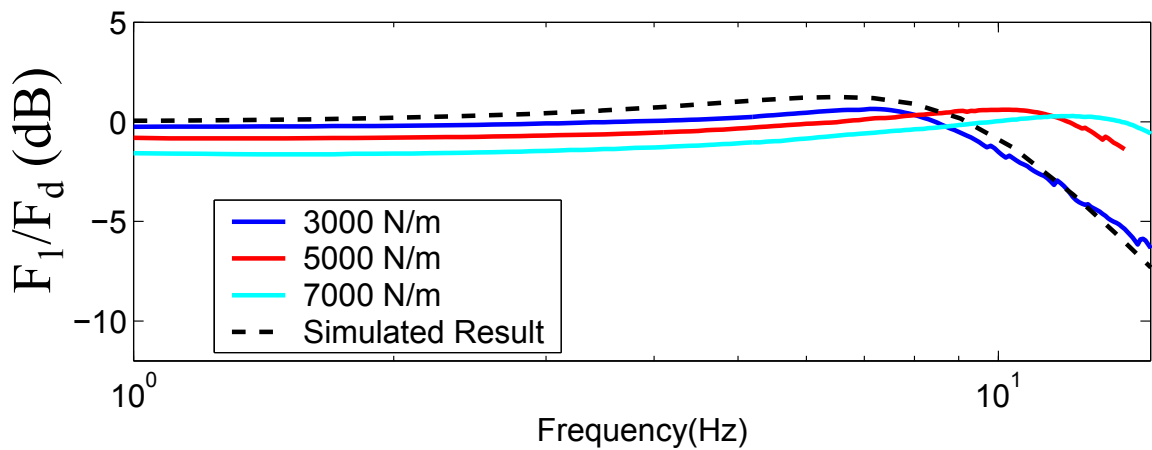
### 4.4.2 The AMASC as a Manipulator

A number of researchers have built mechanisms with variable compliance [Laurin-Kovitz et al., 1991, Mills, 1990, Morita and Sugano, 1995] for manipulation tasks. Most of these mechanisms use antagonistic motor pairs, which must exert forces both to pre-compress the springs and to move the joint. The required motor size and mass for such an antagonistic system is much larger than the AMASC, which uses one small motor with an electric brake to change the pre-compression (or pretension) of the springs. Any forces applied by the set-point motor are transmitted directly to knee torque, and do not need to overcome the opposing force of an antagonistic motor.

The stiffness function of other variable compliance mechanisms can be measured, but not chosen; the opposing springs tend to be a discrete component such as a coil spring or an air cylinder. The spring function is not a design freedom of the mechanism, as it is with the AMASC. In addition, the motors for all of these mechanisms must be placed at the actuated joint. This added mass creates difficulty for a multi-jointed arm, where the base joint must lift all of the other joint motors as well



(a) Series Elastic Actuator, plot reproduced with permission from David Robinson's thesis [Robinson, 2000].



(b) AMASC, bandwidth measured in experiment replicated from those done on MIT-SEA.

Figure 4.16: Comparison of force control bandwidth between the Series elastic actuator and the AMASC. A sine-wave force is commanded to both actuators, and the ratio of commanded/measured force at a range of frequencies provides a Bode plot and a clear bandwidth limit.

as any payload. In contrast, the AMASC allows remote placement of the electric motor, while the structure and springs that are placed at the joint have low mass.

One difference between variable compliance designs for manipulation and designs for legged locomotion are the energy storage requirements. For locomotion, it is important to have springs that are large enough to store the energy of a running gait. For manipulation tasks, little or no energy is stored—the physical compliance is mainly for safety or control system stability.

## Chapter 5

### BiMASC

The Biped with Mechanically Adjustable Series Compliance, or BiMASC, is the first application of ideas demonstrated on the AMASC. Like the AMASC, the BiMASC has control of the set point and stiffness of one joint, the leg length. The BiMASC can also adjust the leg angle, with a standard electric motor and rigid transmission. Although the design specified two legs, a single prototype leg was built and tested; it is a monopod rather than a biped. The prototype was designed and built at the Carnegie Mellon University Robotics Institute, in collaboration with Professor Jessy Grizzle at the University of Michigan. This chapter provides an introduction to the design philosophy of this robot, along with some mechanical design details.

The purpose of the BiMASC is twofold. First, we seek to explore the role of compliance in running gaits. This goal is motivated by evidence from biomechanical studies and from simulations, which indicate that physical leg springs are important for energy efficiency and robustness in the presence of environmental disturbances; however, the problem of choosing the correct leg stiffness for a particular situation remains an open question. Second, the BiMASC is a prototype test platform for exploring control strategies that utilize the mechanical springs in order to achieve more efficient running and walking over smooth surfaces as well as robust locomotion over rough terrain.

Our guiding principle in constructing the BiMASC is dynamic simplicity. The passive dynamics are intentionally designed to match a simple, biomechanically-inspired mathematical model, such that a model-based control system will behave in a predictable manner. We have attempted to create a “clean” system, with measurable and predictable torques and forces, low friction, conveniently located mass concentrations, more than sufficient motor power, ample proprioceptive sensing, minimal backlash in the transmission, and no loose wires or components which can vibrate.

Finally, we discuss details of the mechanical design. We have spent considerable time and effort on the high-level mechanical design of the BiMASC as well as on the design details, because the mechanical system is the most fundamental part of the machine’s dynamic behavior. We use a system of five cable differentials to transmit power between the three motors, two springs, and the thigh and shin associated with each leg. Each motor corresponds to specific combinations of joints constrained by the differentials, rather than corresponding to a single leg joint, so that the complete set of components behaves like a simple and predictable system.

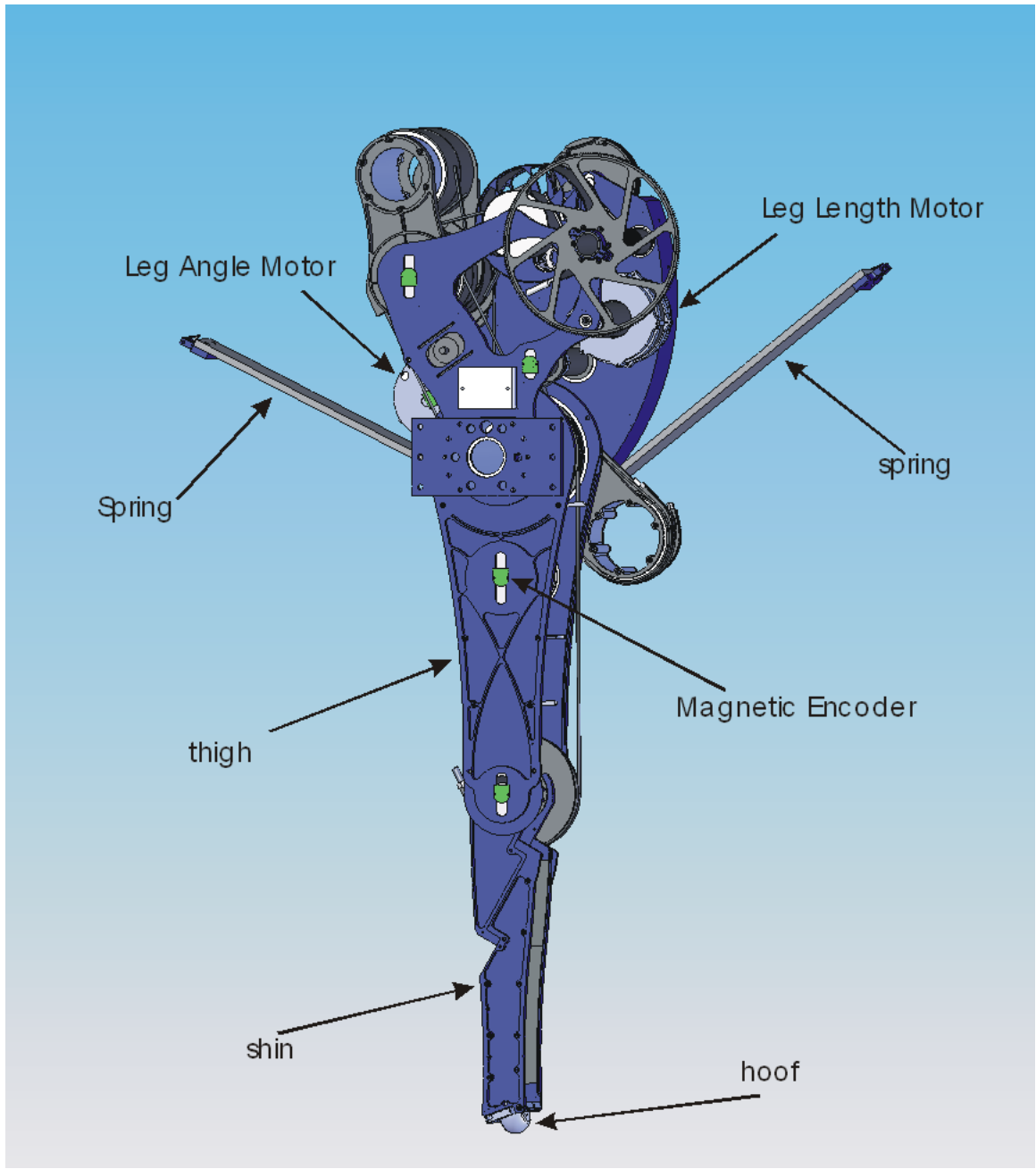


Figure 5.1: SolidWorks rendering of the BiMASC, left side.

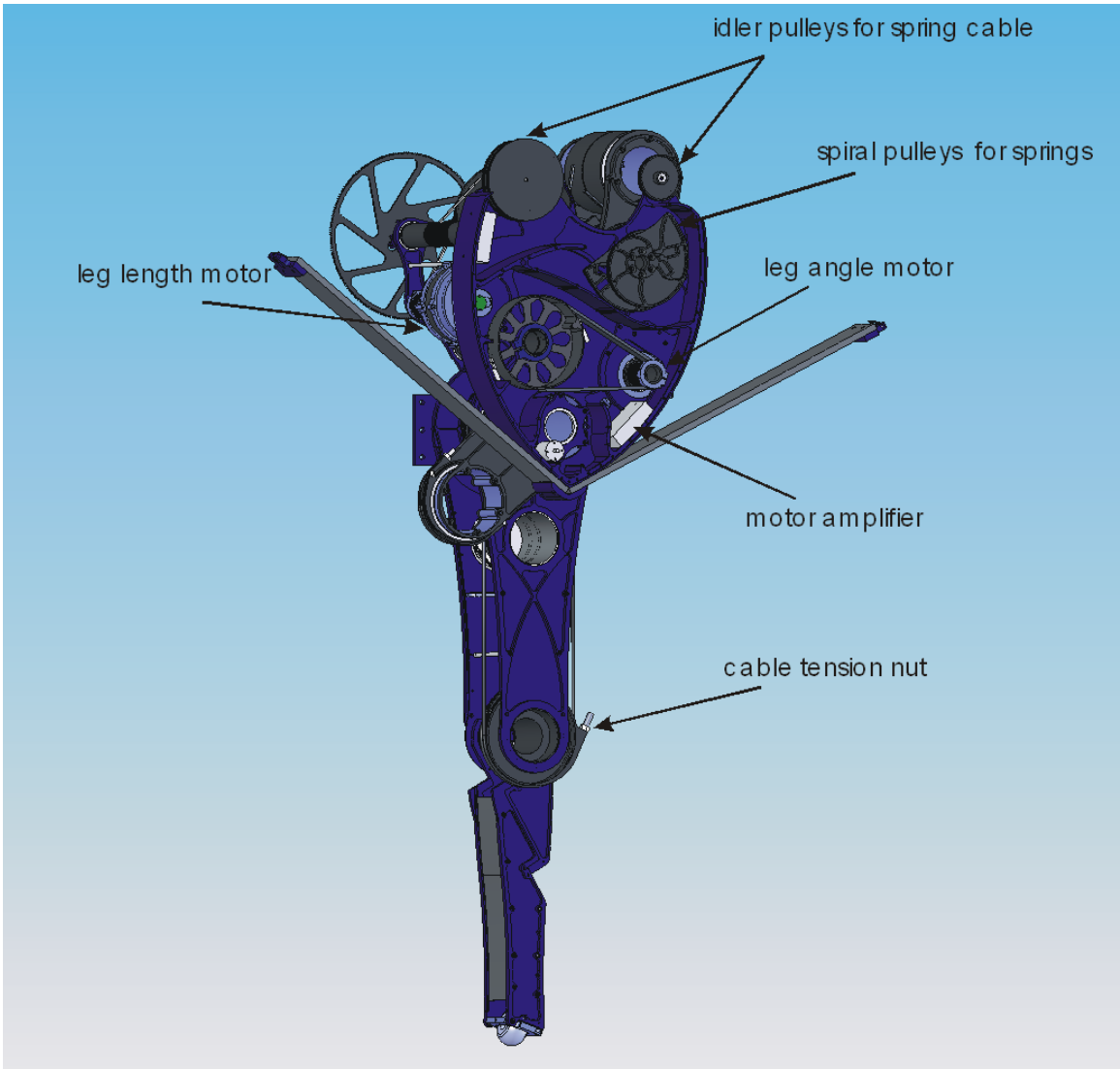


Figure 5.2: SolidWorks rendering of the BiMASC, right side.

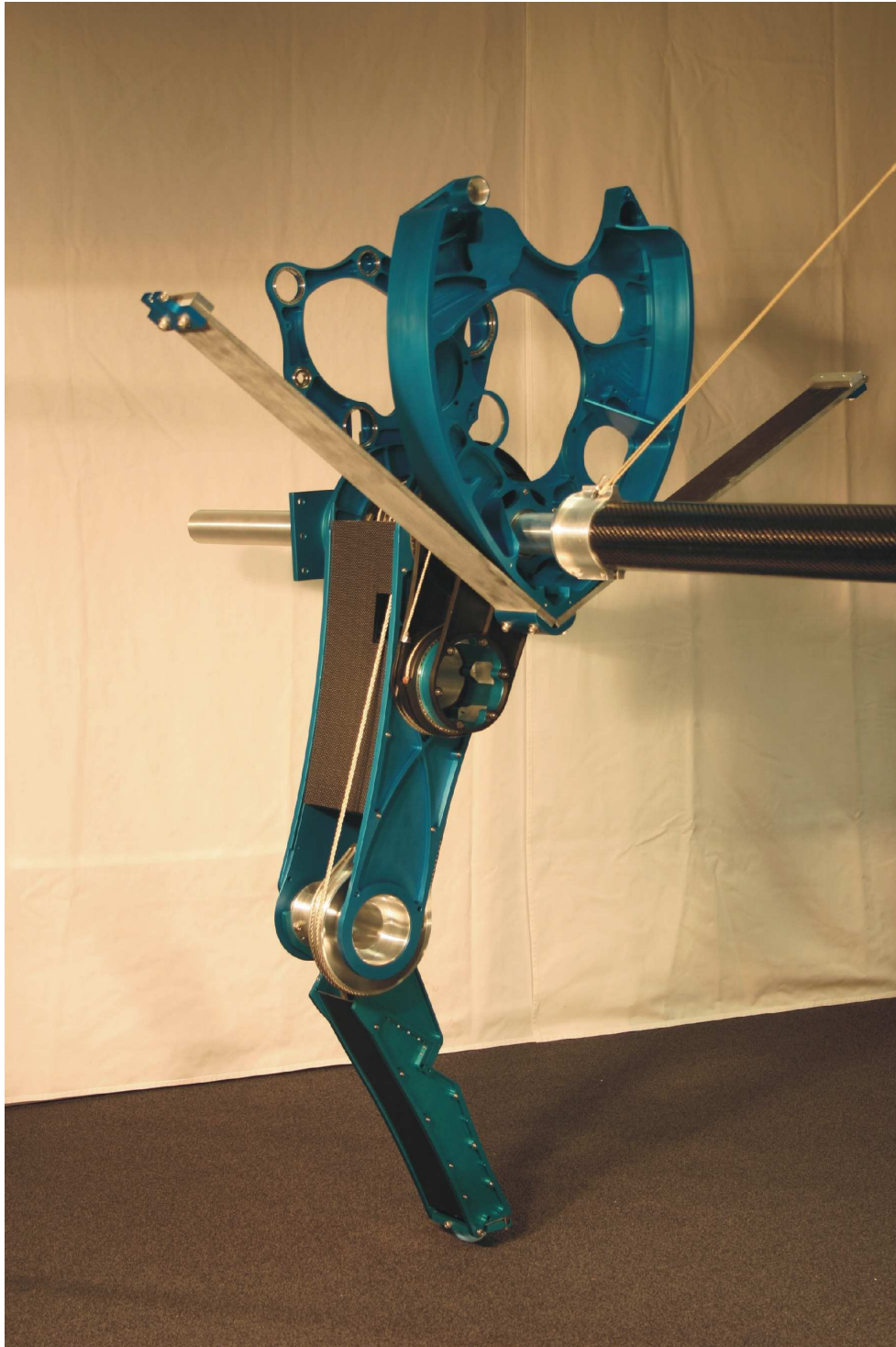


Figure 5.3: One of the BiMASC's legs, partially assembled. There are two joints, one at the hip and one at the knee. The length of the leg, from the toe to the hip, is approximately 1 meter. The long bars protruding from the front and back of the body are fiberglass springs, which attach to the pulleys of the robot with a steel cable.

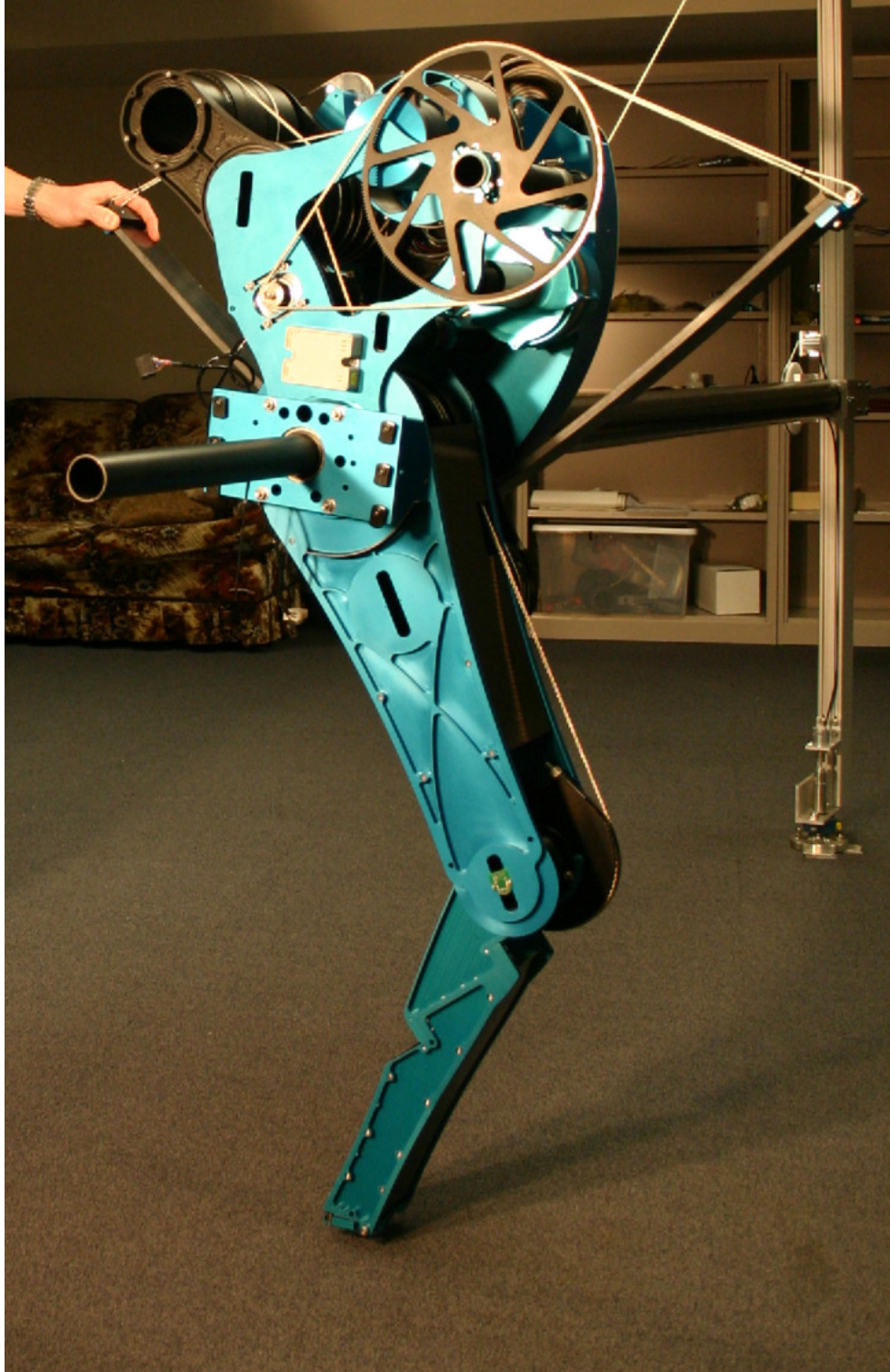


Figure 5.4: An assembled prototype leg of the Biped with Mechanically Adjustable Series Compliance, or BiMASC. This prototype used many of the same ideas from the AMASC, including co-contraction of antagonistic springs for stiffness adjustment. Based on testing of the BiMASC, the decision was made to eliminate the mechanically adjustable stiffness, and instead use active methods for on-the-fly adjustment of the leg spring behavior on the ECD Leg.

## 5.1 Background

The BiMASC is designed to exhibit dynamic behavior that closely matches a simple mathematical model. This model, in turn, is based on approximations of animal running behavior. The BiMASC incorporates ideas from the field of biomechanics, from direct observations of animal behaviors, and from existing running robots.

### 5.1.1 Comparable Robots

Many robots have been built for the purpose of walking and running. There are generally two classes: robots that utilize mechanical springs to store and release kinetic energy during a running gait (much like animals), and robots that do not. The planar biped from MIT's Leg Lab [Hodgins and Raibert, 1991] is an example of a spring-mass robot, using air springs for energy storage. This robot could also adjust the pre-load of air pressure in the cylinder, which affects the leg stiffness. Experiments used this degree of freedom to control aspects of the gait such as step length.

The planar biped was capable of high performance behavior such as front flips, because it was tethered to a large hydraulic compressor and air compressor. In contrast to the high power of many of Raibert's machines, the Bowleg Hopper from Carnegie Mellon University and the ARL Monopod II from McGill University both have defensible claims to being the most efficient running robots [Ahmadi and Buehler, 1999, Zeglin and Brown, 1998]. Both gain their efficiency by utilizing leg springs to effectively store and release energy during each stride, so the electric motors do relatively little work during a normal running gait.

The MIT Leg Lab's Spring Flamingo does use springs, but not for energy storage. The springs on the MIT-style Series Elastic Actuator (MIT-SEA) are primarily for force sensing and mechanical filtering purposes [Pratt and Pratt, 1998, Robinson et al., 1999]. An important distinction between the MIT-SEA and the AMASC is that although both systems consist of springs in series between the motor and the output, the springs in a MIT-SEA are at least an order of magnitude smaller and stiffer. The springs of a MIT-SEA are essentially a soft load cell, acting as a force sensor for the low-level controller. At low frequencies, the MIT-SEA acts as a more sensitive and robust force actuator than a gearmotor and load cell. While the AMASC can behave as a MIT-SEA, the purpose of the adjustable spring in the AMASC is to store energy during a running gait and to create desirable natural dynamics for a range of gaits.

Recent bipeds have also been constructed which can change the stiffness of their joints [Ham et al., 2005, Vanderborght et al., 2006]. However, these bipeds are not designed for running, and are similar to the MIT-SEA in that they do not store significant amounts of energy in their springs. Additionally, when using pneumatic actuators for the joint stiffness control [Vanderborght et al., 2006], the resulting system can be difficult to model and control precisely.

Robots with rigid transmissions such as Rabbit and Asimo do not use springs [Chevallereau et al., 2003]. This difference is important. If these robots are capable of an aerial phase, it is only at the expense of great motor power output and high energetic cost, with relatively unpredictable dynamic behavior at ground impact.

## 5.2 Philosophy

Our goal is to understand the principles of running, and to then leverage those principles to enable the creation of robots that effectively locomote in real-world environments. We seek to capture the essence of the physics and dynamics exhibited by a locomoting animal, rather than merely mimic the motion. By understanding the underlying dynamics, we hope to attain the stability, efficiency, and

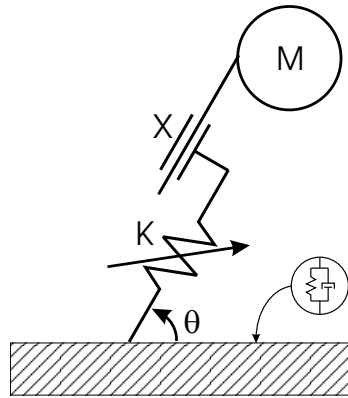


Figure 5.5: The spring-loaded inverted pendulum model.

robustness required to achieve effective running and walking. Our goal is not necessarily to create a robot that appears to run like an animal, although we believe that if the principles of running are understood and implemented properly, the outcome may be animal-like.

Determining which aspects of the behavior should be implemented in hardware and which aspects may be implemented through software control is a significant challenge of the robot design. The software can determine the robot behavior only within the limits of the mechanical system. For example, a gearmotor with a rigid connection to the leg cannot accurately simulate a spring during an impact event. This limitation is a crucial factor, because impacts are common in running.

We treat the behavior of the robot as an integrated system of mechanical, electrical, and software control components. The dynamics of the mechanism, sometimes referred to as the natural dynamics, are critical; properly tuned mechanical springs and close attention to leg mass and actuator dynamics (such as inertia) are as much a part of the control system as the software. The natural dynamics of the mechanism can create a basic cycle, analogous to a mechanical clock, and the software controller nudges the system to change speed or step length. The controller can also aid in recovery from disturbances. However, when the gait is undisturbed and cyclic, little influence is required from the software control system.

The BiMASC is designed to behave in a dynamically simple manner, closely following the SLIP model. While the complex dynamics of an animal may not be perfectly represented through simple models such as the SLIP, such simplifications are important to enable a useful understanding of the system behavior. Many existing mathematical models and control strategies are based on the SLIP model, and if the robot behavior closely matches that of the SLIP model, then model-based controllers can be applied directly to the robot. This attempt at dynamic simplicity has led to mechanical complexity and non-traditional mechanical design, with more moving parts than would normally be required for so few degrees of freedom.

### 5.3 Mechanical Design

The BiMASC is designed to be a highly dynamic running and walking planar robot. This project represents a challenging mechanical design problem, in part because there will be regular impacts between the toe and the ground, positive and negative torques about the joints that will accentuate any backlash, and high power density requirements for lifting the robot off the ground repeatedly.

These issues are addressed through careful attention to the natural dynamics, as well as some unusual design choices.

### 5.3.1 Design Choices

There are a number of decisions made at the beginning of the design that determine the basic morphology of the robot. Following our design philosophy, the BiMASC is intended to be a dynamically simple system, which can be modeled and controlled using the simple spring-loaded inverted pendulum (SLIP) model. This means the robot should have point feet, a prismatic leg spring with controllable stiffness that is large enough to store gait energy, control of hip angle and spring set point, low friction, and low leg mass. Practical considerations include low or zero backlash, and a clean mechanical design with no loose wires or parts that would oscillate during impacts.

We have chosen to add knees to the BiMASC, so that it may walk with dynamic gaits that are similar to human walkers. This choice is somewhat arbitrary—successful walkers and runners have bird-like legs, human-like legs, or even prismatic joints [Raibert, 1986]. We have also chosen to include onboard computing, to reduce the length of control wires and to gain experience towards building autonomous machines in the future. Only power is provided through a tether.

To achieve the goals of low backlash, low leg mass, and low friction, nearly all of the mechanical power transmission is implemented through highly efficient cable drives [Townsend, 1988]. Cable drives are rarely utilized, but are ideal for this particular application. Unlike gears or timing belts, they do not allow for continuous rotation; however, a legged robot requires only a limited range of motion on each joint. More importantly, cable drives have no backlash, because cables are tensioned against each other or against the antagonistic springs. They are lightweight for their torque capacity, because they can use thin aluminum shells for pulleys, compared to the thick steel required for gears. The torque capacity is limited primarily by the strength of the cable, which can be quite high. Cable drives can be very efficient (up to 96%) if properly implemented [Townsend and Salisbury, 1988].

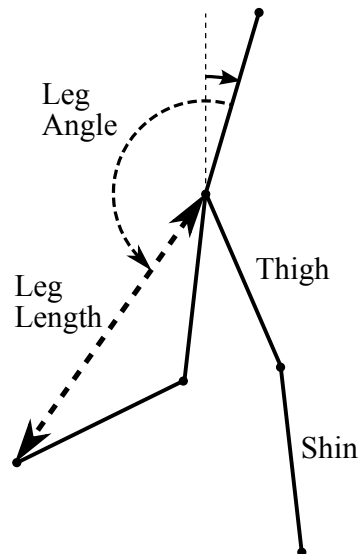


Figure 5.6: The basic configuration of the robot is a familiar humanoid leg shape. The thigh and shin are equal length, and the foot ends in a point contact. The leg length and leg angle are actuated through a series of differentials, rather than direct actuation of the hip and the knee.

In addition, the cables can transmit power across lengths of the leg, so the motors can be placed inside the body of the robot, with the legs remaining largely free of components and their mass.

The basic actuation of the BiMASC is based on the AMASC, using fiberglass springs and electric motors to implement a mechanically adjustable leg stiffness. In addition, the AMASC can use software control to accurately simulate zero torque at a joint, enabling passive leg swings for walking gaits.

Although the BiMASC has knees, the leg spring acts in the leg length direction, rather than acting on a particular joint. This transmission is implemented through the use of a series of five cable differentials, explained in detail in the following section.

### 5.3.2 Layout of Differentials

A differential is a special connection of three components ( $A$ ,  $B$ , and  $C$ ), and an internal, unobserved idler ( $D$ ). The kinematic equation for a differential is given by  $\frac{A+B}{2} = C$ . The components are constrained such that the average motion of two of the components ( $A$  and  $B$ ) is equal to the motion of the third ( $C$ ). Consequently,  $A$  and  $B$  can move in opposite directions if  $C$  is held stationary, and the motion of  $C$  will be half the speed of  $A$  if  $B$  is held stationary.

The differentials in the BiMASC are implemented through the cable drive, as depicted in Figure 5.7. Figure 5.8 illustrates the cable drive layout of one leg of the BiMASC. The cable drive system is made up of five cable differentials and three motors. Two differentials at the hip translate the shin angle and the thigh angle into leg length and leg angle, two more differentials allow the springs to be mounted to the body but still act in series with the motor, and the final differential separates the pretension from the set point, so one motor controls stiffness while the other controls position.

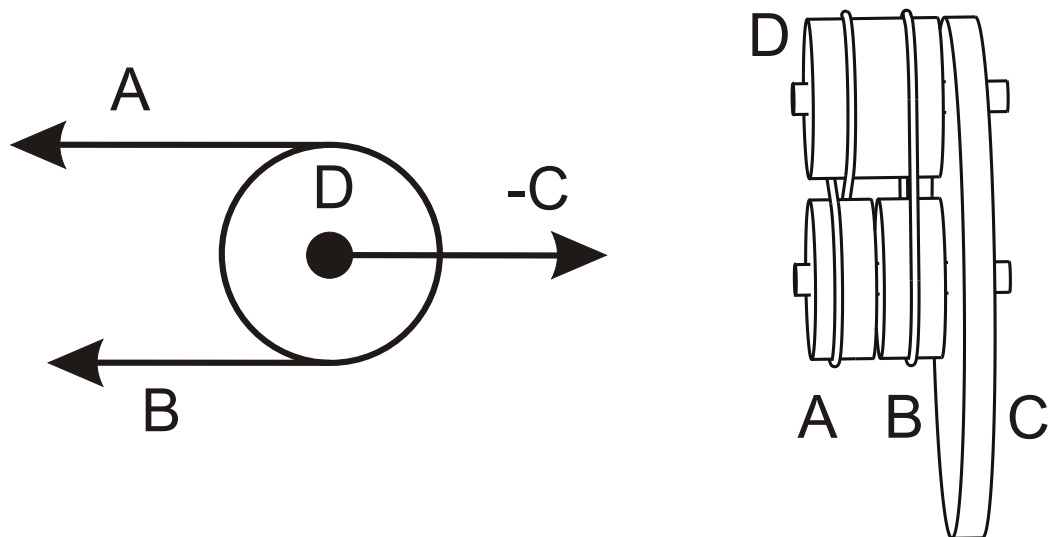


Figure 5.7: Implementations of a differential, identical in operation to an automotive differential, following the velocity constraint  $A + B = 2C$ . The AMASC uses the implementation shown at left, while The BiMASC uses the implementation on the right.

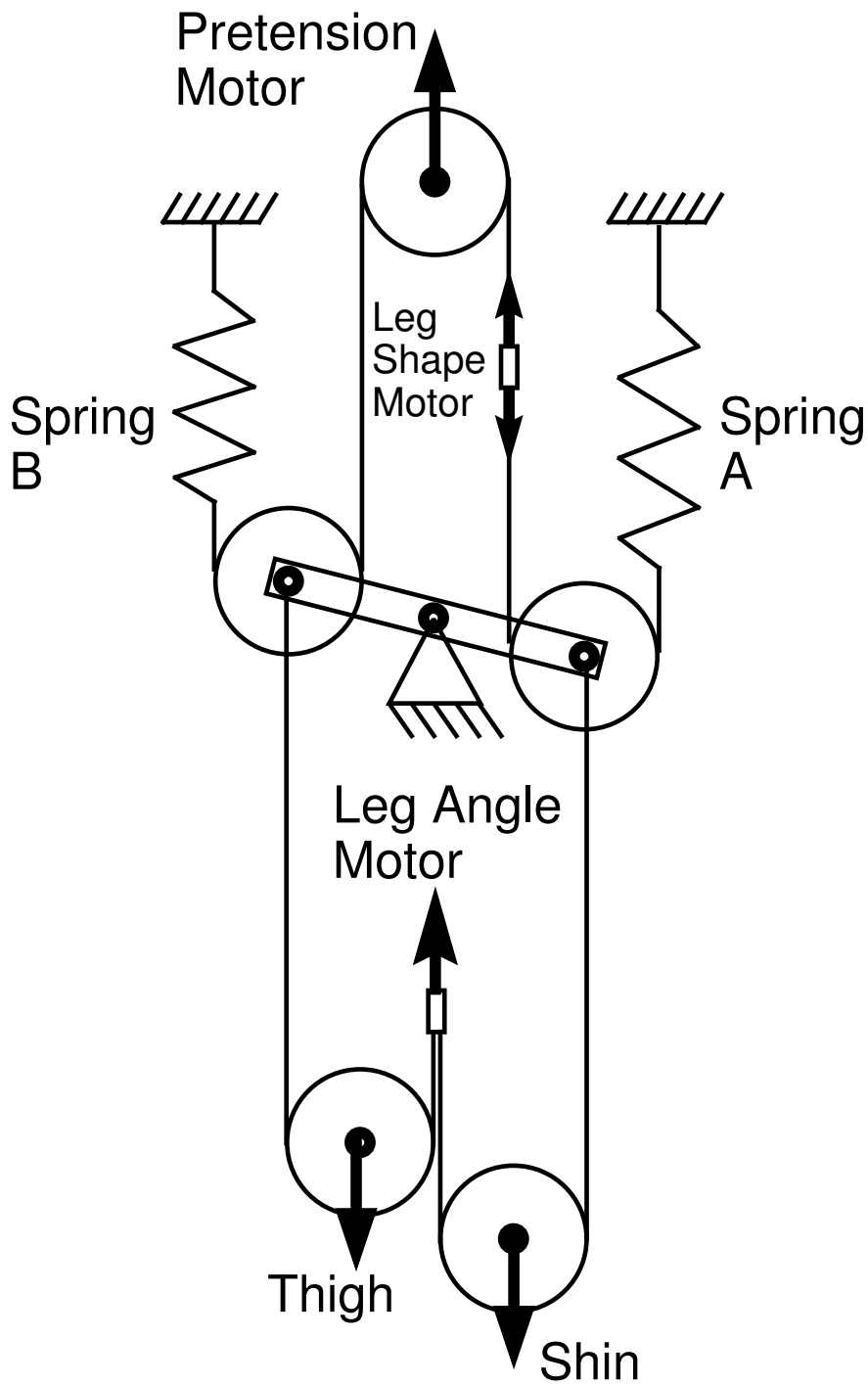


Figure 5.8: Conceptual diagram of differential placement in the BiMASC. Linear displacement of “Thigh” and “Shin” in the diagram correspond to rotational displacements relative to the body of those links on the robot. If the shin and thigh move in the same direction, the leg angle changes. If the shin and thigh move in opposite directions, the leg shape motor changes or the springs deflect differentially.

## Leg Length and Leg Angle

There are two degrees of freedom on the BiMASC, aside from leg stiffness: Leg Length, and Leg Angle. A pair of differentials in the hip translate the shin and thigh angles to leg length and leg angle, as in Figure 5.11, so the motors are actually linked to leg length and leg angle, and not to a particular kinematic leg joint. To translate from the conceptual diagram in Figure 5.8 to the robot kinematics in Figure 5.6, imagine linear displacements on the conceptual diagram corresponding to rotational displacements on the thigh and shin joints, relative to the body.

Notice that if the thigh angle and shin angle move by the same amount, the leg angle changes while the leg shape stays the same. In addition, because the thigh and shin are the same length, if the thigh angle and shin angle are changed by opposite amounts, the leg length changes while the leg angle stays the same. As a result, the hip differential is a transmission with leg length and leg angle as inputs, and thigh angle and shin angle as outputs. By connecting the leg length pulley to the AMASC made up of the top three differentials, the spring in the AMASC acts only along the leg length direction.

## Adjustable Spring Function

To adjust the spring stiffness along the leg length direction, we use two antagonistic springs. After creating a desired nonlinear spring function using the fiberglass spring and shaped spiral pulleys, placing two such spring/pulley systems in direct opposition results in a single effective torsional spring whose stiffness is determined by the pretension on each individual nonlinear spring. This configuration is identical to the AMASC.

The leg spring acts in series between the leg length motor and the actual leg length. To prevent the need for the entire spring to move when the set point changes, we connect each spring to the leg length motor via a differential, as shown in Figure 5.10. This configuration allows one end of the spring to remain grounded on the torso at all times, but still act in series between the motor and the leg length. These two differentials (one for each spring) are shown in the middle of Figure 5.8.

## Control of Set Point and Stiffness

The fifth differential in the BiMASC translates the set position of the two individual springs into an overall set position of the antagonistic pair, and the pretension of the springs, which corresponds to the leg stiffness. In other words, rather than controlling both springs independently, one motor controls the leg shape set point and one motor controls the leg stiffness. This functionality is identical to the AMASC. By separating the function of the motors into set point and pretension, different sizes and capabilities can be chosen for each motor. The pretension motor is relatively small and has a mechanical brake, so a particular stiffness value can be maintained without expending energy. The set point motor is large and powerful, to handle most of the energy of a running gait.

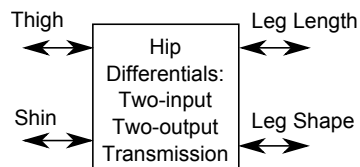


Figure 5.9: The hip differentials serve to translate the leg length AMASC and the leg angle motor into angular positions of the thigh and shin.

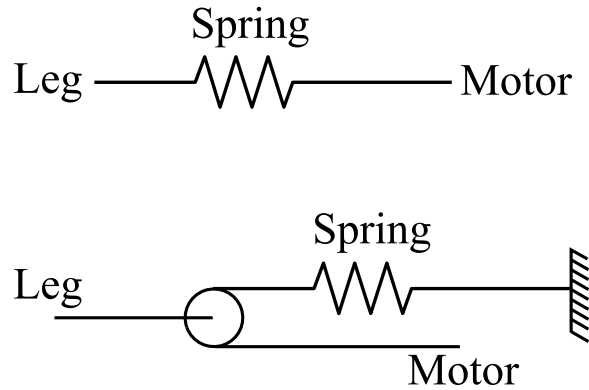


Figure 5.10: *TOP*: Series elastic element without differential. The entire spring moves back and forth. *BOTTOM*: With the differential, the spring can remain grounded at one end.

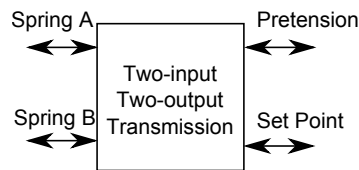


Figure 5.11: The top differential serves to translate the spring deflections of each spring into an overall set point and pretension.

### 5.3.3 Cables

There are many constraints to using stainless steel cables for cable drives. They must wrap around a sufficiently large diameter pulley, to prevent stretching and failure of the cable. They must be supported by a groove, to reduce wear and prevent the cable from rubbing on itself. The terminations must also be done carefully, to support the full load of the cable. To eliminate some of the pulley diameter constraints and to reduce overall weight, we hoped to use a more flexible cable material than steel, such as a polymer material. After some research, we ruled out most polymers, including Spectra, because they are subject to creep—over time, they will “relax” and lose their tension. Kevlar and similar materials are abrasive, and after some wrapping around a pulley, will tend to self-destruct. Vectran and Xylon were promising alternatives, with very high strength and low weight, and they were advertised to have no creep. Xylon is subject to significant weakening over time based on exposure to ultraviolet radiation, and after a few days the color of the material changed, so we chose to test only the Vectran cable.

Vectran is a recently developed material spun from liquid crystal polymer, and to our knowledge has not been used in a cable drive or high speed pulley-wrapping application. Before using Vectran in the design of the robot, we built a test rig to test the durability of the material while wrapping around a small pulley, shown in Figure 5.12. A DC motor moved the cable back and forth over an idler pulley in a sine-wave velocity curve, while a coil spring held the cable tension at approximately 20% of its breaking strength, the advertised working load.

The results of the experiment were disappointing, with cable failure after only a few minutes. The outside frayed quickly, and a waxy substance was left on the surface of the pulley, as can be seen in Figure 5.13. We speculate that the high internal damping of the Vectran cable, combined



Figure 5.12: The test setup for Vectran cable. A DC motor on the bottom right runs a linkage, which rotates the large pulley at the upper right of the device back and forth. The cable then rolls back and forth repeatedly on the small pulley at the upper left.

with the repeated stretch-relax cycle of wrapping around a pulley, caused high internal temperatures and melting of the material. Removing the cable after a test run, the section that had wrapped around the pulley was stiff and no longer flexible. It had a shiny surface under the fibers, as if there were melted wax inside the cable. In addition, a waxy substance was left on the aluminum surface of the pulley.

After this experiment, we chose to use the more standard steel cables, and design the pulleys of the robot according to the minimum pulley diameters and limits of the steel. In several locations, we have used a pair of cables to bear the necessary load, while still wrapping around a small diameter pulley.

## 5.4 Discussion

Designing the BiMASC for dynamic simplicity led to some unusual and novel mechanical solutions. For example, there are no gears or gearboxes; most of the transmissions are implemented with steel cables wrapped around aluminum pulleys. The motors are connected to the joints through a system of cable differentials, so forces from a single motor (or a spring) can be applied in directions that are unrelated to a single joint. We hope these ideas will be applied to future robotic systems with similar constraints.

After initial construction of the prototype BiMASC leg, we tested some of the basic functionality. We moved all of the joints through their entire range of motion, to verify that there was no



Figure 5.13: After just a few seconds, the cable started to fray, and leave a waxy substance on the pulley. We speculate that high internal damping leads to sufficiently high temperatures to melt the cable.

mechanical interference. We tested the robustness of the safety harness and the robot hard stops by lifting the machine in the air and throwing it towards the ground. We locked the motor shafts and manually bounced the robot in place. While most of the test results were encouraging and informative, it became apparent that antagonistic springs have significant tradeoffs. The springs, while physically very large and capable of storing significant energy, did not store enough energy as an antagonistic pair to convincingly bounce the robot in the air. This issue was the most significant of several small oversights in the design of the BiMASC.

There are several effects that can reduce the energy storage capacity of antagonistic springs by an order of magnitude over a single spring of the same size, shown mathematically in Appendix B. First, only one of the springs is actually compressing when the joint compresses—halving the potential energy storage—and the other spring is actually relaxing, and releasing energy into the compressing spring rather than into the joint. This effect accounts for approximately a factor of three. Additionally, the individual spring deflections are the sum of both the co-contraction and the joint deflection ( $p + x$ ), so increasing the co-contraction will reduce the maximum allowable joint deflection if we assume an upper and lower limit on the spring deflection. If the joint stiffness is to be adjusted by a factor of three (for example), then the maximum joint deflection will be reduced by a similar factor. Combining these two effects, the energy storage capacity of the springs for this example is reduced by a factor of 15. Aside from the reduction in energy storage capacity, using antagonistic pairs of springs increases internal forces beyond the applied joint forces, which increases friction and requires stronger parts. There is also an extra actuator for stiffness adjustment and other additional parts, which add mass and complexity to the system.

There are several methods for implementation of stiffness behavior in a running machine, and co-contraction of antagonistic springs is only one of them. After implementing the differential design used in the BiMASC and observing that it did not have sufficient energy storage for a running gait, the costs seem to be higher than the benefits. Although improvements could certainly be made to the mechanical design, the fundamental issues of high internal forces and reduced spring energy storage cannot be overcome, and present a useful piece of information for the design of variable stiffness mechanisms.



## Chapter 6

### The Electric Cable Differential Leg

The Electric Cable Differential (ECD) Leg is the final revision of the BiMASC design. We created three copies of the ECD Leg: one is the monopod named Thumper, in our lab at Carnegie Mellon University. Two are bolted together as a bipedal pair of ECD Legs, named MABEL and assembled in Professor Grizzle's lab at the University of Michigan. MABEL will be used as a platform to explore advanced feedback control theory for legged locomotion, and has already taken several steps of a walking gait [Westervelt et al., 2007].

In this chapter, we will briefly describe the software architecture and simulation of the robot, as well as the control algorithms, both derived from existing work. The mechanical design, a contribution of this thesis, is described in more detail, including the pulley transmission layout and its mathematical representation. Finally, we present experimental results from Thumper and from simulations of Thumper, hopping in place and hopping at forward speed. The experiments show that there is an energetically optimal leg stiffness for hopping in place or at speed.

#### 6.1 Robot Software and Simulation

The software framework for Thumper and MABEL's control system is based on RHexLib, a system architecture originally developed for RHex, a running hexapod robot [Saranli et al., 2001]. RHexLib provides tools for implementing robot controllers, switching between controllers, communicating over the network with a graphical user interface running on a different computer, and logging data, among other things. It runs on the QNX real-time operating system, and all controllers for Thumper run at 1kHz.

The dynamic model of Thumper is created using SD/FAST (<http://www.sdfast.com/>), which generates C code for simulating articulated rigid bodies. This simulation is designed as a development tool for robot controllers, and interfaces with the gait controller and the graphical user interface in exactly the same way as the robot. Thus, gait tuning and operation of the simulated robot uses the exact same interface as gait tuning and operation of the real robot, and much of the software can be tested and debugged on the simulation rather than on the real robot.

We represent the leg links, the torso, and the motor shafts as inertial bodies. However, we do not represent all of the pulleys in the transmission as independent inertial bodies, but rather combine those pulleys that are constrained to move together. Specifically, the simulation is made up of the following bodies: torso, thigh, shin, leg shape motor ( $q_{MLS}$ ), and leg angle motor ( $q_{MLA}$ ). Custom code specifies the forces on the inertial bodies in the system, such as spring forces and differential constraints.

The ground contact forces are modeled as a spring and damper in the vertical direction, with the added constraint that the ground can not pull the foot downward. Frictional force is modeled via

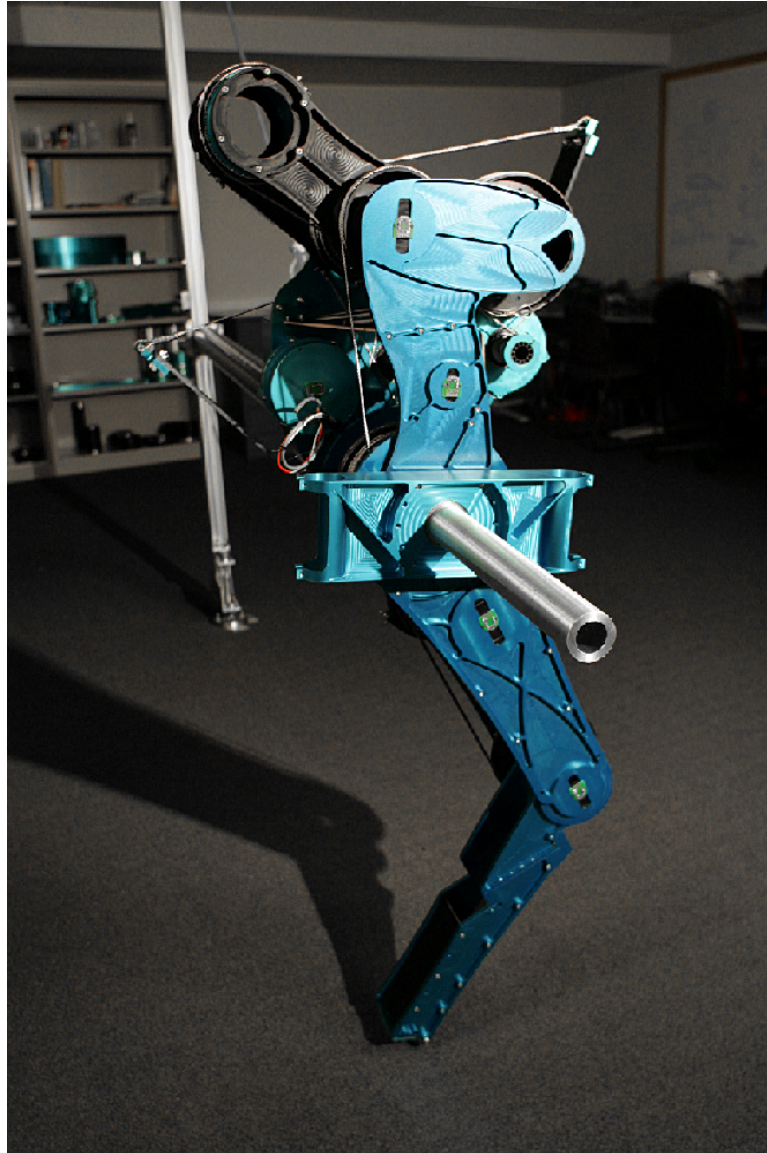


Figure 6.1: The Electric Cable Differential (ECD) Leg.

high damping in the horizontal direction. This model is inaccurate in comparison to real friction, but because the dynamics of the leg spring dominate the dynamics of the robot, the toe contact details are much less significant than they would be in a model without leg springs. The important aspect of toe contact is that the kinetic energy of the toe is removed within a small percentage of the overall stance time.

There are many differences between the simulation and the robot. Many of the machine parameters are estimates, such as knee damping, and many of the details of the machine are simplified in the simulation. Thus, it should be expected that the gait parameters that enable a stable running gait are slightly different between the robot and the simulation, and the optimal stiffness values are all different between the robot and the simulation.

Table 6.1: Simulation Parameters.

Torso Mass	23.1kg
Torso Rotational Inertia	0.894kg · m <sup>2</sup>
Thigh Mass	2.88kg
Thigh Rotational Inertia	0.317kg · m <sup>2</sup>
Shin Mass	2.54kg
Shin Rotational Inertia	0.114kg · m <sup>2</sup>
$q_{MLS}$ Rotational Inertia	$7.3 \times 10^{-4}$ kg · m <sup>2</sup>
$q_{MLA}$ Rotational Inertia	$3.6 \times 10^{-4}$ kg · m <sup>2</sup>

## 6.2 Robot Controller

The software control for experiments with Thumper is derived from the control methods described in “Legged Robots That Balance” [Raibert, 1986]. The control can be broken into three separate components: hopping height, forward speed, and body pitch. While all three aspects of the running gait may affect each other, the controller treats them as if they were decoupled.

The hopping height is regulated by adjusting the amount of energy that the leg length motor inserts while the robot is on the ground. The motor holds position while the leg spring compresses in the first half of stance, and just as the spring begins to decompress and lift the robot, the motor compresses the spring slightly further, adding to its stored energy. The peak height of the resulting hop is measured, and the amount of motor-induced spring compression is adjusted accordingly, to regulate the hopping height to the desired value.

Body pitch can only be controlled while the robot is on the ground and able to use ground reaction forces to apply torques to the body. The body pitch is servoed to a fixed angle relative to the ground, using a simple proportional-derivative controller. When the toe leaves the ground, the body may have some accidental rotational velocity, which will change the pitch of the body throughout the flight phase. This pitch error is corrected after landing again.

Forward velocity of the robot is controlled by adjusting the leg angle at touchdown. During the flight phase, while the robot is in the air, the forward velocity is measured. The leg servos to a position that is proportional to the measured velocity; faster velocity corresponds to a steeper leg angle and longer stride length. To increase the speed, the leg angle is set farther back, causing the robot to lean forward and accelerate. To decrease the speed, the leg angle is set farther forward, causing the robot to lean backwards and decelerate.

We noted that Thumper’s body pitches forward at each liftoff, perhaps due to the abrupt deceleration of the leg as it reaches its full extension. In order to correct this observed instability, we added an additional control law, beyond that described in “Legged Robots That Balance”: the commanded angle of the torso during stance is a function of the leg spring deflection, imparting a backwards rotation to the torso at liftoff, canceling the forward body pitch. This control law enabled stable hopping gaits, and was used for all experiments of Thumper hopping in place. However, the added control law did not stabilize body pitch for hopping at speed, because the leg must swing forward during each flight phase, causing the body of the robot to pitch as angular momentum is conserved. To counter this problem, we added long bars and weights to Thumper’s torso, significantly increasing the rotational inertia. The increased torso inertia eliminated the need for the added pitching control law, and enabled hopping at higher speeds. We used this increased torso inertia for all simulation and experiments of hopping at speed.

Thumper was designed so the natural dynamics of the machine would match a simple controllable model. Successful running with these simple controllers shows that the mechanical design

met this goal. We believe that more advanced controllers would significantly improve and expand the performance of this machine, although these basic controllers served as an excellent proof of concept.

## 6.3 Mechanical Design

The ECD Leg is designed to behave in a dynamically similar manner to the spring-mass model of Figure 5.5, so the dynamic behaviors can be quantified and controlled. There are two motors—one to control the leg angle, and another to control the leg length, with a large spring placed in series between the leg length motor and the actual leg length. The ECD Leg has a knee joint, partly to enable human-like ballistic walking, and partly to incorporate an adjustable mechanical advantage for leg stiffness adjustment. The leg ends in a simple rounded toe, with no articulation or actuation.

Like the earlier prototypes, the ECD Leg uses electric motors, a cable drive transmission, and mechanical differentials to implement the desired relationships between motors and joints. However, leg stiffness adjustment is achieved through modification of the physical spring behavior using active software control during the toe's ground contact time. The stiffness adjustment is also achieved through changes to the knee angle upon landing. The ECD Leg has no antagonistic springs, and cannot adjust its stiffness mechanically, like the BiMASC or AMASC. It is, however, lower mass and mechanically simpler than the BiMASC, which we believe to be a worthwhile tradeoff.

A series of mechanical differentials determine the relationship between the motors and the legs. Three cable differentials are used to convert leg length and leg angle to shin and thigh angles, and for placing springs in series, although they are bolted to the body, the same as the BiMASC. However, there are two fewer differentials, because we have eliminated the top differential and one spring differential, significantly simplifying the system. Each pulley in the system has a label, which does not necessarily correspond directly with a configuration variable such as  $q_{LS}$  or  $q_{LA}$ . In this section, we will describe the function and layout of each differential, with a diagram illustrating the location of each pulley and the label for each relevant component. The ECD Leg is philosophically similar to the BiMASC, described in Chapter 5, so basic ideas are not repeated in this chapter; however, many of the detailed calculations about the differentials, springs, and cable forces are recorded here.

### 6.3.1 System Notation

Analysis of the differentials and control of the ECD Leg requires a clear notation defining all degrees of freedom. Our system coordinates begin with those defined in Figure 6.2, and all other coordinates are based on these basic coordinates. The leg angle,  $q_{LA}$ , is the angle between the torso and a line drawn from the hip to the toe, and is related to the thigh angle and shin angle:

$$q_{LA} = \frac{\theta_{Ct} + \theta_{Cs}}{2}. \quad (6.1)$$

The Leg Shape,  $q_{LS}$ , is associated with leg length:

$$LL = 2d \cos(q_{LS}) \quad (6.2)$$

$$q_{LS} = \arccos\left(\frac{LL}{2d}\right), \quad (6.3)$$

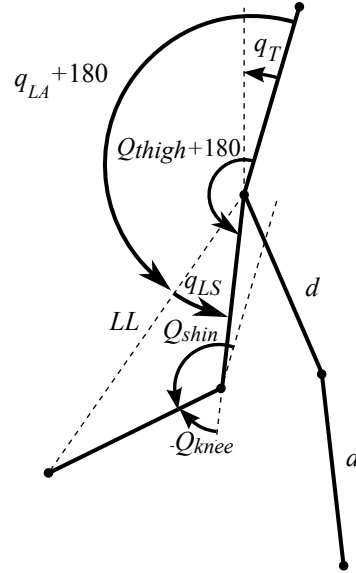


Figure 6.2: Official notation for all calculations on the ECD Leg. Leg Length,  $LL$ , is the length of the line from the hip to the toe, and leg angle,  $q_{LA}$ , is measured between that line and the torso angle,  $q_T$ . The leg shape,  $q_{LS}$ , is a rotational angle, and related by a sine function to the leg length.

but it is maintained as an angle rather than a length for our calculations. The physical representation of the leg shape is the angle from the dotted line between the toe and the hip to the thigh, and it relates the leg angle,  $q_{LA}$ , to the thigh angle,  $q_{thigh}$ :

$$q_{LA} + q_{LS} = \theta_{Ct}. \quad (6.4)$$

The angle of the knee is related to the angle of the shin and thigh:

$$\theta_{knee} = \theta_{Cs} - \theta_{Ct}, \quad (6.5)$$

and the leg shape is related to the thigh angle and shin angle:

$$q_{LS} = -\frac{\theta_{knee}}{2} = \frac{\theta_{Ct} - \theta_{Cs}}{2}. \quad (6.6)$$

### 6.3.2 Mechanical Differentials in General

Differentials can be implemented in a variety of different ways, several of which are illustrated in Figure 6.3. All methods adhere to the following velocity constraints, where  $\omega$  is the rotational velocity of a pulley or linear velocity of a cable, whichever is applicable:

$$\omega_C = \frac{\omega_A + \omega_B}{2} \quad (6.7)$$

$$\omega_D = \frac{\omega_A - \omega_B}{2}. \quad (6.8)$$

A derivation of the velocity constraints for a general differential is presented in Appendix A.

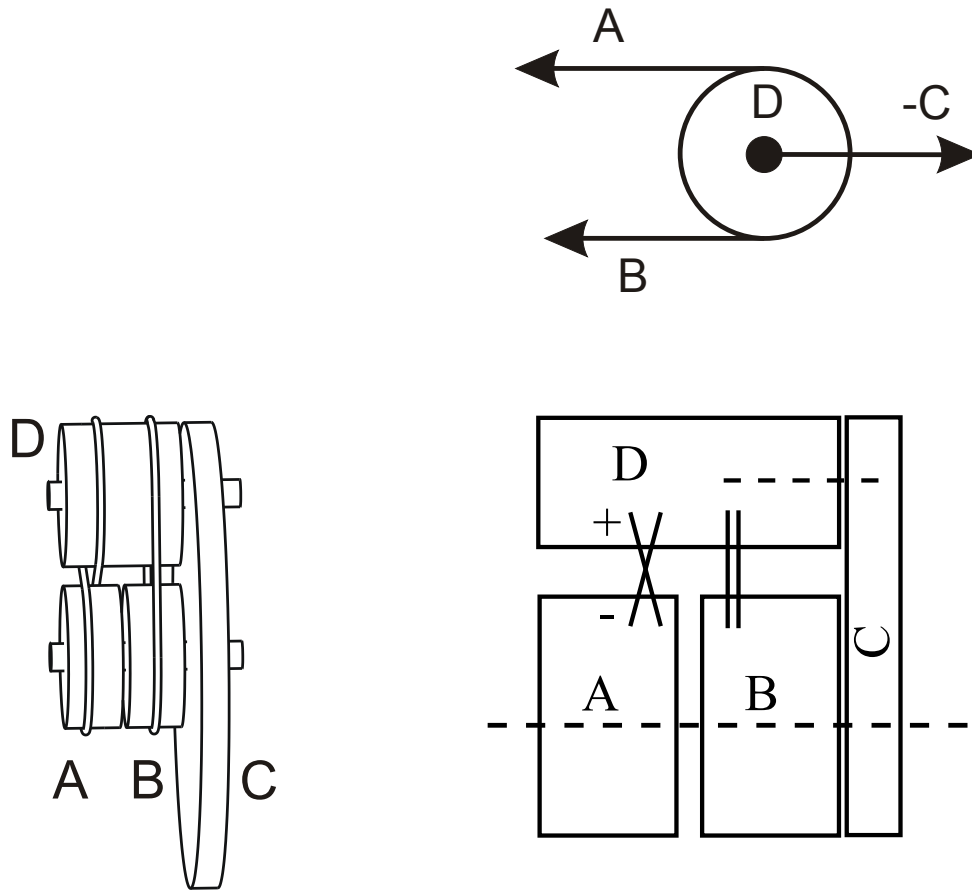


Figure 6.3: Different representations of a differential. The picture on the lower left depicts a cable differential, which is used for this mechanism. It is similar to a planetary differential. The simplified representation of this cable differential, which we use for diagrams and notation, is depicted on the lower right. The crossed and straight lines in between the pulleys depict the figure-eight wrap or the straight wrap of the cables, determining when a sign change takes place between two pulleys. The  $A$ ,  $B$ , and  $C$  pulleys all rotate about the same axis, while the  $D$  pulley rotates about a shaft mounted to the  $C$  pulley.

The torque transmitted through a differential is different than the position or velocity, and is required to calculate the cable tensions and the torque amplification of the motors. To calculate the torques of a differential transmission, we begin by stating known constraints. If the positive direction is the same for each pulley (counterclockwise, for example), then we know that the torque of  $A$  and  $B$  are always the same:

$$\tau_A = \tau_B. \quad (6.9)$$

The velocities are constrained:

$$\omega_A + \omega_B = 2\omega_C, \quad (6.10)$$

and the power must balance:

$$\omega_{ATA} + \omega_{BTB} + \omega_{CTC} = 0. \quad (6.11)$$

From these definitions, we can derive the following:

$$(\omega_A + \omega_B)\tau_A + \omega_C\tau_C = 0 \quad (6.12)$$

$$\omega_C\tau_C + 2\omega_C\tau_A = 0 \quad (6.13)$$

$$\omega_C(\tau_C + 2\tau_A) = 0 \quad (6.14)$$

$$\tau_C + 2\tau_A = 0 \quad (6.15)$$

$$\tau_C = -2\tau_A \quad (6.16)$$

$$\tau_C = -\tau_A - \tau_B \quad (6.17)$$

$$\tau_C + \tau_A + \tau_B = 0. \quad (6.18)$$

The result is a torque balance on each pulley, which matches what is expected of a differential. This equation also implies that the forces on the cables that connect the pulleys will be equal, so they should all be the same strength and size.

### 6.3.3 Mechanical Differential Configuration and Notation for Thumper

The initial design of the differential configuration was done with simple diagrams and sketches, connecting differentials to one another with various constraints. To verify the velocity constraints, we built a Lego model of the BiMASC differential tree, shown in Figure 6.4. However, for the detailed design of the pulleys, a more careful analysis must be done, to determine the exact range of rotation for each pulley and the forces on each cable. The range of pulley rotation determines the location of the cable termination, which must be machined into the shape of the pulley. Knowing the cable forces is necessary to appropriately size the cables, and to design the entire mechanism to minimize the pulley and cable sizes, while still supporting the stresses throughout the system.

We begin with the following definitions:

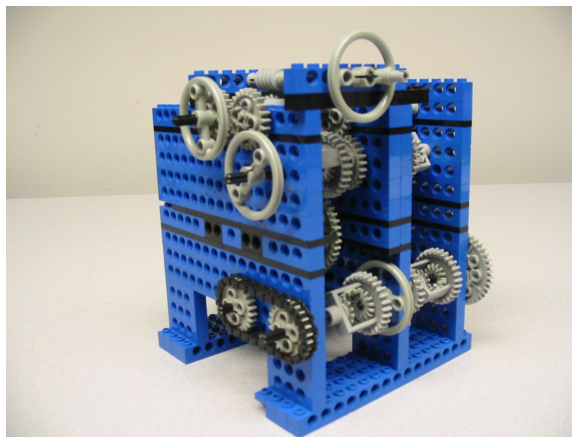


Figure 6.4: A prototype of the BIMASC differential tree, built from Legos, verifying the mathematical representation of the differentials.

- Each pulley has a unique label, which can be used in calculations.
- $q$  is used to describe the coordinate system angles, and completely define the configuration of the robot. The controller interacts only with the  $q$  variables, and motors are all labeled with  $q$  variables.
- $\theta$  refers to a rotational angle of a labeled pulley.
- $r$  refers to the radius of a labeled pulley.
- $\tau$  is the torque of a motor or an outside force.
- $X$  is a linear displacement, such as that of a cable unwrapping from a pulley.
- a superscript “\*,” as in  $LL^*$ , indicates a desired value rather than a measured value.

For the analysis and calculations of cable stress and pulley rotation, we assume that the system is in static equilibrium, thus no pulley inertias affect the cable forces. We also ignore any effects of friction, which are negligible compared to the overall loads. Although the cable pairs on each pulley have a pre-load to tension them against each other, we are considering only the difference in the cable tension, or the resulting applied torque to the pulley. In the real system, the cables will stretch, and the pre-load is necessary to prevent cables from going slack and falling out of pulley grooves; but if the pre-load is roughly half the peak load that the cables will see in operation, then the peak pulley torque will result in one cable at zero tension and one cable at its peak load. The result is similar to ideal stretch-free cables with no pre-load, so we can safely ignore this detail in the analysis.

## Hip Differential

The hip differential takes two inputs, the shin angle and the thigh angle, and transforms them into the leg angle and the leg shape. Cables connect to the hip differential from the leg shape motor and from the spring differential, which controls the leg length. The hip differential is actually a pair of two discrete cable differentials, constrained in several places to exhibit the desired transmission relationship. To calculate the forces on the cables and the relationships between motor torques and relevant degrees of freedom, we start with some basic force balances and position constraints.

Force balances from the diagram in Figure 6.5:

$$F_{BsDs}r_{Bt} + F_{BtDt}r_{Bt} + F_{BtMLA}r_{Bt} = 0 \quad (6.19)$$

$$F_{BtMLA} = \frac{\tau_{MLA}}{r_{MLA}} \quad (6.20)$$

$$F_{AtDt} = F_{AtCsp} = F_{BtDt} \quad (6.21)$$

$$F_{AsDs} = -F_{AsCsp} = F_{BsDs} \quad (6.22)$$

$$F_{AtDt}r_{At} + F_{BtDt}r_{Bt} + \tau_{thigh} = 0 \quad (6.23)$$

$$r_{At} = r_{Bt} \quad (6.24)$$

$$F_{AtDt}r_{At} + F_{BsDs}r_{Bt} + \tau_{shin} = 0. \quad (6.25)$$

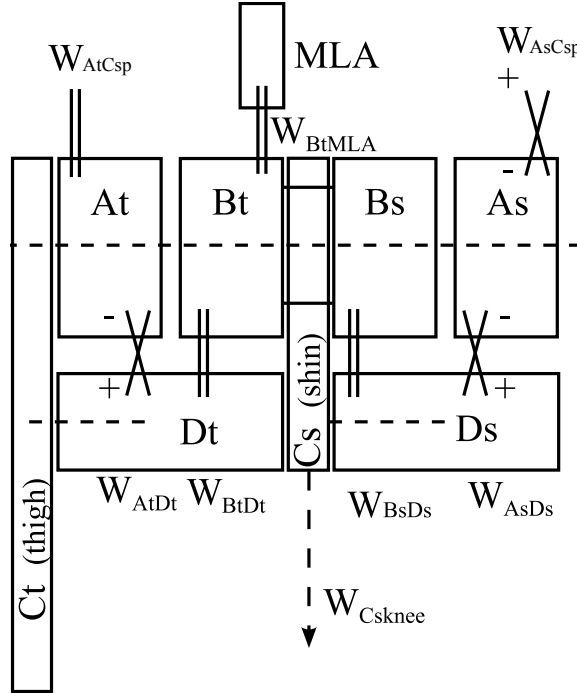


Figure 6.5: Hip differential, including labeled cables. Dashed lines depict axes of rotation, with the  $D$  pulley axes fitted to the rotating frame of reference of their corresponding  $C$  pulleys.  $B_t$  and  $B_s$  are physically the same pulley, representing a constraint between the thigh and shin differentials. The leg angle motor,  $qMLA$ , connects to them.  $C_s$  connects directly to the knee joint, and corresponds to the angle of the shin.  $A_t$  and  $A_s$  both connect to the same pulley ( $C_{sp}$ ) on the spring differential, and are thus constrained to rotate equal and opposite each other.  $C_t$  is actually the thigh itself, which houses the  $D_t$  pulley and rotates about the same axis as  $A_t$ ,  $B_t$ ,  $B_s$ , and  $A_s$ .

Position constraints from the diagram in Figure 6.5:

$$\theta_{B_t} + \theta_{A_t} = 2\theta_{C_t} \quad (6.26)$$

$$\theta_{B_s} + \theta_{A_s} = 2\theta_{C_s} \quad (6.27)$$

$$\theta_{B_t} r_{B_t} = q_{MLA} r_{MLA} \quad (6.28)$$

$$\theta_{B_s} = \theta_{B_t} \quad (6.29)$$

$$\theta_{A_t} = -\theta_{A_s}. \quad (6.30)$$

The motors are referred to by the variable  $q$ , and are related to the physical pulleys  $\theta$  by a constant ratio:

$$\theta_{B_t} r_{B_t} = q_{MLA} r_{MLA}. \quad (6.31)$$

Many of the radii of the differential pulleys are the same, which simplifies the equations:

$$r_{A_t} = r_{B_t} = r_{B_s} = r_{A_s}. \quad (6.32)$$

Based on these equations, we can derive the following:

$$F_{BtDt}r_{Bt} = \frac{-\tau_{thigh}}{2} \quad (6.33)$$

$$F_{AtCsp} = \frac{-\tau_{thigh}}{2r_{At}} \quad (6.34)$$

$$F_{BsDs}r_{Bs} = \frac{-\tau_{shin}}{2} \quad (6.35)$$

$$F_{AsCsp} = \frac{\tau_{shin}}{2r_{As}}. \quad (6.36)$$

Combining equations 6.19, 6.20, 6.33, and 6.35, and keeping in mind that many pulley radii are identical from (6.32), we can find the relationship between the leg angle motor and the shin and thigh:

$$-\frac{\tau_{shin}}{2} - \frac{\tau_{thigh}}{2} + \tau_{MLA} \frac{r_{Bt}}{r_{MLA}} = 0 \quad (6.37)$$

$$\tau_{MLA} \frac{r_{Bt}}{r_{MLA}} = \frac{\tau_{shin} + \tau_{thigh}}{2}. \quad (6.38)$$

### Spring Differential

The spring differential places the fiberglass bar springs in series between the leg shape motor,  $q_{MLS}$ , and the actual leg shape. Because of this differential, the springs can be physically bolted to the body of the robot, sharing a base with the motors, rather than shuttling back and forth with the motion of the leg. Bolting the springs to the body of the robot allows us to make them much larger and store sufficient energy for a running gait, while avoiding the leg mass of leg-mounted springs.

Positions from Figure 6.6:

$$\theta_{Asp} + \theta_{Bsp} = 2\theta_{Csp} \quad (6.39)$$

$$\theta_{Asp}r_{Asp} = q_{MLS}r_{MLS}. \quad (6.40)$$

Forces and torques from Figure 6.6:

$$F_{MLS}r_{Asp} - F_{AspDsp}r_{Asp} = 0 \quad (6.41)$$

$$F_{AspDsp}r_{Asp} + F_{BspDsp}r_{Bsp} + F_{AtCsp}r_{Csp} + F_{AsCsp}r_{Csp} = 0 \quad (6.42)$$

$$F_{AspDsp}r_{Dsp} - F_{BspDsp}r_{Dsp} = 0 \quad (6.43)$$

$$F_{MLS}r_{Asp} - F_{AtCsp}r_{Csp} - F_{AsCsp}r_{Csp} = 0 \quad (6.44)$$

$$F_{MLS}r_{MLS} = \tau_{MLS}. \quad (6.45)$$

Equivalences:

$$F_{AspDsp} = F_{BspDsp} = F_{MLS}. \quad (6.46)$$

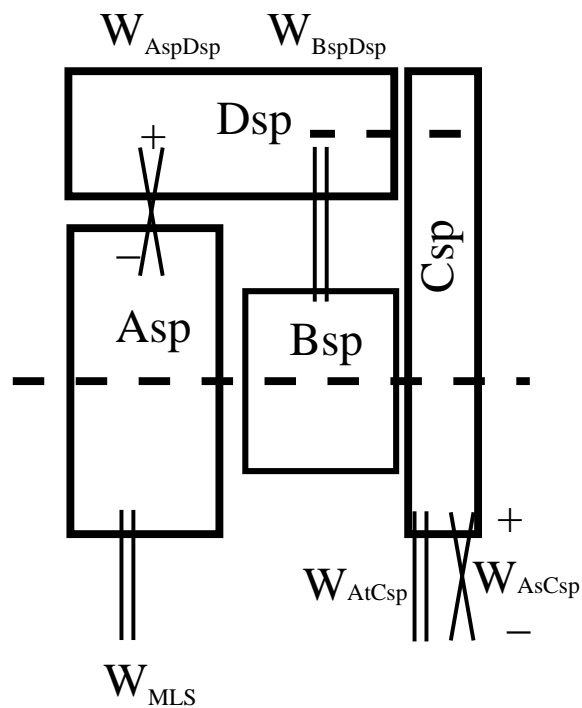


Figure 6.6: Spring differential, including labeled cables. The purpose of this differential is to allow the fiberglass bar springs to be bolted to the body of the robot, but still act as if they were in series with the leg shape motor like a springy tendon. Dashed lines depict axes of rotation, with the  $D$  pulley axes fitted to the rotating frame of reference of the  $C$  pulley.  $W_{AtCsp}$  and  $W_{AsCsp}$  cables connect the spring differential to the hip differential.  $W_{MLS}$  connects to the leg shape motor. The  $B_{sp}$  pulley connects directly to the fiberglass bar springs, and acts as a linear torsional spring.

Combining equations 6.45, 6.33, 6.35 and 6.45, we can calculate the relationship between leg shape torque,  $\tau_{MLS}$ , and the thigh and shin torques,  $\tau_{thigh}$  and  $\tau_{shin}$  :

$$F_{MLS} = F_{AtCsp}r_{Csp} + F_{AsCsp}r_{Csp} \quad (6.47)$$

$$F_{MLS} = \frac{\tau_{shin}}{2r_{As}r_{Asp}} - \frac{\tau_{thigh}}{2r_{At}r_{Asp}} \quad (6.48)$$

$$\tau_{MLS} = \tau_{shin} \frac{r_{MLS}}{2r_{As}r_{Asp}} - \tau_{thigh} \frac{r_{MLS}}{2r_{At}r_{Asp}}. \quad (6.49)$$

Because  $A_s$  and  $A_t$  are the same diameter, equal shin and thigh torques will cancel and transmit no torque to the leg shape motor. Conversely, equal and opposite torques will be entirely transmitted to the leg shape motor.

### 6.3.4 Pulley Workspace

The workspace of the leg is determined by an imaginary line drawn from the hip to the toe, as shown in Figure 6.2. The angle of this line relative to the body is called Leg Angle,  $q_{LA}$ . The length of this line is directly related to the Leg Shape,  $q_{LS}$ , where the actual leg length is  $LL = 2d \cos(q_{LS})$ .

Home position for the robot is with the springs completely relaxed, the Leg Angle completely vertical, and the Leg Length fully extended. The Leg Shape can move an additional  $5^\circ$ , to slightly hyperextend the knee, but the home position places the thigh and shin parallel to each other. For a given cable, the home position is the line drawn between two pulleys; if a pair of pulleys is contained in a moving frame of reference, as is the case for several of the differential pulleys, the home position for that pair can move relative to the body coordinates. However, the home position of the robot fixes and completely defines the home positions for all of the pulleys.

Our constraints are chosen based on the range limits of the leg and the deflection limits of the springs:

- Spring pulleys may only rotate 160 degrees.
- Leg Shape,  $q_{LS}$ , can range from  $-5^\circ$  to  $55^\circ$ , which implies that the thigh range is  $-5^\circ$  to  $55^\circ$ , and the knee joint range is  $-10^\circ$  to  $110^\circ$ .
- Leg Angle has a range of  $\pm 45^\circ$ .

Given these constraints, we can derive the range of motion of the entire system from the equations that describe the differentials. The range of motion of each pulley is required for their detailed design, to locate the cable terminations correctly on each pulley, as shown in Figure 6.7. Beginning with a list of pulleys and pulley radii:

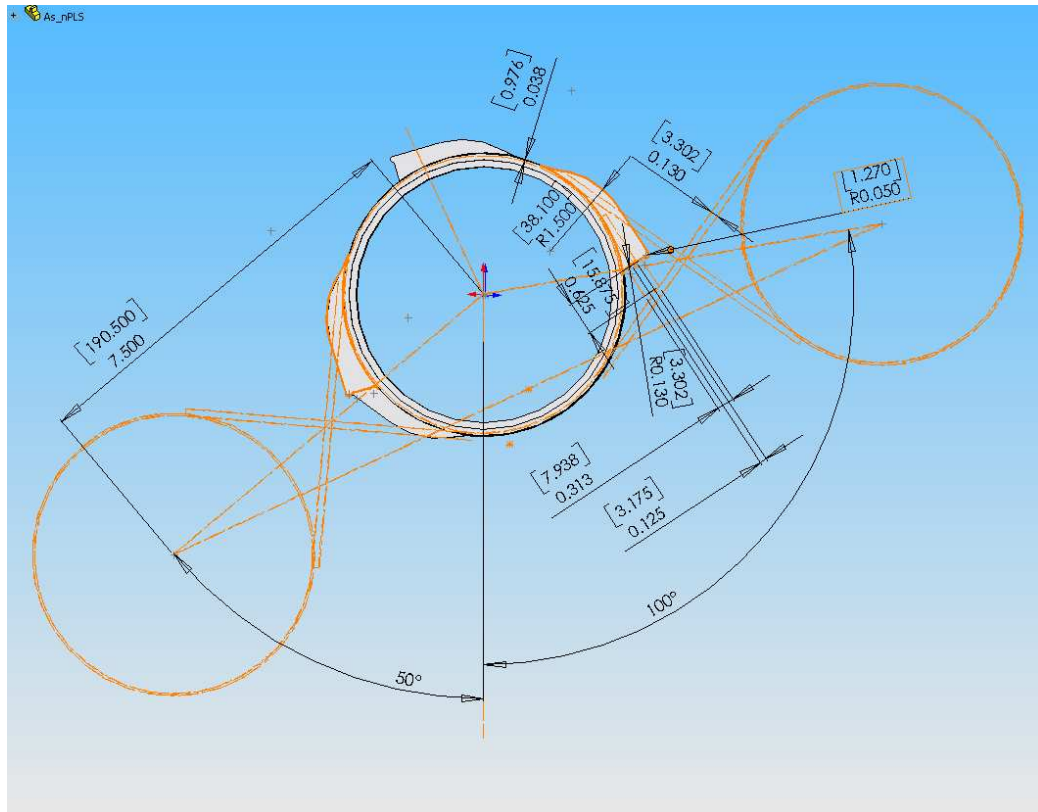


Figure 6.7: An example drawing from SolidWorks, showing the  $A_s$  pulley (center of image) and  $W_{AsDs}$ , the cable that interacts with the  $D_s$  pulley. The two shadowed pulley images show the maximum and minimum possible extent of the range of motion for the  $D_s$  pulley, relative to the  $A_s$  pulley. The calculated range of motion of the cable interaction is  $[-50, 100]$ . Positive rotation is counter-clockwise, as defined by Figure 6.2. From our standard notation of A, B, C, and D pulleys, only the A and D pulleys are shown in this image. The line from the A to the D pulley corresponds to the orientation of the C pulley (not shown).

$r_{As}$	2.60
$r_{Asp}$	2.60
$r_{At}$	2.60
$r_{Bs}$	2.60
$r_{Bsp}$	1.62
$r_{Bt}$	2.60
$r_{Cs}$	3.18
$r_{Csp}$	2.60
$r_{Ds}$	2.60
$r_{Dsp}$	2.60
$r_{Dt}$	1.75
$r_{LA}^b$	3.00
$r_{LA}^s$	0.825
$r_{LS}^b$	3.50
$r_{LS}^s$	1.25
$r_{mLA}$	0.750
$r_{mLS}$	0.750

We now describe the relations that define the three individual differentials in the ECD Leg transmission. The thigh differential:

$$r_{At}\theta_{At} + r_{Bt}\theta_{Bt} - (r_{At} + r_{Bt})\theta_{Ct} = 0 \quad (6.50)$$

$$\theta_{At} - \theta_{Bt} + r_{Dt}(1/r_{At} + 1/r_{Bt})\theta_{Dt} = 0. \quad (6.51)$$

the shin differential:

$$r_{As}\theta_{As} + r_{Bs}\theta_{Bs} - (r_{As} + r_{Bs})\theta_{Cs} = 0 \quad (6.52)$$

$$\theta_{As} - \theta_{Bs} + r_{Ds}(1/r_{As} + 1/r_{Bs})\theta_{Ds} = 0. \quad (6.53)$$

and the spring differential:

$$r_{Asp}\theta_{Asp} + r_{Bsp}\theta_{Bsp} - (r_{Asp} + r_{Bsp})\theta_{Csp} = 0 \quad (6.54)$$

$$\theta_{Asp} - \theta_{Bsp} + r_{Dsp}(1/r_{Asp} + 1/r_{Bsp})\theta_{Dsp} = 0. \quad (6.55)$$

Finally, the equations that define interconnections of the differentials to form the ECD Leg's transmission;  $B_t$  and  $B_s$  are physically the same pulley, linking the shin and thigh differentials:

$$\theta_{Bt} - \theta_{Bs} = 0. \quad (6.56)$$

The  $C_{sp}$  pulley on the spring differential is connected to the  $A_s$  pulley on the shin differential with a straight connection, and to the  $A_t$  pulley on the thigh differential with a crossed cable:

$$r_{Csp}\theta_{Csp} + r_{As}\theta_{As} = 0 \quad (6.57)$$

$$r_{Csp}\theta_{Csp} - r_{At}\theta_{At} = 0. \quad (6.58)$$

The small side of the leg angle speed reducer pulley is connected to  $B_t$  (same as  $B_s$ ) of the thigh and shin differentials, with a crossed cable:

$$r_{LA}^s\theta_{LA}^s + r_{Bt}\theta_{Bt} = 0. \quad (6.59)$$

The leg angle and leg shape speed reducer pulleys both have two different diameters, but each consist of only one shaft:

$$\theta_{LA}^s - \theta_{LA}^b = 0 \quad (6.60)$$

$$\theta_{LS}^s - \theta_{LS}^b = 0. \quad (6.61)$$

The  $q_{MLA}$  leg angle motor pulley is connected to the larger diameter of the leg angle speed reducer pulley, while the leg shape motor is connected to the larger diameter of the leg shape speed reducer:

$$r_{mLA}q_{mLA} - r_{LA}^b\theta_{LA}^b = 0 \quad (6.62)$$

$$r_{mLS}q_{mLS} - r_{LS}^b\theta_{LS}^b = 0. \quad (6.63)$$

The leg shape pulley is attached to  $A_{spring}$  of the spring differential:

$$r_{LS}^s\theta_{LS}^s - r_{Asp}\theta_{Asp} = 0. \quad (6.64)$$

The standard coordinate for leg shape,  $q_{LS}$ , is related to the physical pulleys by the following relationship:

$$q_{LS} + (\theta_{Cs} - \theta_{Ct})/2 = 0, \quad (6.65)$$

and the standard coordinate for leg angle,  $q_{LA}$ , is related to physical pulleys by the following relationship:

$$q_{LA} - (\theta_{Cs} + \theta_{Ct})/2 = 0. \quad (6.66)$$

The sets of equations (6.50) through (6.66) can be combined to yield seventeen equations in twenty variables. They can be solved in terms of any three variables, using a solver such as Matlab. Solving in terms of  $q_{LA}$ ,  $q_{LS}$  and  $\theta_{Bsp}$  and substituting for our range of motion limitations,  $-45^\circ \leq q_{LA} \leq 45^\circ$ ,  $-5^\circ \leq q_{LS} \leq 55^\circ$ , and  $0^\circ \leq \theta_{Bsp} \leq 160^\circ$ , results in the range of motion of each pulley in the system:

$\theta_{As}$	$-2q_{LS}$	$[-110, 10]$
$\theta_{Aasp}$	$-0.625\theta_{Bsp} + 3.25q_{LS}$	$[-116.25, 178.75]$
$\theta_{At}$	$2q_{LS}$	$[-10, 110]$
$\theta_{Bs}$	$2q_{LA}$	$[-90, 90]$
$\theta_{Bt}$	$2q_{LA}$	$[-90, 90]$
$\theta_{Cs}$	$-q_{LS} + q_{LA}$	$[-100, 50]$
$\theta_{Csp}$	$2q_{LS}$	$[-10, 110]$
$\theta_{Ct}$	$q_{LA} + q_{LS}$	$[-50, 100]$
$\theta_{Ds}$	$q_{LA} + q_{LS}$	$[-50, 100]$
$\theta_{Dsp}$	$0.625\theta_{Bsp} - 1.25q_{LS}$	$[-68.75, 106.25]$
$\theta_{Dt}$	$-1.4857q_{LS} + 1.4857q_{LA}$	$[-148.5714, 74.2857]$
$\theta_{LA}^b$	$-6.3030q_{LA}$	$[-283.6364, 283.6364]$
$\theta_{LA}^s$	$-6.3030q_{LA}$	$[-283.6364, 283.6364]$
$\theta_{LS}^b$	$-1.3\theta_{Bsp} + 6.76q_{LS}$	$[-241.8, 371.8]$
$\theta_{LS}^s$	$-1.3\theta_{Bsp} + 6.76q_{LS}$	$[-241.8, 371.8]$
$\theta_{mLA}$	$-25.212q_{LA}$	$[-1134.5455, 1134.5455]$
$\theta_{mLS}$	$-6.0667\theta_{Bsp} + 31.547q_{LS}$	$[-1128.4, 1735.0667]$

Most of the pulleys are mounted to the frame of the robot, and interact with other pulleys also mounted to the frame of the robot. For these pulleys, the range of motion of the individual pulley provides sufficient information to calculate the location of the cable terminations. However, some pulleys are mounted on rotating frames of reference, such as the Ds pulley mounted in the Cs pulley, shown in Figure 6.8. To calculate the range of motion of the actual cable interaction, rather than just the pulley rotation, we add the range of the pulley to the range of its frame of reference, if the frame of reference moves. The range of motion of the pulley interactions are described with a range of motion in the coordinate system of the base pulley. For example,  $Bt \rightarrow Dt$  will show the range of motion of that cable in the local coordinates of  $Bt$ . If a line is drawn between the base pulley and the interacting pulley, the range swept by that line is a number pair contained in the list below:

This complete list of pulley interactions and ranges of motion is used to define the location of each cable termination on each pulley. Because most of the pulley ranges are less than a full revolution, most of the cables can be wrapped in a straight line around the pulley rather than in a spiral, and the cable will not wrap on top of itself. However, because the cable terminations are a potential weak point, we attempt to maximize the amount of cable that is in contact with the pulley,

to maximize the friction and reduce the forces on the cable terminations. Using the range of motion and the sketch in SolidWorks, the termination is placed such that it will have a small clearance from interfering with itself at its maximum rotation. This small clearance means that if the hard stops on the robot were to fail, many cables would rotate farther than their maximum designed range of motion, and they would run into themselves and cause damage. This problem occurred once during robot experiments, but the cables were relatively easy to replace.

$Cs \rightarrow knee$	$-\theta_{Cs} + \theta_{Ct}$	$[-10.0, 110.0]$
$knee \rightarrow Cs$	$-\theta_{Cs} + \theta_{Ct}$	$[-10.0, 110.0]$
$As \rightarrow Ds$	$-\theta_{As} + \theta_{Cs}$	$[-50.0, 100.0]$
$Ds \rightarrow As$	$-\theta_{Ds}$	$[-100.0, 50.0]$
$Bs \rightarrow Ds$	$-\theta_{Bt} + \theta_{Cs}$	$[-100.0, 50.0]$
$Ds \rightarrow Bs$	$-\theta_{Ds}$	$[-100.0, 50.0]$
$As \rightarrow Csp$	$-\theta_{As}$	$[-10.0, 110.0]$
$At \rightarrow Dt$	$-\theta_{At} + \theta_{Ct}$	$[-100.0, 50.0]$
$Dt \rightarrow At$	$-\theta_{Dt}$	$[-74.3, 148.6]$
$Bt \rightarrow Dt$	$-\theta_{Bt} + \theta_{Ct}$	$[-50.0, 100.0]$
$Dt \rightarrow Bt$	$-\theta_{Dt}$	$[-74.3, 148.6]$
$At \rightarrow Csp$	$-\theta_{At}$	$[-110.0, 10.0]$
$Csp \rightarrow At$	$-\theta_{Csp}$	$[-110.0, 10.0]$
$Csp \rightarrow As$	$-\theta_{Csp}$	$[-110.0, 10.0]$
$Bsp \rightarrow Dsp$	$-\theta_{Bsp} + \theta_{Csp}$	$[-170.0, 110.0]$
$Dsp \rightarrow Bsp$	$-\theta_{Dsp}$	$[-106.25, 68.75]$
$Asp \rightarrow Dsp$	$-\theta_{Asp} + \theta_{Csp}$	$[-106.25, 68.75]$
$Dsp \rightarrow Asp$	$-\theta_{Dsp}$	$[-106.25, 68.75]$
$Asp \rightarrow LS_s$	$-\theta_{Asp}$	$[-178.75, 116.25]$
$LS_s \rightarrow Asp$	$-\theta_{LS^s}$	$[-371.8, 241.8]$
$LS_b \rightarrow q_{MLS}$	$-\theta_{LS^s}$	$[-371.8, 241.8]$
$q_{MLS} \rightarrow LS_b$	$-\theta_{q_{MLA}}$	$[-1128.4, 1735.1]$
$Bt \rightarrow LA_s$	$-\theta_{Bt}$	$[-90.0, 90.0]$
$LA_s \rightarrow Bt$	$-\theta_{LA^s}$	$[-283.6, 283.6]$
$LA_b \rightarrow q_{MLA}$	$-\theta_{LS^s}$	$[-283.6, 283.6]$
$q_{MLA} \rightarrow LS_b$	$-\theta_{q_{MLA}}$	$[-1134.5, 1134.5]$

Table 6.2: Parameters for Thumper.

Leg Length, fully extended	1.0m
Leg Length, fully retracted	0.5m
Leg Angle range	$\pm 45^\circ$ from vertical
Robot mass	38kg
“Knee” stiffness	512-585 Nm/rad
Motor peak torque	30Nm
Speed reduction between motor and knee	31.5



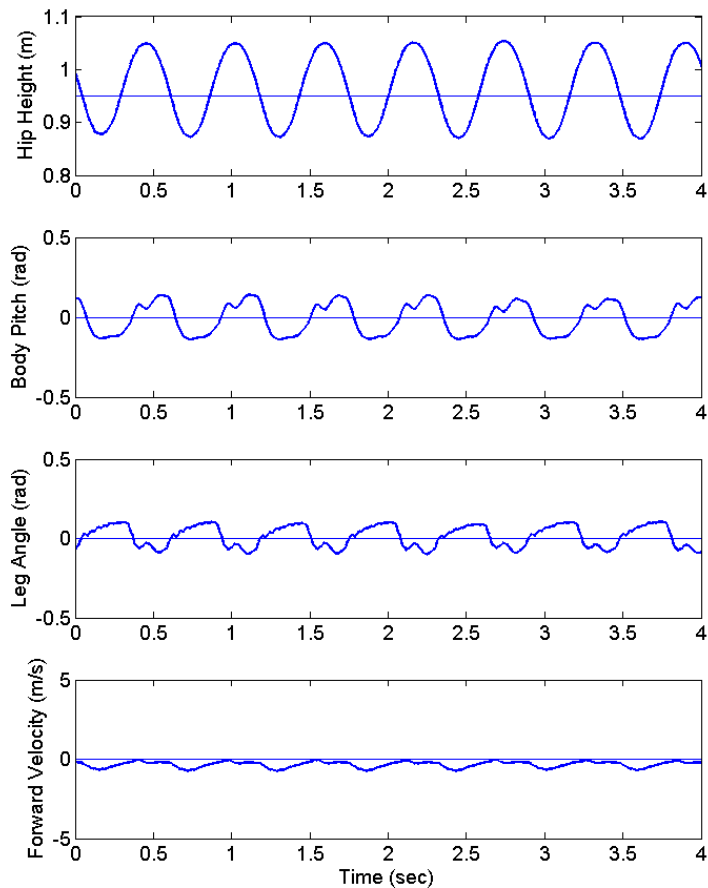


Figure 6.9: Data recorded from Thumper, hopping with approximately zero forward velocity. A small time-section of the data has been plotted, so details of the motion are visible, but the rest of the data set is similar. The length of the leg at full extension is 1m, but the leg length at touchdown is held at 0.95m for this experiment. Any values for hip height above 0.95m are an aerial phase of running, while values below 0.95 are stance phases. The knee stiffness in this experiment was 524Nm/rad.

approximately 1m/s with three different spring stiffnesses, and the results are shown in Figure 6.14. From subjective observations of the running gait, it seemed that higher leg stiffnesses resulted in better running gaits with this added mass and higher forward speed, but the data showed a minimum energy use at the second highest stiffness we could achieve.

Experiments in simulation and on the robot are done by creating a specific leg stiffness, either by defining it in simulation or by bolting it on to the robot, and manually tuning the controller until the robot is hopping in a steady-state gait. Data is recorded for approximately ten hops from the robot, or three hops from the simulation, because the simulation data tends to be much more consistent than the robot data and does not require as many data points for averaging. From the plot of the spring deflection, we calculate the amount of energy stored in the spring as the robot lands and its vertical velocity comes to zero. From the plot of the motor deflection, we calculate the amount

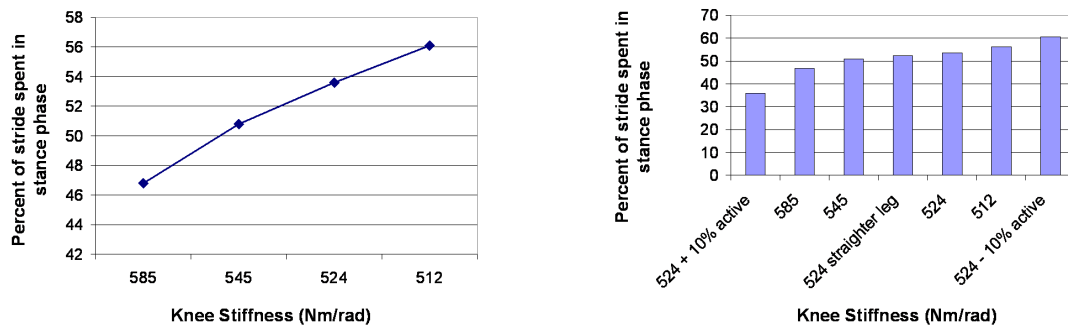


Figure 6.10: The duty factor, or percent of gait cycle spent on the ground, as a function of knee stiffness. The graph on the left shows only the effect of physical springs, with values adjusted by swapping springs between experiments. The bar graph on the right shows the effect of active control in adjusting leg stiffness, significantly affecting duty factor, without changing the physical spring. Also shown is an example of changing leg stiffness through the mechanical advantage of the knee, by landing with a leg length of 0.97m, rather than the standard 0.95m.

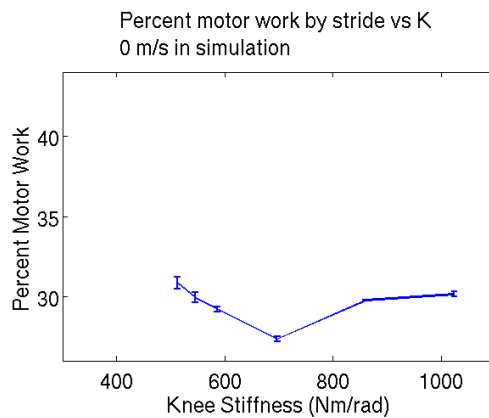


Figure 6.11: Data from the simulation of Thumper, showing the percentage of the total gait energy that is inserted by the motor with each hop, as a function of the leg stiffness, while hopping in place. The total energy for hopping in place is the combined spring and motor energy required to lift the robot from the bottom of stance to the apex of the flight phase. The error bars represent one standard deviation calculated from data from three simulated hops. The mass of the robot is 38kg.

of mechanical energy the motor inserts to maintain a constant gait. These values are summed to calculate the total amount of energy required to lift the robot from the bottom of stance to the top of flight, and also the percent of this total energy that the motor inserts with each hop to maintain a consistent gait. The values are averaged and a standard deviation is calculated, resulting in a data point on the final plot. This process is repeated for each different leg stiffness, to provide a picture of motor work as a function of leg stiffness.

The energy insertion for our experiments is calculated by measuring the deflection of the motor at each millisecond, and the deflection of the spring at that point in time, which corresponds to the applied force at the motor shaft. By measuring only the mechanical work, we avoid the effects of the motor technology, such as inertia or stall inefficiencies, and the results of our experiments can more

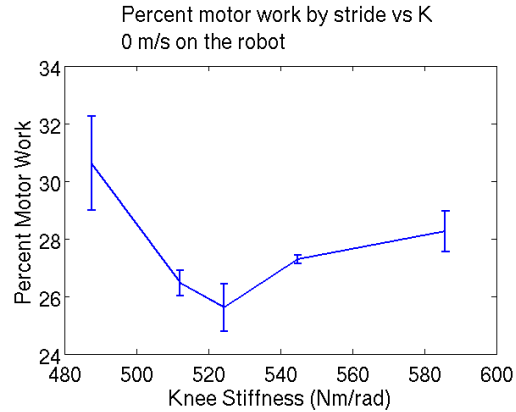


Figure 6.12: Data from the experiments with Thumper, showing the percentage of the total gait energy that is inserted by the motor with each hop, as a function of the leg stiffness, while hopping in place. Error bars represent one standard deviation calculated from data from ten hops. The mass of the robot is 38kg.

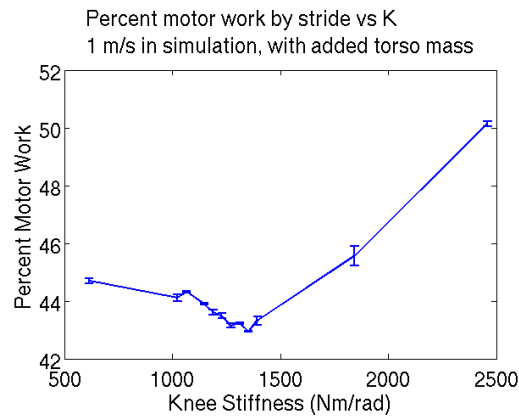


Figure 6.13: Data from the simulation of Thumper, showing the percentage of the total gait energy that is inserted by the motor with each hop, as a function of the leg stiffness, while hopping at 1.04m/s. The error bars represent one standard deviation calculated from data from three simulated hops. The mass of the robot with the added torso inertia was 42.5kg.

easily be compared to robots using other actuation technologies. We also avoid consideration of the software controller in the calculation of work insertion; the energy can be inserted in a way that is electrically inefficient, using high torques and accelerations, without affecting the results of our experiment. This way, we are certain that the energy savings come from some mechanical effect, such as minimization of collision losses or frictional losses.

During hopping experiments with the ECD Leg, we found that the steel cables stretch by a significant amount when under load. This behavior did not affect the operation of the robot, because the compression of the fiberglass spring dominates the behavior of the system. The cable stretch only caused a problem when the preload on the cable pairs was low enough that the unloaded cable went slack and fell out of the cable groove. As long as the preload is at least half of the peak

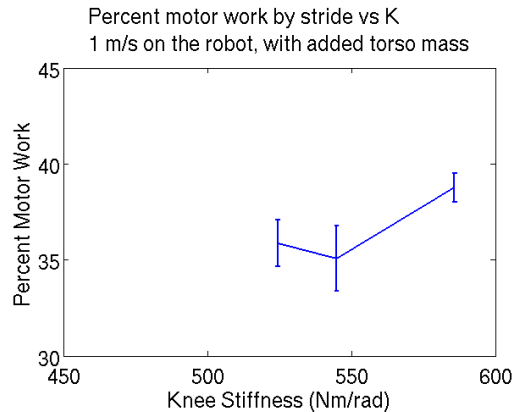


Figure 6.14: Data from the experiments with Thumper, showing the percentage of the total gait energy that is inserted by the motor with each hop, as a function of the leg stiffness, while hopping at approximately 1m/s. Error bars represent one standard deviation calculated from data from ten hops. The forward speed could not be well-regulated, so the speed ranged from 0.6m/s to 1.4m/s in this experiment. The mass of the robot with the added torso inertia was 42.5kg.

forces, one side will reach peak load while the other reaches no load, and the cables will stay in their groove.

After several hours of hopping, we observed that the cables associated with the Leg Angle degree of freedom had worn through the hard anodized coating in a repeating pattern, like a dashed line. The cables also seem to be wearing faster, with whiskers of steel protruding from the side of the cables. The cables on the Leg Length degree of freedom did not appear to have this same accelerated wear. We speculate that the damage to the Leg Angle pulleys is caused by impacts with the ground, where the inertia of the Leg Angle motor,  $q_{LA}$ , resists the instantaneous acceleration and causes large force spikes through the cable transmission. In contrast, the force spikes of the leg length pulleys will not be as large, because the inertia of the leg length motor,  $q_{LS}$ , is insulated from the ground impacts by the series spring. Only the relatively small inertia of the leg and pulleys will contribute to the forces of impact. This observation is a solid advertisement for series elasticity in the design of actuators that regularly encounter impacts.

Thumper tends to be somewhat loud while hopping on the ground, and this noise necessarily corresponds to energy loss. The construction of the legs is similar in many ways to an acoustic instrument, with slightly curved sheets of carbon fiber captured by two aluminum plates. With every ground impact, the “clack” is amplified. It does not seem to negatively affect the function of the robot, but for future robots, this particular design feature may be avoided for aesthetic considerations.

Thumper was designed to behave like a simple mass-spring model for hopping, and for the most part, it does; controllers are straightforward, and derived from those described in Raibert’s book [Raibert, 1986]. However, the robot seems to have a preference for hopping backwards rather than forwards, where the direction is defined by similarity to human hopping. The impacts with the ground are much louder when the robot hops forward, and the robot is more sensitive to falling while hopping forward. Although the shin and thigh are constrained by a differential to act like a prismatic joint, there are still asymmetries due to the inertia of the two links. We speculate that this asymmetry is the cause of the instability; when running forward, the effective toe inertia is actually higher than when running backwards. Figure 6.15 shows a simplified hopping robot much like

Thumper, running forwards and backwards. At ground impact, the toe abruptly changes velocity. For the backwards-running robot, most of this toe velocity causes the shin to rotate, while the forwards-running case results in translation of the shin. The impulse required to rotate the shin is lower than the impulse required to translate the shin, and thus, ground impacts are greater for forward-running in Thumper.

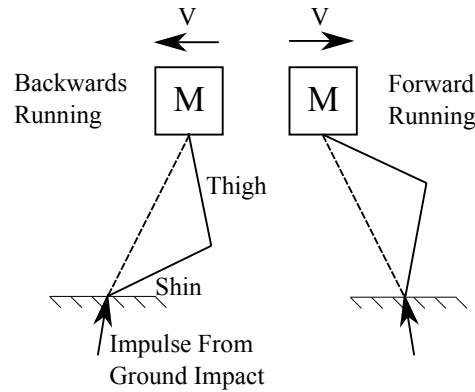


Figure 6.15: Two simplified hopping robots with knees, moving at equal and opposite velocities. The ground impact imparts a discontinuous velocity change to the toe, which corresponds to a rotational and a linear velocity change to the shin link. For the robot on the left, running backwards, the resulting rotational velocity of the shin is higher and linear velocity lower than the robot on the right, running forward.

The inertia of the motors accelerating and decelerating quickly seem to affect the dynamics of the robot. For example, when the leg is extending during liftoff, the abrupt stop seems to pitch the robot forward. We have added control laws to add rotational inertia in the opposite direction to the body to partially cancel this effect. For future designs of electric running robots, this effect should be taken under consideration.

One problem with Thumper is that the robot has some difficulty running at high speeds, due to the leg swing. The body pitches forward quickly in response to the leg swinging forward during the flight phase. In later experiments of running at speed, we added long horizontal bars with weights at the ends to increase Thumper's rotational inertia. This problem should not exist for MABEL, which can use the left leg to counter the inertia of the right leg, and vice-versa.

There are a number of additional experiments that could be done with this machine. Better stability at forward running speeds would allow us to find the energetically optimal leg stiffness for a range of speeds, and show a correlation between forward speed and optimal leg stiffness. Experiments running on surfaces of different stiffness might allow us to determine the mechanisms of energy loss in the hopping gait, and allow us to explore methods for accommodating the changing surface.

Many aspects of the ECD Leg are successful demonstrations of new ideas, or, alternatively, a new application and refinement of old ideas. The series springs are clearly important and contribute to the successful hopping gait, with better than 70% restitution. The cable differentials create relationships between joints with no backlash, and relatively low mass. Although cable differentials are not new, the concentric shape of this implementation, similar to a planetary gear box, is novel. In addition, there are many engineering details in the design of the ECD leg that will be used in our legged machine designs in the future, and hopefully in the designs of other researchers and engineers. For example, the methods for calculating the locations of cable terminations, the design and manufacture of the grooves in both straight and spiral configurations to support the cable, the

methods for using fiberglass leaf springs, and the integration of the brushless motors into the body of the robot. Thumper and MABEL demonstrate, for the first time, a cable drive paired with series elasticity for a running machine. To our knowledge, the AMASC is the first demonstration of a differential and a brake being used to maintain pretension in a pair of antagonistic springs. This implementation maintains a given joint stiffness with no energy cost, while a different motor controls the set point. The AMASC is also the first demonstration of series elasticity implemented via a mechanical differential, and the BIMASC, Thumper, and MABEL all utilize this same concept. In conclusion, Thumper hops, MABEL walks, and future designs will surely build upon this successful example of a walking and running machine.



## Chapter 7

### Conclusions and Future Work

#### 7.1 Future Work

I believe there are general rules that determine the ideal series impedance for actuators, especially in force control and legged locomotion applications, and this is the first topic I plan to explore in the near future. A well known analogy is the design of a servomotor system to quickly accelerate an inertial load. Common practice is to maximize the peak acceleration by sizing the gearbox to match the reflected inertia of the motor with the inertia of the load. A higher gear ratio would cause the motor inertia to limit the peak acceleration, while a smaller gear ratio would cause the inertia of the load to limit the peak acceleration, so there is a clear optimal value.

In force control applications, series elasticity clearly improves the performance and stability [Robinson, 2000]. But a generic “force actuator” cannot be sufficiently general to serve all force control purposes—there are still limits to the bandwidth, depending on the task. For example, if the desired task is to apply changing forces to a load that will not move, then a rigid transmission would be ideal; because there is no acceleration, forces are directly transmitted from the electronics of the motor to the end effector. Adding series compliance would only limit the performance, by requiring accelerations of the motor to compress the series spring and apply the desired forces.

If the desired task for a force-controlled actuator is to absorb the energy of an unexpected impact, such as heel strike during a walking gait, the ideal mechanical system is less obvious. I suggest that there is a quantitative relationship between the series impedance and motor inertia that will allow good force control on an unexpected impact of limited velocity, yet maintain acceptable bandwidth for changes in applied force. The ideal actuator would have zero inertia, along with infinite stiffness—bandwidth for impacts and for applied forces would be limited only by the speed of the control computer. However, all motors have some inertia, and series impedance is required to prevent large force spikes during impacts. In addition to inertia, all motors have a torque limit, which combine to create a limit on acceleration. If a stiff, undamped, spring is placed in series with a low-acceleration motor, an impact will result in a rebound or uncontrollable oscillation, as the natural frequency of the spring is faster than the acceleration of the motor. A soft spring, in contrast, would allow the motor to accelerate and match the impact velocity as the spring compresses to then slow the impact, while preventing large force spikes. As a drawback, a soft series spring limits the bandwidth of the actuator to apply changing forces to a stationary object. Essentially, I propose that a force control actuator should be as stiff as possible, with the limit imposed by the acceleration of the motor and the maximum expected velocity of an unexpected impact.

For legged locomotion, the goal for actuation may be much more complex than just force control. It is an oscillating system with many tuned parts, analogous to a mechanical clock, but with more energy transfer between components and more degrees of freedom. As the second primary

interest for future research, I would like to understand this oscillation, to create a mechanical system that can support robust, efficient walking and running. Building the AMASC, BiMASC, and ECD Leg has resulted in a better understanding of methods for the implementation of spring-like behavior for running, as well as some information regarding the importance and difficulties of variable stiffness. However, there is much more to do.

The ECD Leg was designed to have simple dynamic behaviors, with only a few complexities arising from the knee and leg inertia. Future work will involve addition of potentially interesting complexities. For example, hip springs have been shown to be useful for improving efficiency in robotic legged locomotion. The ARL Monopod was first built with only a leg spring, and the ARL Monopod II incorporated a hip spring, with significant energy savings [Ahmadi and Buehler, 1999]. We do not currently use hip springs, but they could be added in the future to the ECD Leg.

Adding feet will allow the robot to stand in one place, and may also lead to efficiency and stability gains. Coordination of a foot spring with the larger leg springs could reduce the effective toe mass, for improved efficiency during running. For a ballistic walking gait, additional leg weights could tune the natural dynamics to improve the performance.

In the near future, I would like to design and build a bipedal robot based on the lessons from the AMASC, BiMASC, and ECD Leg. My mental image is a 3-foot tall bird-like machine, capable of running quickly across somewhat uneven terrain, taking small dips and rises in stride without much effect on the gait. I would like to replicate, with a robotic system, the experiments done by Daley et al. on guinea fowl running over a large, unexpected drop in ground level [Daley et al., 2006]. The birds were able to absorb this disturbance and continue running. I believe force control combined with large springs for storing the energy of the running gait can replicate this level of performance, and the software will be no more complex than current running controllers.

The robot design may use discrete actuators on each different joint, or some simple transmission to create a carefully considered linkage between joints. The goal of the actuation will be to allow good force control on all degrees of freedom through the use of series impedance, so ballistic walking will be possible, but also allow for SLIP-model running gaits with mechanical energy storage. The robot will be designed to operate both on and off of a planar boom, to aid in control system design and tuning. Animals provide a proof of example, so it can certainly be done, and I believe the mechanical system can be reasonably simple compared to the complexity of biological systems.

## 7.2 Discussion

The theme of this thesis is the implementation of actuators for running robots, and specifically the creation of variable compliance behaviors. Through the implementation of three different devices, the mechanical design has evolved, with effective ideas being retained and problematic ideas being revised. For example, the AMASC used a block-and-tackle system for speed reduction in the cable drive. The many pulleys and bearings imposed a large amount of friction, especially under large pretension loads. One set of pulleys was suspended in the middle of a length of cable, and this weight oscillated on the tensioned cable like a plucked string. However, the cable drive itself provided very good power transmission with no backlash, an important trait for a system which regularly applies torque in a changing direction.

With the BiMASC, we took the AMASC from a bench-mounted prototype to implementation on a legged robot. Although the fundamental ideas remained the same, much of the engineering was refined and improved. We replaced the block and tackle with a concentric cable differential, and developed methods for terminating the cables on the pulleys and for tensioning the cables. We prototyped and tested the basic structure of the robot, such as the carbon fiber and aluminum

“torsion box” structure of the legs and the archery bow style of the fiberglass springs. We also tested the durability of the robot, by throwing it a few times, and relying on the boom to catch it. This first implementation and set of tests was invaluable in creating the ECD leg.

In choosing to remove the adjustable stiffness capability of the BiMASC and AMASC for the ECD Leg revision, we made a subjective engineering decision. The internal forces of the antagonistic springs, along with the additional mechanism associated with our implementation, seemed to have greater costs than the benefits could warrant. Because different engineering implementations may achieve better performance than ours, we cannot conclude that the variable stiffness mechanism is not worthwhile. Our experiments have illustrated some energetic effects of different leg stiffnesses in a real system, and future work could show greater effects for running at speed.

When choosing the leg springs for testing the energy use on Thumper, we first calculated the necessary energy storage capacity based on the mass and the hopping height, and verified that our springs would be physically large enough. After construction of the robot, we tried various different springs to find the one that provided a subjective “best” running gait. We then ran experiments with springs that were slightly softer and slightly stiffer. The very soft springs resulted in long leg deflections that neared the limits of leg deflection, while very stiff springs resulted in harsh ground impacts that destabilized the gait. We do not believe that it is coincidental that the subjective “best” leg stiffness also resulted in the best spring restitution for the robot, although the influence of leg stiffness on spring restitution was somewhat weak. The curves in Figures 6.12 and 6.14 might be much more pronounced for significant forward velocities or for more highly-damped natural ground surfaces.

### 7.3 Conclusions

The focus of much of this thesis work has been creating mechanical systems that match simple dynamic models, so the behavior can be readily understood, modeled, and controlled. The primary application has been legged locomotion, showing an optimal leg stiffness, showing how to implement stiffness behavior, and showing that physical springs are important for legged locomotion in particular.

The important message to take from this thesis is that a robot is a unified dynamic system comprised of electronics, software, and mechanical components, and for certain tasks such as running, a significant portion of the behavior is best exhibited through natural dynamics of the mechanism. Therefore, the mechanical system must be specialized for the task, and designed with the same care for dynamic control as the software control system.

In constructing the ECD Leg, we have attempted to follow this philosophy and design the mechanical system for the specific tasks of walking and running. The prototype actuator, with dynamics verified by testing, exhibited behavior that enabled running in simulation. The ECD Leg builds on design revisions from the BiMASC prototype; Thumper successfully hops and MABEL successfully walks. The design of these robots is significantly different from other running or walking machines, and in addition to the mechanical implementation, the exploration of series stiffness and methods for stiffness adjustment will be a reference for future designs.



# Appendices



## Appendix A

### Derivation of a Mechanical Differential

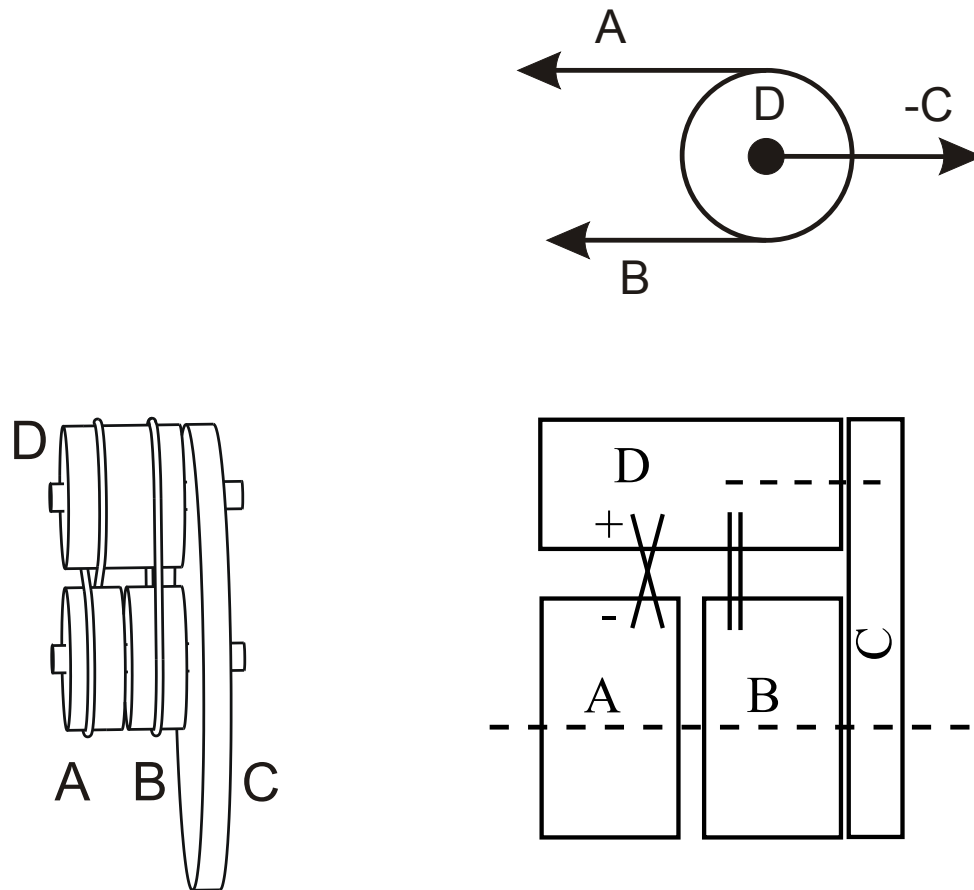


Figure A.1: Representations of a differential. A standard gear differential in upper left, pulley differential as used on the AMASC in upper right, the BiMASC and ECD Leg cable differential in lower left, and abstracted representation in lower right.

For a standard mechanical differential, there are four gears, pulleys, levers, or equivalent components. Using a standard automotive differential as an example, the four gears are the driveshaft, the right wheel, left wheel, and an internal idler gear. We arbitrarily label the left and right wheels A and B, the driveshaft C, and the internal idler pulley D. In the case of the ECD Leg and the BiMASC,

the differentials are created using steel cables and aluminum pulleys, as shown in Figure A.1. To design the combination of differentials which will provide the desired relationships between the shin and thigh links, we must quantitatively calculate the relative position and velocity of each pulley relative to the other, even if the pulleys are all different diameters. We assume the radius of D (the idler pulley) is the same where it interacts with the A pulley and with the B pulley. In practice this may be untrue, but the diameter of the A and B pulleys should be adjusted accordingly, so the ratio between A and D is correct, and the ratio between B and D is correct. The diameter of the C pulley is not relevant, because it does not interact with any of the other pulleys of the differential.

Starting with a generic constraint equation, the velocity of three pulleys,  $\omega_A$ ,  $\omega_B$ , and  $\omega_C$ , are constrained to a linear relationship (in other words, only round pulleys are allowed), using generic variables  $a$ ,  $b$ , and  $c$ :

$$a\omega_A + b\omega_B + c\omega_C = 0 \quad (\text{A.1})$$

If we assume that  $c$  is 1,  $a$  and  $b$  can be scaled appropriately and the equation will still be true:

$$a\omega_A + b\omega_B + \omega_C = 0. \quad (\text{A.2})$$

We know intuitively that if pulleys  $A$  and  $B$  are rotating at the same rate, pulley  $C$  will also rotate at that rate:

$$\omega_A = \omega_B = \omega_C. \quad (\text{A.3})$$

Combining those equations:

$$a + b + 1 = 0. \quad (\text{A.4})$$

We also know from observation that, when  $\omega_C$  is zero, the  $\omega_A$  and  $\omega_B$  rotate at the same rate, proportional to their radii:

$$\omega_A r_a = -\omega_B r_b \quad (\text{A.5})$$

$$\omega_A = -\frac{\omega_B r_b}{r_a} \quad (\text{A.6})$$

and

$$a\omega_A + b\omega_B = 0. \quad (\text{A.7})$$

Combining those relationships,

$$-a\frac{\omega_B r_b}{r_a} + b\omega_B = 0 \quad (\text{A.8})$$

$$b = \frac{r_b}{r_a} a \quad (\text{A.9})$$

$$r_b a = r_a b. \quad (\text{A.10})$$

Solving for  $a$  in terms of  $r_a$  and  $r_b$ :

$$a + b + 1 = 0 \quad (\text{A.11})$$

$$a + a \frac{r_b}{r_a} + 1 = 0 \quad (\text{A.12})$$

$$a \frac{r_b + r_a}{r_a} + 1 = 0 \quad (\text{A.13})$$

$$a = -\frac{r_a}{r_b + r_a} \quad (\text{A.14})$$

and  $b$ :

$$b = -\frac{r_a}{r_b + r_a} \frac{r_b}{r_a} \quad (\text{A.15})$$

$$b = -\frac{r_b}{r_b + r_a}. \quad (\text{A.16})$$

Substituting  $a$  and  $b$  into the original linear relationship:

$$-\frac{r_a}{r_b + r_a} \omega_A - \frac{r_b}{r_b + r_a} \omega_B + \omega_C = 0 \quad (\text{A.17})$$

$$\omega_C = \frac{r_a}{r_b + r_a} \omega_A + \frac{r_b}{r_b + r_a} \omega_B. \quad (\text{A.18})$$

This relationship describes the angular rate of the three pulleys that interact with the outside world, given the reduction ratios between them, depicted by the radii. If all of the radii are equal, then we are left with the familiar equation for a differential:

$$\omega_C = \frac{\omega_A + \omega_B}{2}. \quad (\text{A.19})$$

For our uses, we also need to calculate the relative velocity of the idler pulley  $\omega_D$ . So, starting at almost the same starting point of a linear relationship between the pulleys, but with  $\omega_D$  instead of  $\omega_C$ :

$$a\omega_A + b\omega_B + \omega_D = 0. \quad (\text{A.20})$$

If  $\omega_D = 0$ , then

$$a\omega_A + b\omega_B = 0 \quad (\text{A.21})$$

and

$$\omega_A = \omega_B. \quad (\text{A.22})$$

Combining the two equations results in a useful equation linking  $a$  and  $b$ :

$$a\omega_A + b\omega_A = 0 \quad (\text{A.23})$$

$$a + b = 0 \quad (\text{A.24})$$

$$a = -b. \quad (\text{A.25})$$

The direct contact of the pulleys can be represented:

$$\omega_A r_a = -\omega_D r_d \quad (\text{A.26})$$

$$\omega_A = -\frac{r_d}{r_a} \omega_D \quad (\text{A.27})$$

$$\omega_B r_b = \omega_D r_d \quad (\text{A.28})$$

$$\omega_B = \frac{r_d}{r_b} \omega_D \quad (\text{A.29})$$

Notice that the direction of one pulley is reversed from the other—which one is an arbitrary decision. In a standard gear differential, the axis of rotation of  $\omega_D$  is perpendicular to the axis of rotation of  $\omega_A$  and  $\omega_B$ , so a sign change is not very informative, the sign half-changes (rotates 90 degrees twice) between them. However, in representing mathematically, one of them has to be an opposite sign for the mechanism to be a differential. Also, our implementation of a cable differential is similar to a planetary gearbox, in that all the axes of rotation are parallel. Thus, we use one cable that is straight, like a regular pulley belt, and another cable that is a figure eight, to switch the sign of rotation. For our convention, we have decided that the sign change is always on the cable that interacts with the  $A$  pulley, while the straight cable is always on the  $B$  pulley.

Combining equations:

$$-a\frac{r_d}{r_a}\omega_D + b\frac{r_d}{r_b}\omega_D + \omega_D = 0 \quad (\text{A.30})$$

$$-a\frac{r_d}{r_a} + b\frac{r_d}{r_b} + 1 = 0 \quad (\text{A.31})$$

$$-a\frac{r_d}{r_a} - a\frac{r_d}{r_d} + 1 = 0 \quad (\text{A.32})$$

$$a\left(\frac{r_d}{r_a} + \frac{r_d}{r_b}\right) = 1 \quad (\text{A.33})$$

$$a\left(\frac{r_d r_b + r_d r_a}{r_a r_b}\right) = 1 \quad (\text{A.34})$$

$$a = \frac{r_a r_b}{r_d r_b + r_d r_a} \quad (\text{A.35})$$

$$a = \frac{r_a r_b}{r_d(r_a + r_b)} \quad (\text{A.36})$$

$$(\text{A.37})$$

Because we know that  $a = -b$ , we can substitute  $a$  and  $b$  into the original linear relationship:

$$\frac{r_a r_b}{r_d(r_a + r_b)}\omega_A - \frac{r_a r_b}{r_d(r_a + r_b)}\omega_B + \omega_D = 0 \quad (\text{A.38})$$

$$r_a r_b \omega_A - r_a r_b \omega_B + r_d(r_a + r_b)\omega_D = 0 \quad (\text{A.39})$$

## Appendix B

### Energy Storage in Antagonistic Spring Pairs

In the ECD Leg, as in many robots and in all animals, physical springs store the energy of a running gait. The AMASC and the BiMASC adjust the leg stiffness through co-contraction of antagonistic springs, as in Figure B.1, and this approach leads to significantly lower energy storage capacity for a given pair of springs than a more efficient parallel pairing, as in Figure B.2. There are two main reasons: first, a parallel set of springs can both store energy during a load deflection, while the antagonistic pairs do not. Second, a range of stiffness adjustment values requires a range of pretension values, and the corresponding spare spring deflection. For a particular energy storage at a particular stiffness, only a small part of the total spring deflection may be used.

#### B.1 Antagonistic vs. Parallel Springs

With two springs opposed across a single joint, the deflection of the joint,  $x$ , stretches one spring while relaxing the other. Co-contraction of the springs,  $p$ , stretches both springs equally. For the

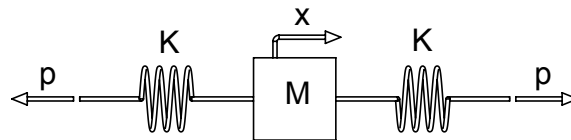


Figure B.1: Two opposing springs in co-contraction across a single linear joint. Spring constant  $K$ , joint deflection  $x$ , joint load mass  $M$ , and co-contraction  $p$ . The co-contraction is always larger than the joint deflection, such that the springs are always in tension.

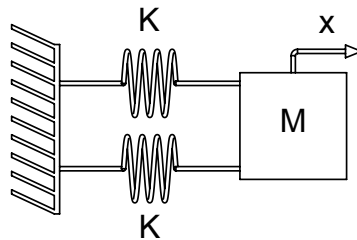


Figure B.2: The same two springs, but in parallel, working together rather than antagonistically. They have the same stiffness  $K$ , joint deflection  $x$ , and joint load mass  $M$ . There is no co-contraction.

co-contraction to affect the joint stiffness, the springs must be nonlinear. For the mathematically convenient example of antagonistic quadratic springs,  $F_1 = K(p + x)^2$  and  $F_2 = K(p - x)^2$ , the combined force on the joint is

$$F = F_1 - F_2 \quad (\text{B.1})$$

$$F = K(p + x)^2 - K(p - x)^2 \quad (\text{B.2})$$

$$F = K(p^2 + 2px + x^2) - K(p^2 - 2px + x^2) \quad (\text{B.3})$$

$$F = 4Kpx, \quad (\text{B.4})$$

where the co-contraction  $p$  can be considered as part of the spring constant that determines the resultant forces of a joint deflection  $x$ . Integrating to calculate the energy storage gives

$$\int F dx = 4Kp \int x dx \quad (\text{B.5})$$

$$E = 2Kpx^2. \quad (\text{B.6})$$

Assuming a maximum spring deflection  $x_{max}$  and a minimum deflection  $x = 0$ , a pretension of  $p = \frac{1}{2}x_{max}$  will provide the greatest possible deflection of the load mass  $M$ . Because one spring is relaxing at an equal and opposite rate of the other, a deflection of  $x = \frac{1}{2}x_{max}$  will result in one spring reaching zero deflection while the other reaches its maximum. Substituting the pretension and load deflection values into the energy equation, the recoverable energy stored in the springs is

$$E = 2K\left(\frac{1}{2}x_{max}\right)\left(\frac{1}{2}x_{max}\right)^2 \quad (\text{B.7})$$

$$E = \frac{1}{4}Kx_{max}^3. \quad (\text{B.8})$$

By comparison, placing the springs in parallel rather than in opposition allows their forces to add:

$$F = F_1 + F_2 \quad (\text{B.9})$$

$$F = 2Kx^2 \quad (\text{B.10})$$

and the corresponding energy storage is

$$\int F dx = 2K \int x^2 dx \quad (\text{B.11})$$

$$E = \frac{2}{3}Kx^3. \quad (\text{B.12})$$

The parallel springs can both deflect to the maximum spring deflection  $x_{max}$ , and the recoverable energy stored in the springs is

$$E = \frac{2}{3}Kx_{max}^3, \quad (\text{B.13})$$

which is larger than the useful energy storage of the antagonistic pair by a factor of 2.66. This factor is large because both springs are recruited for energy storage, rather than one spring relaxing while the other one stretches; in addition, the relaxing spring is releasing energy into the stretching spring, transferring energy within the mechanism rather than storing useful energy through the load mass. Finally, the pretension on the spring reduces the useful deflection of the spring, further reducing the energy storage capacity of the system.

## B.2 Stiffness Adjustment

Humans have been measured adjusting leg stiffness by a factor of three while hopping in place, so we use this as a goal for the stiffness adjustment range of the antagonistic spring pair [Ferris and Farley, 1997]. The calculation from the previous section shows the maximum possible energy storage for the antagonistic spring pair, but this value will drop if the pretension is varied away from  $p = \frac{1}{2}x_{max}$  to adjust the effective stiffness, because the springs will run into a lower or upper deflection limit. Given that our force function at the load is  $F = 4Kpx$ , the coefficient  $4Kp$  can be viewed as the linear stiffness value of the overall spring function, and changing the pretension  $p$  by a factor of three will affect the coefficient by the same amount. Keeping a minimum spring deflection of  $x = 0$  and a maximum spring deflection of  $x = x_{max}$ , the peak deflection of the load at the minimum pretension value will be  $x = p_{min}$  and the peak deflection of the load at the maximum pretension value will be  $x = x_{max} - p_{max}$ . Therefore, the usable energy stored by the system at  $p_{min}$  is

$$E = 2Kpx^2 \quad (\text{B.14})$$

$$E_{pmin} = 2Kp_{min}(p_{min})^2 \quad (\text{B.15})$$

$$E_{pmin} = 2K(p_{min})^3 \quad (\text{B.16})$$

and the usable energy stored by the system at  $p_{max}$  is

$$E_{pmax} = 2Kp_{max}(x_{max} - p_{max})^2. \quad (\text{B.17})$$

$$(\text{B.18})$$

Because we want to vary the pretension by a factor of three,  $p_{max} = 3p_{min}$ , and we can substitute for  $p_{max}$  :

$$E_{pmax} = 6Kp_{min}(x_{max} - 3p_{min})^2. \quad (\text{B.19})$$

$$(\text{B.20})$$

Equating the energy storage capacity of the maximum and minimum stiffness values allows a substitution and simplification:

$$E_{pmin} = E_{pmax} \quad (\text{B.21})$$

$$2K(p_{min})^3 = 6Kp_{min}(x_{max} - 3p_{min})^2 \quad (\text{B.22})$$

$$26p_{min}^2 - 18p_{min}x_{max} + 3x_{max}^2 = 0. \quad (\text{B.23})$$

Solving the quadratic equation,

$$p_{min} = 0.28x_{max} \quad (\text{B.24})$$

$$p_{max} = 0.84x_{max}, \quad (\text{B.25})$$

thus the usable energy stored in the system for either  $p_{min}$  or  $p_{max}$  is

$$E_{pmin} = 2K(p_{min})^3 \quad (\text{B.26})$$

$$E_{pmin} = 0.044Kx_{max}^3 \quad (\text{B.27})$$

$$E_{pmax} = 2K(p_{max})(x_{max} - p_{max})^2 \quad (\text{B.28})$$

$$E_{pmax} = 2K(0.84x_{max})(x_{max}^2 - 2x_{max}(0.84x_{max}) + (0.84x_{max})^2) \quad (\text{B.29})$$

$$E_{pmax} = 0.044Kx_{max}^3 \quad (\text{B.30})$$

which is a factor of 15 less than the parallel springs,  $E = \frac{2}{3}Kx_{max}^3$ .

## Bibliography

- M. Ahmadi and M. Buehler. A control strategy for stable passive running. In *IEEE Conference on Intelligent Systems and Robots*, pages 152–157, 1995.
- M. Ahmadi and M. Buehler. The ARL monopod II running robot: Control and energetics. In *IEEE International Conference on Robotics and Automation*, pages 1689–1694, May 1999.
- R. McN. Alexander. Three uses for springs in legged locomotion. *The International Journal of Robotics Research*, 9(2):53–61, April 1990.
- R. Altendorfer, U. Saranli, H. Komsuoglu, D. E. Koditschek, B. Brown, M. Buehler, E. Moore, D. McMordie, and R. J. Full. Evidence for spring loaded inverted pendulum running in a hexapod robot. In *Experimental Robotics VII*, 2002.
- Adamantios Arampatzis, Falk Schade, Mark Walsh, and Gert-Peter Brüggemann. Influence of leg stiffness and its effect on myodynamic jumping performance. *Journal of Electromyography and Kinesiology*, 11:355–364, 2001.
- David J. Bennett. What are the advantages of variable stiffness control? In *IEEE Engineering in Medicine and Biology*, pages 86–87, December 1992.
- Antonio Bicchi, Giovanni Tonietti, Michele Bavaro, and Marco Piccigallo. Variable stiffness actuators for fast and safe motion control. In *International Symposium on Robotics Research*, 2003.
- Antonio Bicchi and Giovanni Tonietti. Fast and “soft-arm” tactics. *IEEE Robotics & Automation Magazine*, 2004.
- R. Blickhan. The spring-mass model for running and hopping. *Journal of Biomechanics*, 22(11/12):1217–1227, 1989.
- R. Blickhan and R. J. Full. Similarity in multilegged locomotion: Bouncing like a monopode. *Journal of Comparative Physiology*, pages 509–517, 1993.
- R. Blickhan, R. J. Full, and L. Ting. Exoskeletal strain: Evidence for a trot-gallop transition in rapidly running ghost crabs. *Journal of Experimental Biology*, pages 301–321, 1993.
- Giovanni A. Cavagna. Elastic bounce of the body. *Journal of Applied Physiology*, 29(3):279–282, 1970.
- Giovanni A. Cavagna, Norman C. Heglund, and C. Richard Taylor. Mechanical work in terrestrial locomotion: Two basic mechanisms for minimizing energy expenditure. *American Journal of Physiology*, 233(5):R243–R261, 1977.
- Souhaïel M Chelly and Christian Denis. Leg power and hopping stiffness: Relationship with sprint running performance. *Med. Sci. Sports Exerc.*, 33(2):326–333, 2001.

- C. Chevallereau and Y. Aoustin. Optimal reference trajectories for walking and running of a biped robot. *Robotica*, 19(5), September 2001.
- C. Chevallereau, G. Abba, Y. Aoustin, F. Plestan, E. R. Westervelt, C. Canudas de Wit, and J. W. Grizzle. RABBIT: a testbed for advanced control theory. *IEEE Control Systems Magazine*, June 2003.
- C. Chevallereau, E. R. Westervelt, and J. W. Grizzle. Asymptotically stable running for a five-link, four-actuator, planar bipedal robot. *IEEE Transactions on Robotics*, 2008. URL <http://www.eecs.umich.edu/~grizzle/papers/robotics.html>.
- Nicholas P. Chironis. *Mechanisms, Linkages, and Mechanical Controls*, chapter Types of Noncircular Gears, pages 241–244. McGraw Hill, 1965.
- Monica A. Daley, James R. Usherwood, Gladys Felix, and Andrew A. Biewener. Running over rough terrain; guinea fowl maintain dynamic stability despite a large unexpected change in substrate height. *Journal of Experimental Biology*, 209:171–187, 2006.
- Michael H. Dickinson, Claire T. Farley, Robert J. Full, M. A. R. Koehl, Rodger Kram, and Steven Lehman. How animals move: An integrative view. *Science*, 288:100–106, April 2000.
- Audrey Duncan and Martin J. N. McDonagh. Stretch reflex distinguished from pre-programmed muscle activations following impacts in man. *Journal of Physiology*, 526:457–468, 2000.
- Steven D. Eppinger and Warren P. Seering. Understanding bandwidth limitations in robot force control. In *IEEE International Conference on Robotics and Automation*, pages 904–909, 1987.
- C. T. Farley, J. Glasheen, and T. A. McMahon. Running springs: Speed and animal size. *Journal of Experimental Biology*, 185:71–87, 1993a.
- Claire T. Farley and Daniel P. Ferris. Biomechanics of walking and running: Center of mass movements to muscle action. In M.D. John O. Holloszy, editor, *Exercise and Sport Sciences Reviews*, volume 26, chapter 10, pages 253–285. Williams and Wilkins, 1998.
- Claire T. Farley and Octavio Gonzalez. Leg stiffness and stride frequency in human running. *Journal of Biomechanics*, 29(2):181–186, 1996.
- Claire T. Farley, James Glasheen, and Thomas A. McMahon. Running springs: Speed and animal size. *Journal of Experimental Biology*, pages 71–86, 1993b.
- Claire T. Farley, Han H. P. Houdijk, Ciska Van Strien, and Micky Louie. Mechanism of leg stiffness adjustment for hopping on surfaces of different stiffnesses. *The American Physiological Society*, pages 1044–1055, 1998.
- Daniel P. Ferris and Claire T. Farley. Interaction of leg stiffness and surface stiffness during human hopping. *The American Physiological Society*, pages 15–22, 1997.
- Daniel P. Ferris, Mickey Louie, and Claire T. Farley. Running in the real world: adjusting leg stiffness for different surfaces. In *Proceedings of the Royal Society London*, volume 265, pages 989–993, January 1998.
- Daniel P. Ferris, Kailine Liang, and Claire T. Farley. Runners adjust leg stiffness for their first step on a new running surface. *Journal of Biomechanics*, pages 787–974, 1999.

- Robert J. Full and Claire T. Farley. Musculoskeletal dynamics in rhythmic systems - a comparative approach to legged locomotion. In J. M. Winters and P. E. Crago, editors, *Biomechanics and Neural Control of Posture and Movement*. Springer-Verlag, New York, 2000.
- Robert J. Full and Daniel E. Koditschek. Templates and anchors: Neuromechanical hypotheses of legged locomotion on land. *Journal of Experimental Biology*, 202:3325–3332, 1999.
- Robert J. Full and Michael S. Tu. Mechanics of a rapid running insect: Two-, four- and six-legged locomotion. *Journal of Experimental Biology*, pages 215–231, September 1991.
- Robert J. Full, Timothy Kubow, John Schmitt, Philip Holmes, and Daniel Koditschek. Quantifying dynamic stability and maneuverability in legged locomotion. *Integrative and Comparative Biology*, 42:149–157, 2002.
- M. Gienger, K. Löffler, and F. Pfeiffer. Towards the design of a biped jogging robot. In *IEEE International conference on Robotics and Automation*, volume 4, pages 4140–4145, 2001.
- P. Gregorio, M. Ahmadi, and M. Buehler. Design, control, and energetics of an electrically actuated legged robot. In *IEEE Transactions on Systems, Man, and Cybernetics*, pages 626–634, August 1997.
- Ronald Van Ham, Bram Vanderborght, Bjrn Verrelst, Michal Van Damme, and Dirk Lefeber. MAC-CEPA: the mechanically adjustable compliance and controllable equilibrium position actuator used in the controlled passive walking biped veronica. In *Proceedings of the 15th International Symposium on Measurement and Control in Robotics*, 2005.
- N. C. Heglund and C. R. Taylor. Speed, stride frequency and energy cost per stride: how do they change with body size and gait? *Journal of Experimental Biology*, (138), 1988.
- Jessica K. Hodgins and Marc H. Raibert. Adjusting step length for rough terrain. In *IEEE Transactions on Robotics and Automation*, volume 7, 1991.
- T. Horita, P. V. Komi, C. Nicol, and H. Kyrolainen. Interaction between pre-landing activities and stiffness regulation of the knee joint musculoskeletal system in the drop jump: implications to performance. *European Journal of Applied Physiology*, 88:76–84, 2002.
- John R. Hutchinson, Dan Famini, Richard Lair, and Rodger Kram. Are fast-moving elephants really running? *Nature*, (422):493–494, 2003.
- Florence Griffith Joyner, John Hanc, and Jackie Joyner-Kersey. *Running For Dummies*. For Dummies, 1999.
- Takeo Kanade and Donald Schmitz. Development of CMU direct-drive arm II. Technical Report CMU-RI-TR-85-05, Robotics Institute, Carnegie Mellon University, Pittsburgh, PA, March 1985.
- Amy E. Kerdok, Andrew A. Biewener, Thomas A. McMahon, Peter G. Weyand, and Hugh M. Herr. Energetics of human running on surfaces of different stiffnesses. *Journal of Applied Physiology*, pages 469–478, 2002.
- Jeff Koechling. *The limits of running speed: experiments with a legged robot*. PhD thesis, Carnegie Mellon University, 1989.
- T. M. Kubow and R. J. Full. The role of the mechanical system in control; a hypothesis of self-stabilization in hexapedal runners. *Phil. Trans. R. Soc. Lond.*, 1999.

- Sami Kuitunen, Paavo V. Komi, and Heikki Kyrolainen. Knee and ankle joint stiffness in sprint running. *Med. Sci. Sports Exerc.*, 34(1):166–173, 2002.
- Kirsten F. Laurin-Kovitz, J. Edward Colgate, and Steven D. R. Carnes. Design of components for programmable passive impedance. In *Proceedings of the IEEE International Conference on Robotics and Automation*, pages 1476–1481, April 1991.
- Dale A. Lawrence. Actuator limitations on achievable manipulator impedance. In *IEEE International Conference on Robotics and Automation*, pages 560–565, 1989.
- T. A. McMahon. The role of compliance in mammalian running gaits. *Journal of Experimental Biology*, 115:263–282, 1985.
- Thomas A. McMahon and George C. Cheng. The mechanics of running: How does stiffness couple with speed? *Journal of Biomechanics*, 23:65–78, 1990.
- James K. Mills. Hybrid actuator for robot manipulators: design, control and performance. In *IEEE International Conference on Robotics and Automation*, pages 1872–1878, 1990.
- Toshio Morita and Shigeki Sugano. Design and development of a new robot joint using a mechanical impedance adjuster. In *IEEE International Conference on Robotics and Automation*, pages 2469–2475, 1995.
- Ken’ichiro Nagasaka, Yoshihiro Kuroki, Shin’ya Suzuki, Yoshihiro Itoh, and Jin’ichi Yamaguchi. Integrated motion control for walking, jumping and running on a small bipedal entertainment robot. In *Proc. 9th RSJ/JSME Robotics Symposia of Japan*, pages 386–391, 2004.
- Dhiraj R. Nahar and Thomas Sugar. Compliant constant-force mechanism with a variable output for micro/macro applications. In *Proceedings of the 2003 IEEE International Conference on Robotics and Automation*, 2003.
- K. Nishiwaki, T. Sugihara, S. Kagami, F. Kanehiro, M. Inaba, and H. Inoue. Design and development of research platform for perception-action integration in humanoid robot: H6. In *Proceedings of the 2000 IEEE/RSJ International Conference on Intelligent Robots and Systems*, 2000.
- Daniel Joseph Paluska. Design of a humanoid biped for walking research. Master’s thesis, Massachusetts Institute of Technology, 2000.
- Gill A. Pratt and Matthew M. Williamson. Series elastic actuators. In *IEEE International Conference on Intelligent Robots and Systems*, volume 1, pages 399–406, 1995.
- Jerry Pratt and Gill Pratt. Exploiting natural dynamics in the control of a planar bipedal walking robot. In *Proceedings of the Thirty-Sixth Annual Allerton Conference on Communication, Control, and Computing*, September 1998.
- H. Rad, P. Gregorio, and M. Buehler. Design, modelling and control of a hopping robot. In *Proceedings of the 1993 IEEE/RSJ International Conference on Intelligent Robots and Systems*, 1993.
- Marc Raibert. *Legged Robots That Balance*. MIT Press, Cambridge, Mass., 1986.
- Thomas J. Roberts. The integrated function of muscles and tendons during locomotion. *Comparative Biochemistry and Physiology part A*, pages 1087–1099, 2002.

- Thomas J. Roberts, Richard L. Marsh, Peter G. Weyand, and C. Richard Taylor. Muscular force in running turkeys: The economy of minimizing work. *Science Magazine*, 275, February 1997.
- David W. Robinson, Jerry E. Pratt, Daniel J. Paluska, and Gill A. Pratt. Series elastic actuator development for a biomimetic walking robot. In *IEEE/ASME international conference on advanced intelligent mechatronics*, September 1999.
- David William Robinson. *Design and Analysis of Series Elasticity in Closed-Loop Actuator Force Control*. PhD thesis, Massachusetts Institute of Technology, June 2000.
- U. Saranli, M. Buehler, and D. E. Koditschek. RHex: A simple and highly mobile robot. *International Journal of Robotics Research*, 20(7):616–631, July 2001.
- Philippe Sardain, Mostafa Rostami, and Guy Bessonnet. An anthropomorphic biped robot: Dynamic concepts and technological design. In *IEEE Transactions on Systems, Man, and Cybernetics*, volume 28, pages 823–838, November 1998.
- John Schmitt and Philip Holmes. Mechanical models for insect locomotion: dynamics and stability in the horizontal plane i. theory. *Biological Cybernetics*, 83:501–515, 2000a.
- John Schmitt and Philip Holmes. Mechanical models for insect locomotion: dynamics and stability in the horizontal plane - ii. application. *Biological Cybernetics*, 83:517–527, 2000b.
- J. De Schutter. A study of active compliant motion control methods for rigid manipulators based on a generic control scheme. In *IEEE International Conference on Robotics and Automation*, pages 1060–1065, 1987.
- W. J. Schwind and D. E. Koditschek. Approximating the stance map of a 2-dof monopod runner. *Journal of Nonlinear Science*, 2000.
- William J. Schwind and Daniel E. Koditschek. Control of forward velocity for a simplified planar hopping robot. In *IEEE International Conference on Robotics and Automation*, 1995.
- William J. Schwind and Daniel E. Koditschek. Characterization of monopod equilibrium gaits. In *IEEE International Conference on Robotics and Automation*, pages 1986–1992, April 1997a.
- William J. Schwind and Daniel E. Koditschek. Characterization of monopod equilibrium gaits. Technical report, University of Michigan, 1997b.
- William John Schwind. *Spring Loaded Inverted Pendulum Running: A Plant Model*. PhD thesis, The University of Michigan, 1998.
- A. Seyfarth, R. Blickhan, and J. L. Van Leeuwen. Optimum take-off techniques and muscle design for long jump. *The Journal of Experimental Biology*, 203:741–750, 2000.
- Andrew Seyfarth, Harmut Geyer, Michael Gunther, and Reinhard Blickhan. A movement criterion for running. *Journal of Biomechanics*, 35:649–655, November 2001.
- W. T. Townsend. *The Effect of Transmission Design on Force-Controlled Manipulator Performance*. PhD thesis, Massachusetts Institute of Technology, 1988.
- W. T. Townsend and J. K. Salisbury. Mechanical bandwidth as a guideline to high-performance manipulator design. In *IEEE International Conference on Robotics and Automation*, volume 3, pages 1390–1395, 1989.

- W. T. Townsend and J. K. Salisbury. The efficiency limit of belt and cable drives. In *ASME Journal of Mechanisms, Transmissions, and Automation in Design*, volume 110, pages 303–307, September 1988.
- Bram Vanderborght, Bjorn Verrelst, Ronald Van Ham, Michael Van Damme, Dirk Lefeber, Bruno Meira Y Duran, and Pieter Beyl. Exploiting Natural Dynamics to Reduce Energy Consumption by Controlling the Compliance of Soft Actuators. *The International Journal of Robotics Research*, 25(4):343–358, 2006. doi: 10.1177/0278364906064566.
- E.R. Westervelt, J.W. Grizzle, C. Chevallereau, J.-H. Choi, and B. Morris. *Feedback Control of Dynamic Bipedal Robot Locomotion*. Control and Automation. CRC Press, Boca Raton, June 2007.
- Peter G. Weyand, Deborah B. Sternlight, Matthew J. Bellizzi, and Seth Wright. Faster top running speeds are achieved with greater ground forces not more rapid leg movements. *Journal of Applied Physiology*, 89:1991–1999, 2000.
- Jin’ichi Yamaguchi and Atsuo Takanishi. Development of a biped walking robot having antagonistic driven joints using nonlinear spring mechanism. In *IEEE International Conference on Robotics and Automation*, pages 185–192, April 1997.
- G Zeglin and H. B. Brown. First hops of the 3d bow leg hopper. In *The 5th International Conference on Climbing and Walking Robots*, pages 357–364, 2002.
- Garth Zeglin. *The Bow Leg Hopping Robot*. PhD thesis, Robotics Institute, Carnegie Mellon University, Pittsburgh, PA, October 1999.
- Garth Zeglin. Uniroo: A one-legged dynamic hopping robot. Technical report, Massachusetts Institute of Technology, Cambridge, Massachusetts, 1991.
- Garth Zeglin and H. Benjamin Brown. Control of a bow leg hopping robot. In *IEEE International Conference on Robotics and Automation*, May 1998.